International Atomic Energy Agency

INDC(NDS)-234
Distr. L

INDC

INTERNATIONAL NUCLEAR DATA COMMITTEE

MEASUREMENTS AND ANALYSIS OF DOUBLE DIFFERENTIAL NEUTRON SPECTRA IN (P,N) AND (ALPHA,N) REACTIONS

Proceedings of the
Final Meeting of a Co-ordinated Research Programme
organized by the
International Atomic Energy Agency
and held in
Bologna, Italy, 13-15 November 1989

Compiled by

N.P. Kocherov
IAEA Nuclear Data Section

April 1990

IAEA NUCLEAR DATA SECTION, WAGRAMERSTRASSE 5, A-1400 VIENNA

INDC(NDS)-234
Distr. L

MEASUREMENTS AND ANALYSIS OF DOUBLE DIFFERENTIAL NEUTRON SPECTRA IN (P,N) AND (ALPHA,N) REACTIONS

Proceedings of the
Final Meeting of a Co-ordinated Research Programme
organized by the
International Atomic Energy Agency
and held in
Bologna, Italy, 13-15 November 1989

Compiled by

N.P. Kocherov
IAEA Nuclear Data Section

April 1990

Reproduced by the IAEA in Austria
April 1990

90-01661

INTRODUCTION

The IAEA Co-ordinated Research Programme (CRP) on Measurement and Analysis of Neutron Emission Spectra from (p,n) and (alpha,n) Reactions was started at the beginning of 1986. The first Research Co-ordination Meeting took place on 23-27 June 1986 in Vienna. At that meeting the participants have formulated the main objective of the CRP as to extract systematic information about level densities as a function of excitation energies by means of analysis of neutron emission spectra from (p,n) and (alpha,n) reactions on properly selected targets and within proper bombarding energy ranges.

The participants agreed on three bombarding energy regions: 5-10 MeV, 11-15 MeV and 25 MeV. Only those laboratories which had accelerators with beams within these energy ranges and neutron spectrometer facilities could participate in the experimental part of the programme.

The measurements were done at Argonne (P.T. Guenther), Ohio University (S.M. Grimes), Hamburg University (W. Scobel), FEI Obninsk (B.V. Zhuravlev), and at IAE Beijing (Tang Hongqing).

The analysis of the data sets produced was done by IRK Vienna (H.K. Vonach), TU Dresden (H. Märten), BARC Bombay (S.K. Kataria, V.S. Ramamurthy), FEI Obninsk (A.V. Ignatyuk) and also by some of the data producers themselves.

Measurements of double differential neutron spectra have required a considerable experimental effort and a lot of accelerator time. Therefore it was decided during the first CRP meeting to hold the second one in 1.5 years and after the second meeting it was decided to delay the last meeting for almost 2 years to get time enough for participants to finish the measurements.

All participants have agreed that new reliable data sets with an up-to-date accuracy were produced by the CRP and that the volume of the data was sufficient to make an unambiguous analysis using different theoretical approaches.

As a further useful development of this programme the participants stated the need for measurements with alpha-particle beams and targets which would lead to the same compound nuclei as were reached in (p,n) reactions. However, there seems to be very little hope to organize this activity in the nearest future due to lack of experimental facilities capable of fulfilling this task. Therefore no recommendation was made on this point.

On the last day of the Research Coordination Meeting a joint session with the NEANDC Specialists' Meeting on Nuclear Level Densities was organized. The organization of these two meetings adjoint to each other was found very useful by all participants.

The papers presented by the participants during the Research Coordination Meeting are published in this document. They summarize the results of experimental and theoretical work performed under this CRP.

The contribution by Dr. K. Okamoto, who was scientific secretary of this programme during its first two years is gratefully appreciated.

N. P. Kocherov
Scientific Secretary
of the Meeting

CONTENTS

Level Densities for ^{51}Cr and ^{59}Ni Deduced from (p,n) and (α,n) Spectra

S.M. Grimes, R.S. Pedroni, C.E. Brient,
V. Mishra and N. Boukharouba

Ohio University
Athens, Ohio 45701
U.S.A.

ABSTRACT

Measurements of the (p,n) spectrum from targets of ^{51}V and ^{59}Co and the (α,n) spectrum from ^{48}Ti and ^{56}Fe targets have been made. Comparison of the measurements with Hauser–Feshbach calculations allowed level density parameters for ^{51}Cr and ^{59}Ni to be deduced. For proton energies up to 8.5 MeV and alpha energies up to 13 MeV, both reactions are dominated by compound nuclear processes.

The basic assumption underlying the compound nucleus model is that the formation and decay processes are independent. A compound nucleus decay will be consistent with well–established conservation laws, including energy, momentum, angular momentum and parity, but within these constraints the decay is governed by barrier penetration factors and the number of available final states. The lack of a Coulomb barrier for neutrons makes neutron decay the dominant mode of decay for the compound nucleus. This will be true whether the compound nucleus is formed by neutrons, protons or alpha particles. A disadvantage to the use of neutrons as projectiles is the relative difficulty of obtaining a monoenergetic beam of neutrons with minimum background. An (n,n') study would also be more likely to have significant direct reaction contributions than a (p,n) or (α,n) reaction.

One of the first experimental tests of the compound nucleus model was that of Ghosal [1]. In this study, activation cross sections for the (α,n) reaction on ^{60}Ni and the (p,n) reaction on ^{63}Cu over about a 15 MeV range of energy were determined. Since the cross sections were deduced from activation of the final nucleus, no information on the energy distribution of the outgoing neutrons was obtained. The bombarding energy dependence of the cross sections did agree well with the predictions of the compound nucleus theory, showing a sharp fall off for both (p,n) and (α,n) cross sections when the (p,2n) and (α,2n) channels opened up.

More recently, a number of papers [2] have been published which have studied the proton and alpha channel as both entrance and exit channels for a particular compound nucleus. These have the advantage that they are easier to carry out than the corresponding neutron measurements. They are, however, more likely to be contaminated by non–compound contributions to the spectra, since most of the compound nuclei will decay with the emission of a neutron. It was found that for nuclei with $A < 65$ enough cross section in the (α,α'), (α,p), (p,p') and (p,α) reaction channels was due to compound nuclear processes that information on level densities could be obtained.

Other measurements [3,4] focused on comparisons of (p,n) and (α,n) reactions through the same compound nucleus. The direct observation of the shape of the outgoing spectrum and variation of the proton and alpha bombarding energies allowed information on the level density of the residual nuclei to be obtained over a range of about 10 MeV of excitation energy. Although the (p,n) reaction gave angular distributions which were essentially isotropic, the (α,n) angular distributions were symmetric about 90° but not isotropic. This allowed information about the spin cutoff parameter to be inferred.

The present IAEA Coordinated Research Program was organized to allow a thorough examination of the possible problems with such measurements. Comparison of spectra obtained in various laboratories can help check for unexpected experimental problems. All experimental data are to be exchanged between various research groups, allowing independent analyses of the same data. This could help uncover possible problems with the analysis of the data.

As a part of this CRP, we have measured cross sections for the ^{51}V and ^{59}Co (p,n) reactions and ^{48}Ti and ^{56}Fe (α,n) reactions. These have been measured in the Edwards Laboratory of Ohio University. Beams of alpha particles and protons were obtained from a tandem electrostatic accelerator. A pulsing and bunching system produced protons with a width of 1.2 ns and alpha particles with a width of 2 ns, both at a frequency of 1.25 MHz. The neutrons produced in these reactions were detected in NE213 scintillators after traversing a 12 m flight path. Pulse shape discrimination was utilized to minimize background produced by gamma rays. Detector efficiencies were determined by using the T(p,n) and D(d,n) reactions.

Measurements were made at angles from 0° to 150° in 25° steps. The neutron energy resolution ranged from about 20 keV for 2 MeV neutrons to about 140 keV for 9 MeV neutrons. Over most of the energy range, this was less than the spread induced by energy losses in the 2 mg/cm^2 targets, which were nearly 100 keV for protons and about 500 keV for alpha particles.

Examination of the spectra indicated that the bulk of the neutrons were due to compound nuclear processes. Calculations of the expected spectra were made with the Hauser–Feshbach code HF [4]. Decay channels included the neutron, proton and alpha emission channels. Transmission coefficients were obtained for alphas from the potential of McFadden and Satchler [5], while those for protons and neutrons came from Becchetti and Greenlees [6] and Rapaport, Kulkarni and Finlay [7], respectively.

Level density parameters were obtained from a microscopic Fermi gas code for the appropriate residual nuclei using the single particle levels of Seeger and Howard [8]. These values were then varied as needed to obtain a good fit to the data. The resulting values for ^{59}Ni and ^{51}Cr are a = 7.6 and δ = 1.1 (^{59}Ni) and a = 6.5 and δ = .7 (^{51}Cr), and Figs. 1–15 show the corresponding fits to the data.

A single set of level density parameters was used for a given compound nucleus at all bombarding energies and for both projectiles. For both systems, the (p,n) data can be fit better than the (α,n) data. The significance of this difference is not clear. Further adjustments of the level density parameter would be of limited value because the (α,n) data suggest a need for an increase in the total cross section for neutron production and the (α,n) cross section is already 85% of the absorption cross section. The shape of the spectrum for (α,n) does agree with the predictions but we have not found a justification for an overall renormalization of the spectrum. Spin cutoff parameters for both ^{51}Cr and ^{59}Ni were found to be about 3.2 from examination of the anisotropy in the (α,n) spectra.

Comparisons with the data from Beijing [9] were also made as seen in Figs. 16 and 17. These data are for the ^{59}Co(p,n) reaction and span the range $9 \leq E_p \leq 15$ MeV. The present parameters predict a spectral shape which agrees with the Beijing data, but again, the normalization is not correct. No error in the calculation could be found and the discrepancy is still unexplained.

Despite imperfect agreement for some spectra, rather narrow limits on a and δ are set by the requirement that the data for both reactions be fit. Of particular importance is the range of bombarding energy. This helps narrow the uncertainty in the level density parameters.

The study of (p,n) and (α,n) reactions is useful in determining level density parameters. With the availability of data from more sources, direct comparison of data sets should eliminate or reduce experimental errors. A more careful theoretical analysis should also give better values for the spin cutoff parameter.

REFERENCES

[1] S.N. Ghoshal, Phys. Rev. 80, 939 (1950)

[2] C.C. Lu, J.R. Huizenga, C.J. Stephan and A.J. Gorski, Nucl. Phys. A164, 225 (1971);
L.C. Vaz, C.C. Lu and J.R. Huizenga, Phys. Rev. C5, 463 (1972);
A.J. Kennedy, J.C. Pacer, A. Spinzak, J. Wiley and N.T. Porile, Phys. Rev. C5, 500 (1972);
J. Wiley, J.C. Pacer, C.R. Lux and N.T. Porile, Nucl. Phys. A212, 1 (1973)

[3] S.M. Grimes, J.D. Anderson, J.W. McClure, B.A. Pohl and C. Wong, Phys. Rev. C3, 645 (1971)

[4] S.M. Grimes, J.D. Anderson, J.W. McClure, B.A. Pohl and C. Wong, Phys. Rev. C10, 2373 (1974)

[5] L. McFadden and G.R. Satchler, Nucl. Phys. 84, 177 (1966)

[6] F.D. Becchetti, Jr. and G.W. Greenlees, Phys. Rev. 182, 1190 (1969)

[7] J. Rapaport, V. Kulkarni and R.W. Finlay, Nucl. Phys. A330, 15 (1979)

[8] P.A. Seeger and W.M. Howard, Nucl. Phys. A238, 491 (1975)

[9] Z. Zuying, T. Hongqing, S. Jun, S. Qingchang, Q. Bujia, Y. Chunying and S. Guanren, contribution to this meeting.

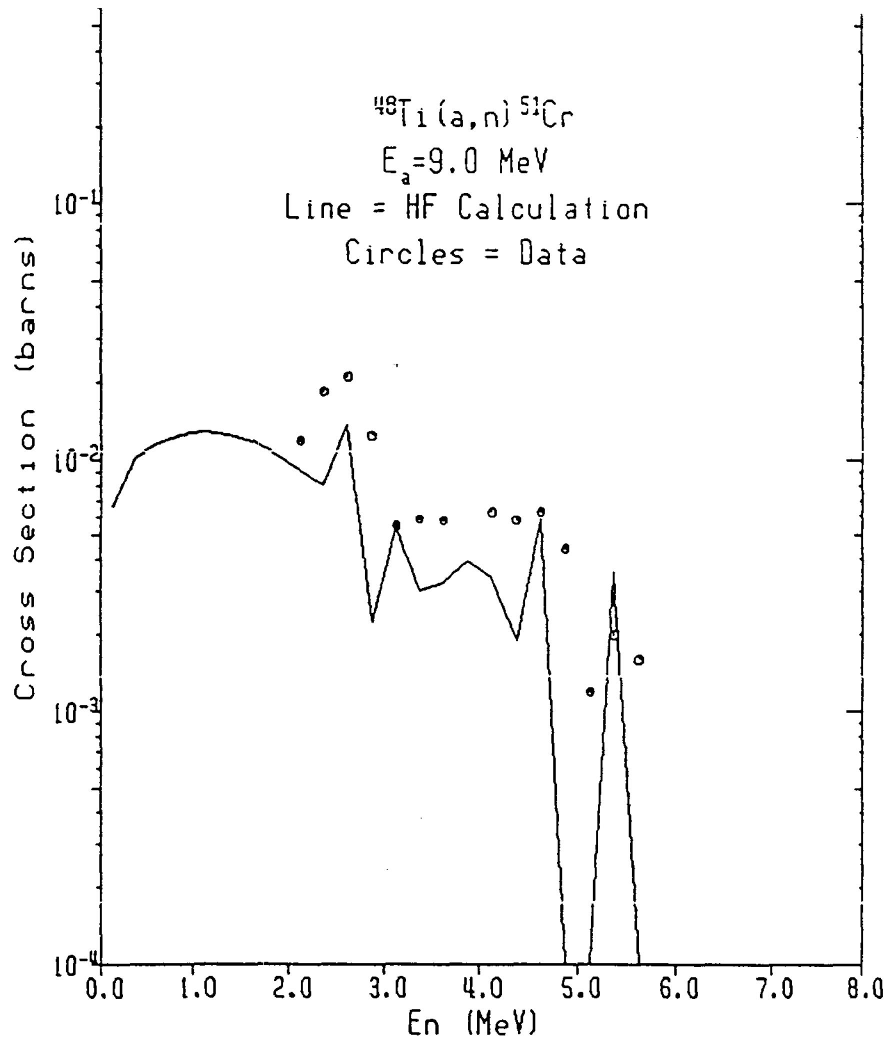

Figure 1

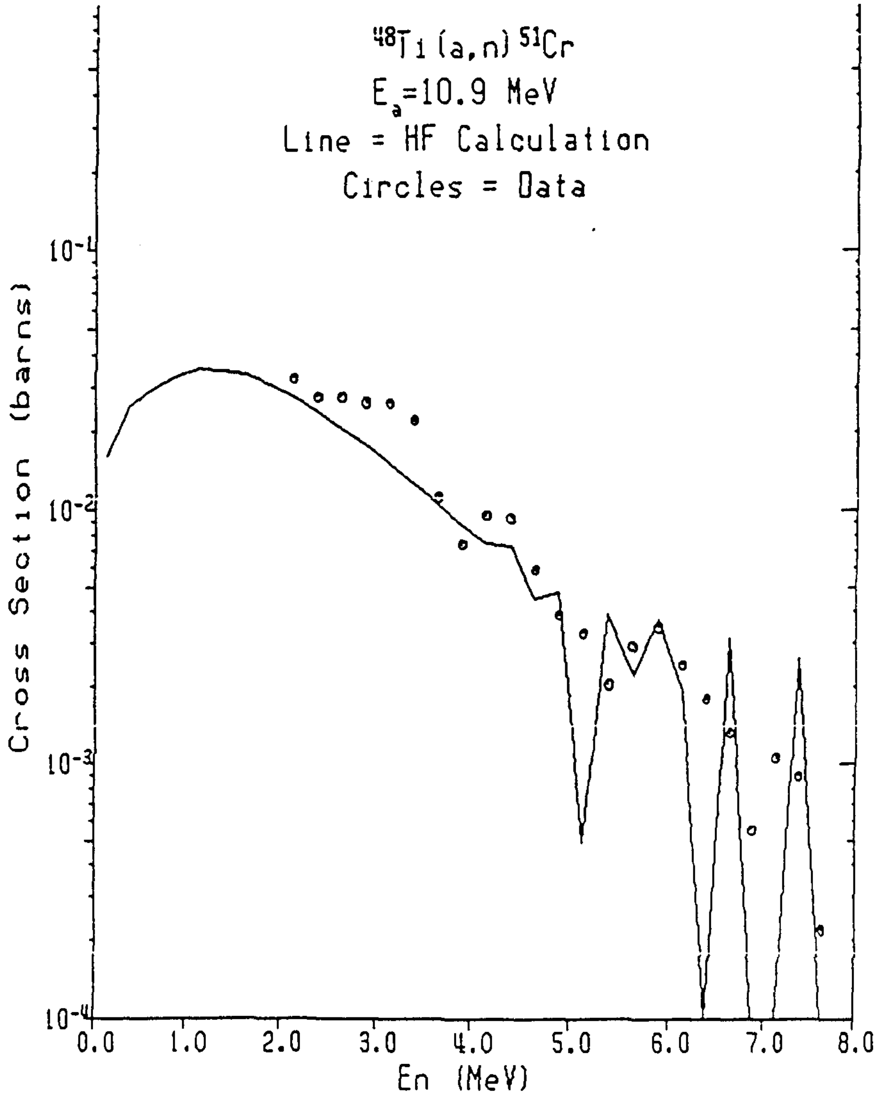

Figure 2

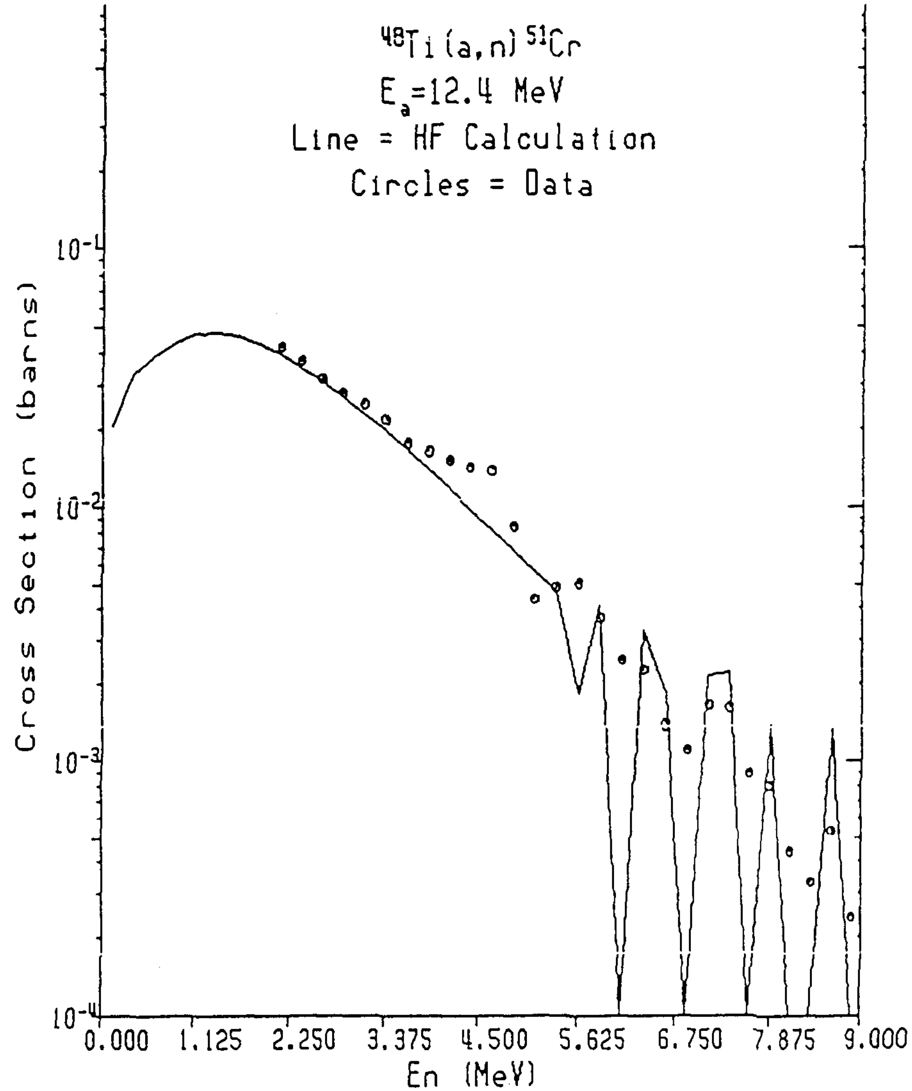

Figure 3

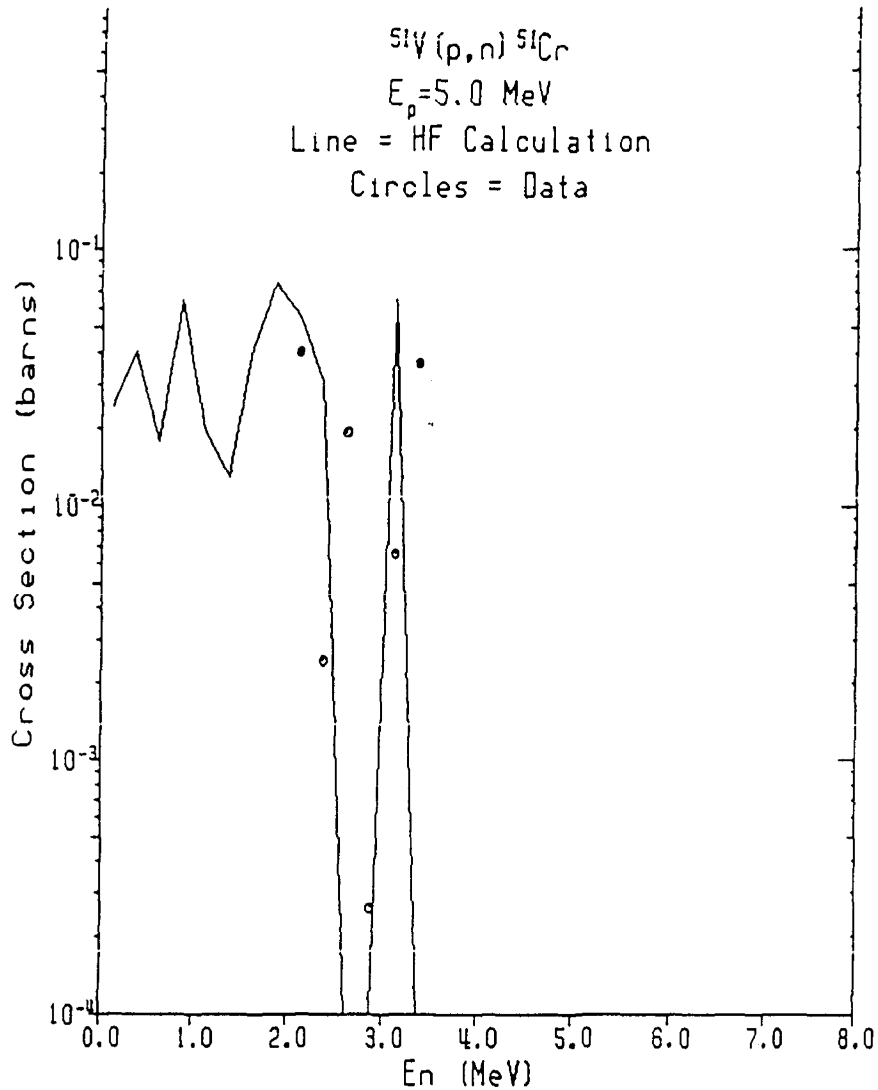

Figure 4

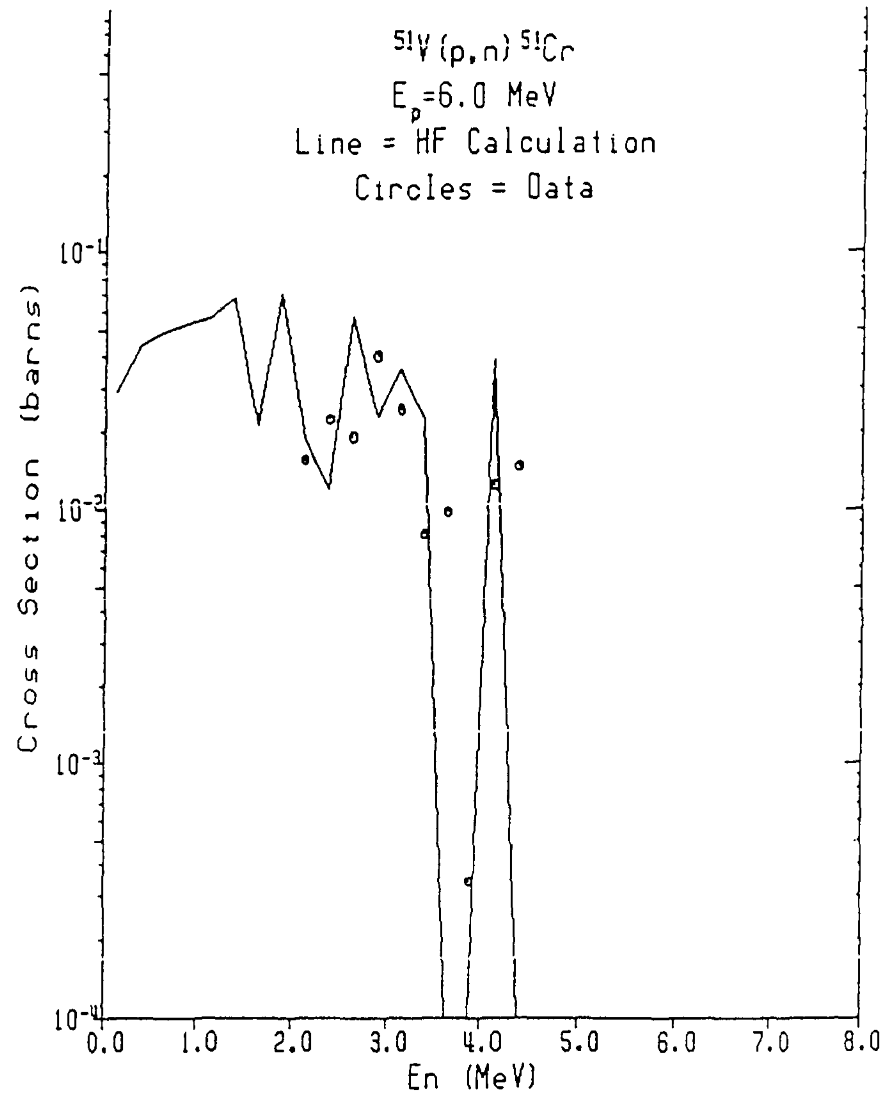

Figure 5

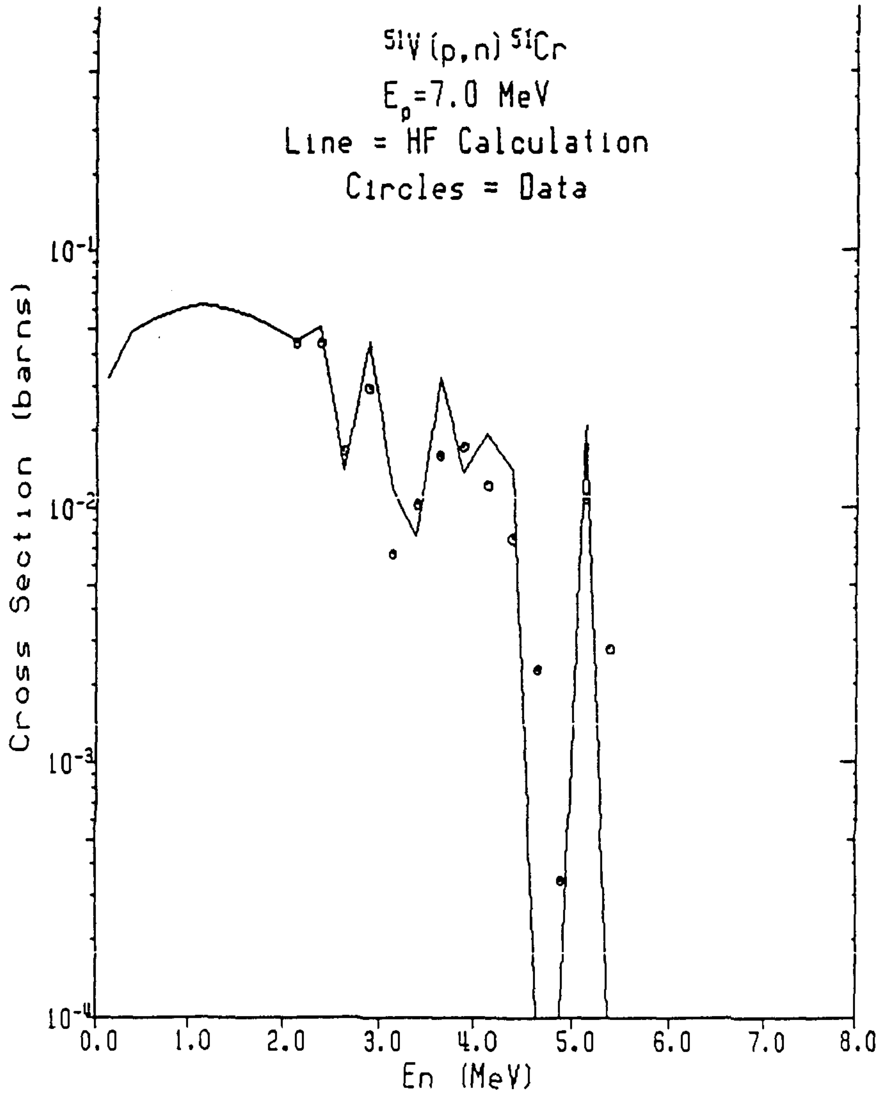

Figure 6

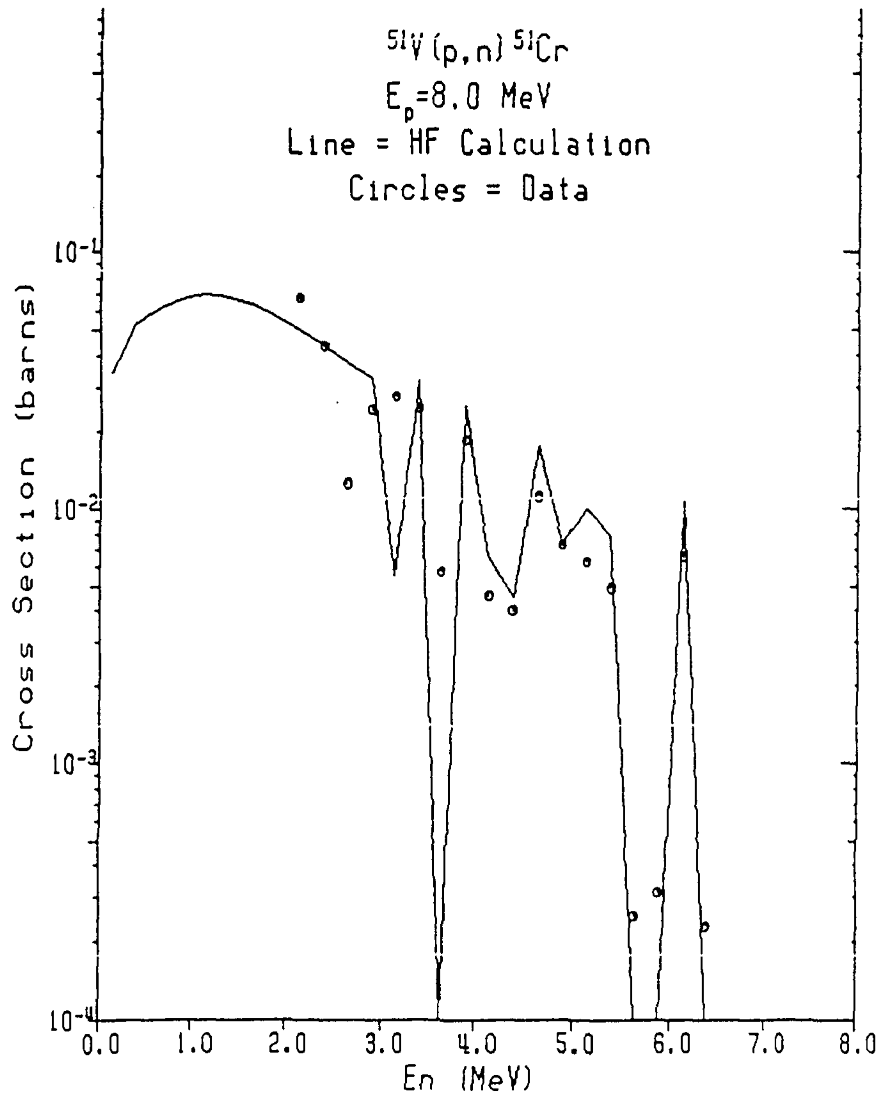

Figure 7

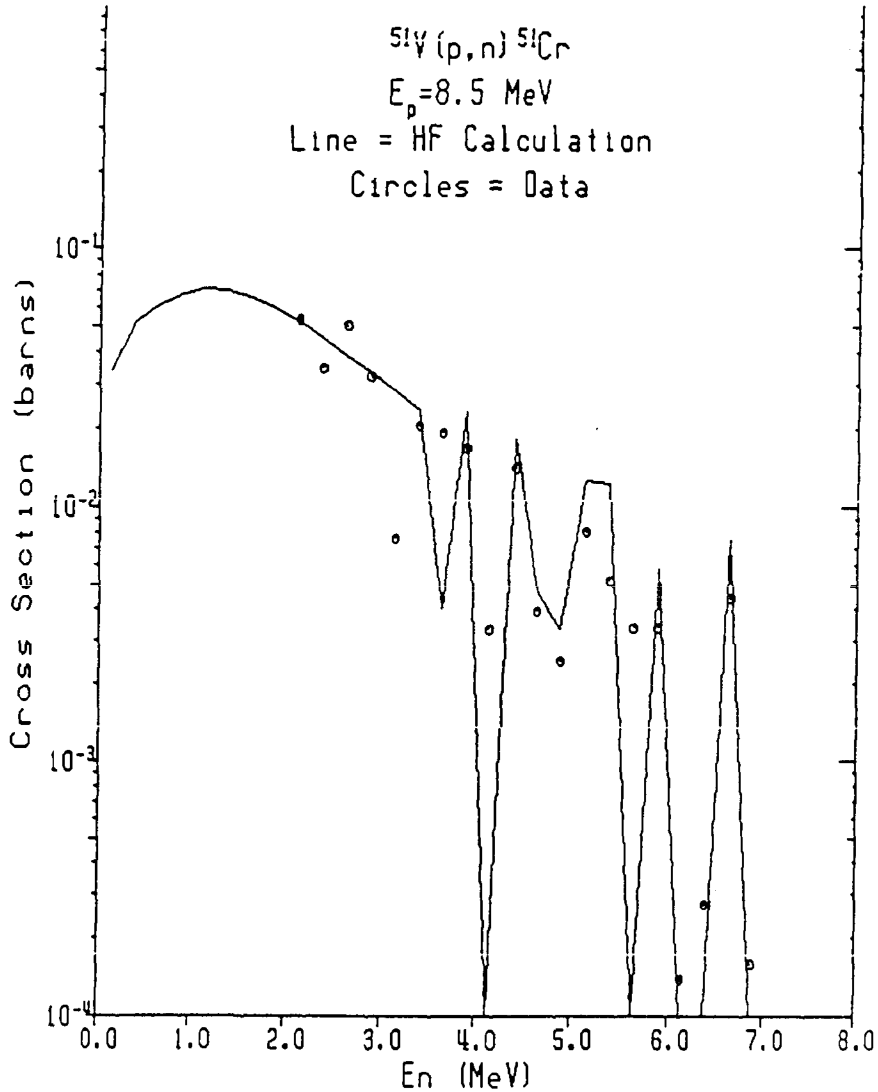

Figure 8

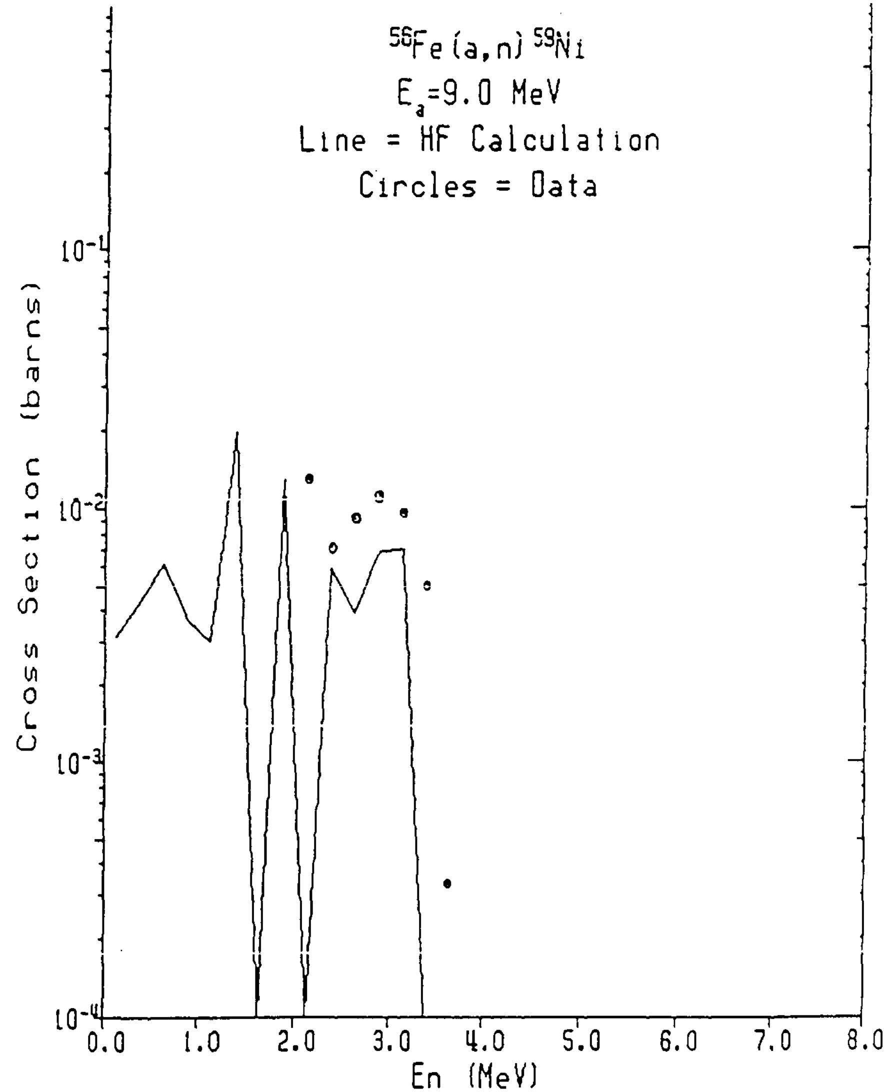

Figure 9

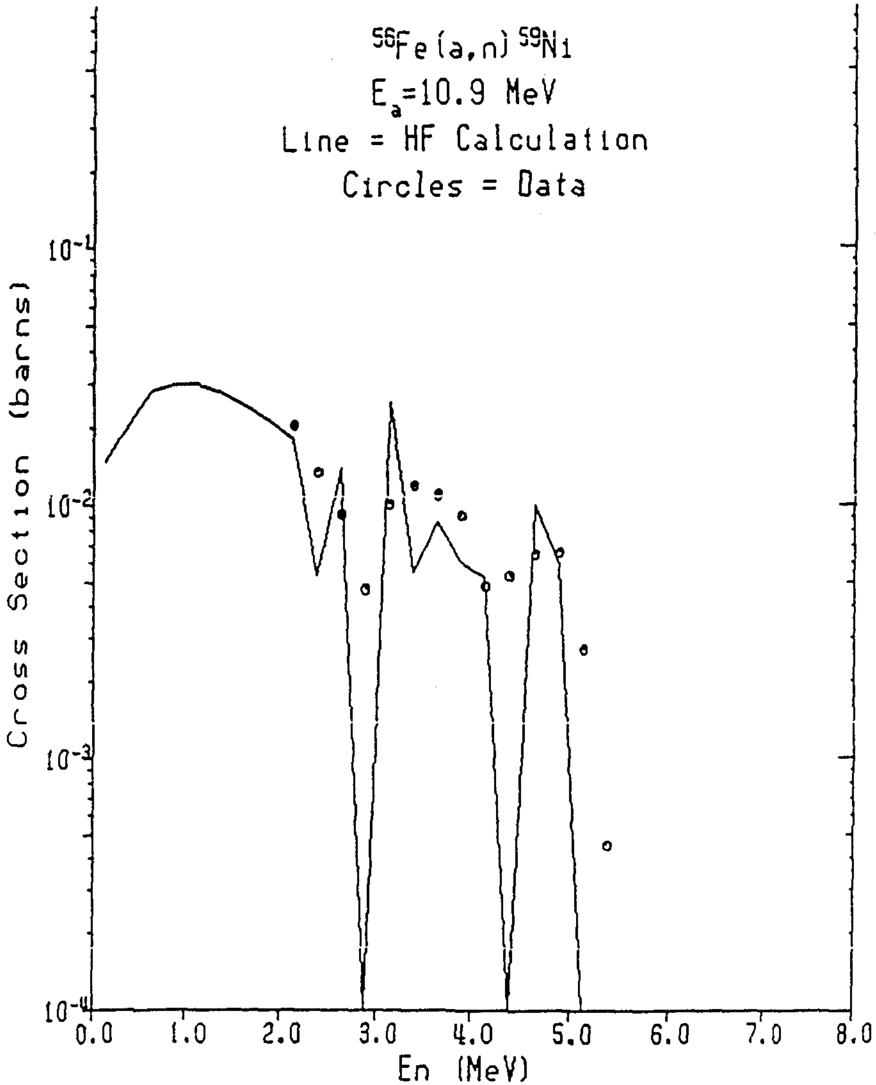

Figure 10

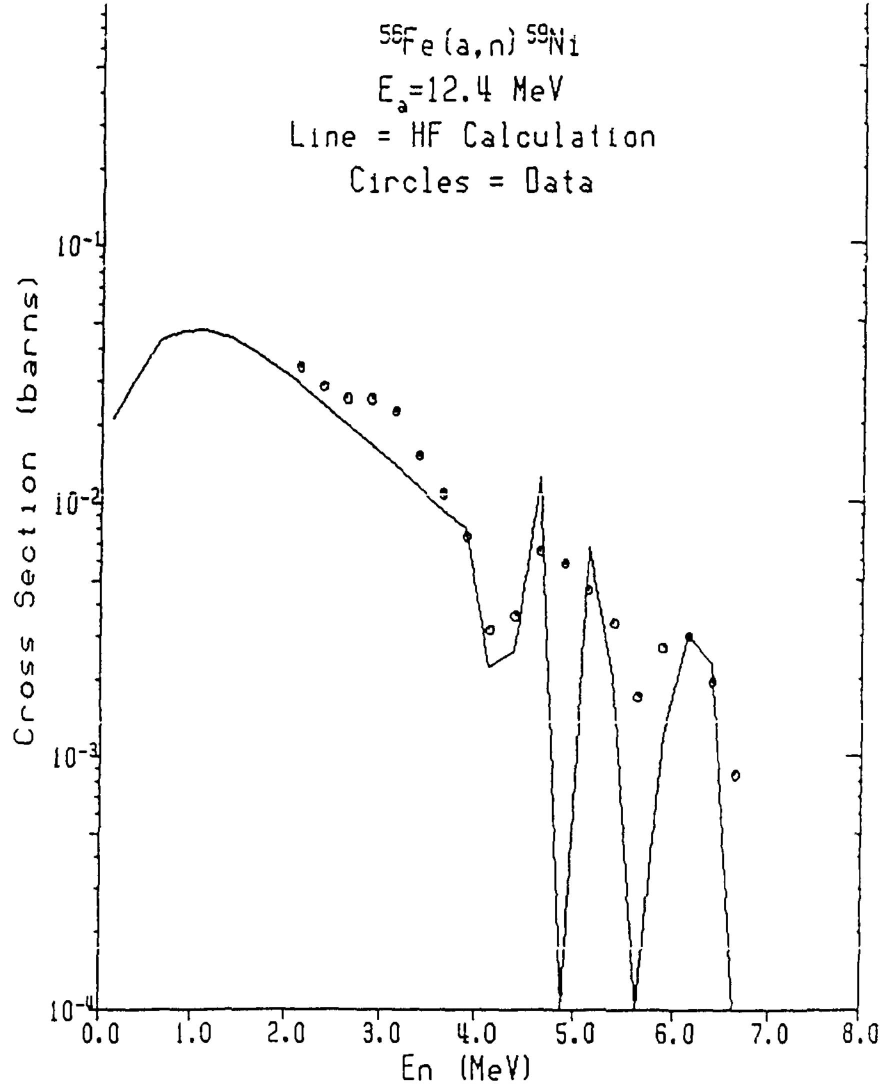

Figure 11

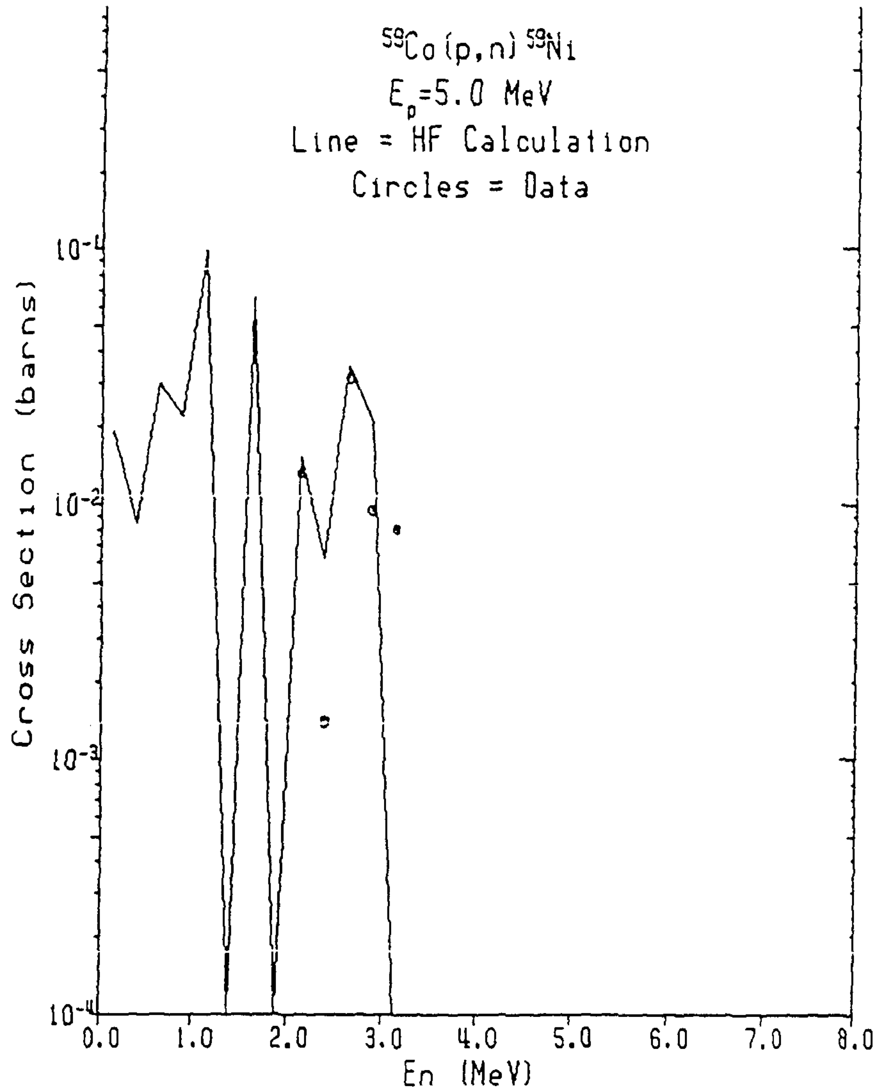

Figure 12

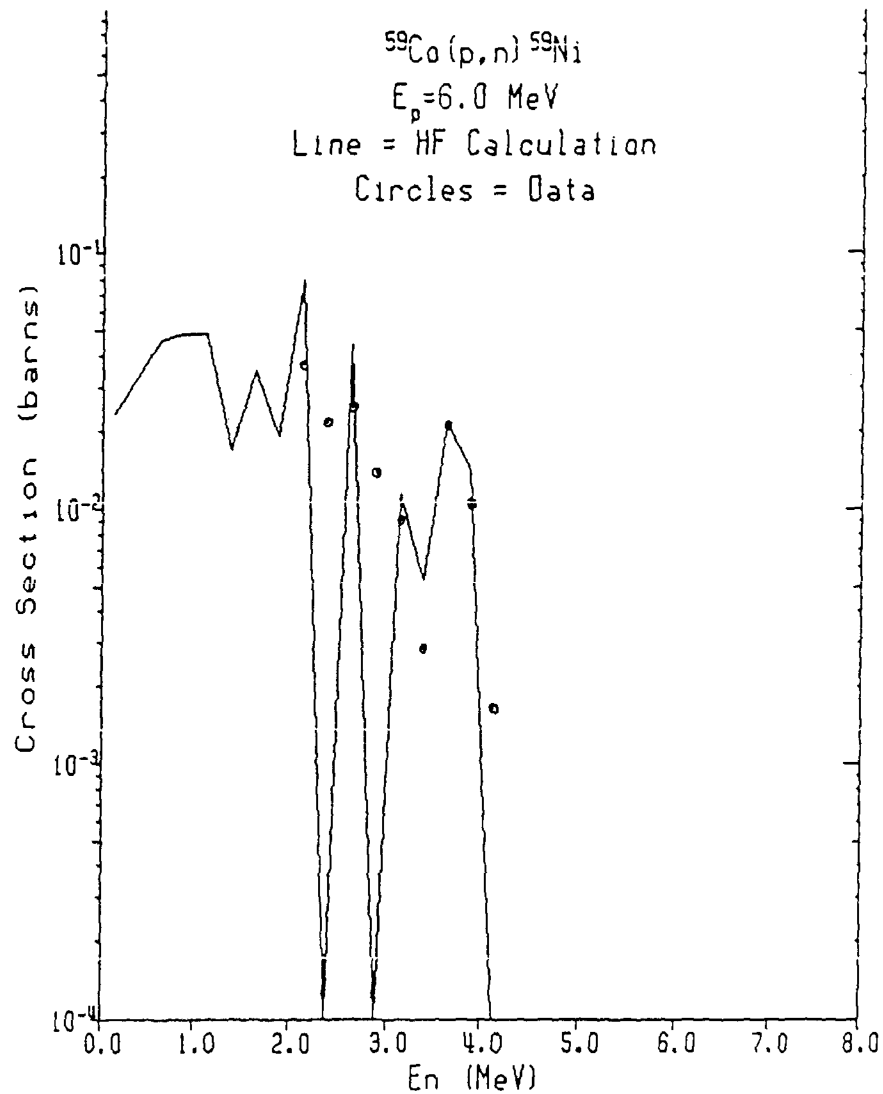

Figure 13

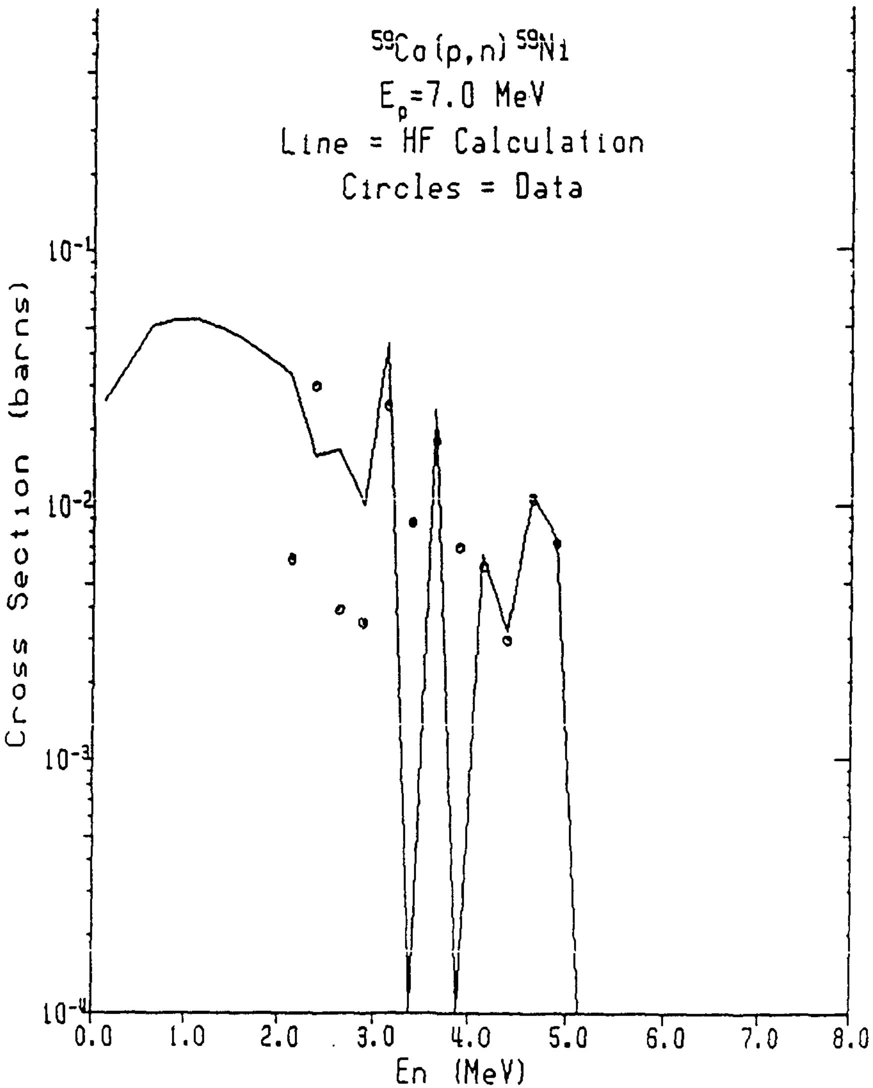

Figure 14

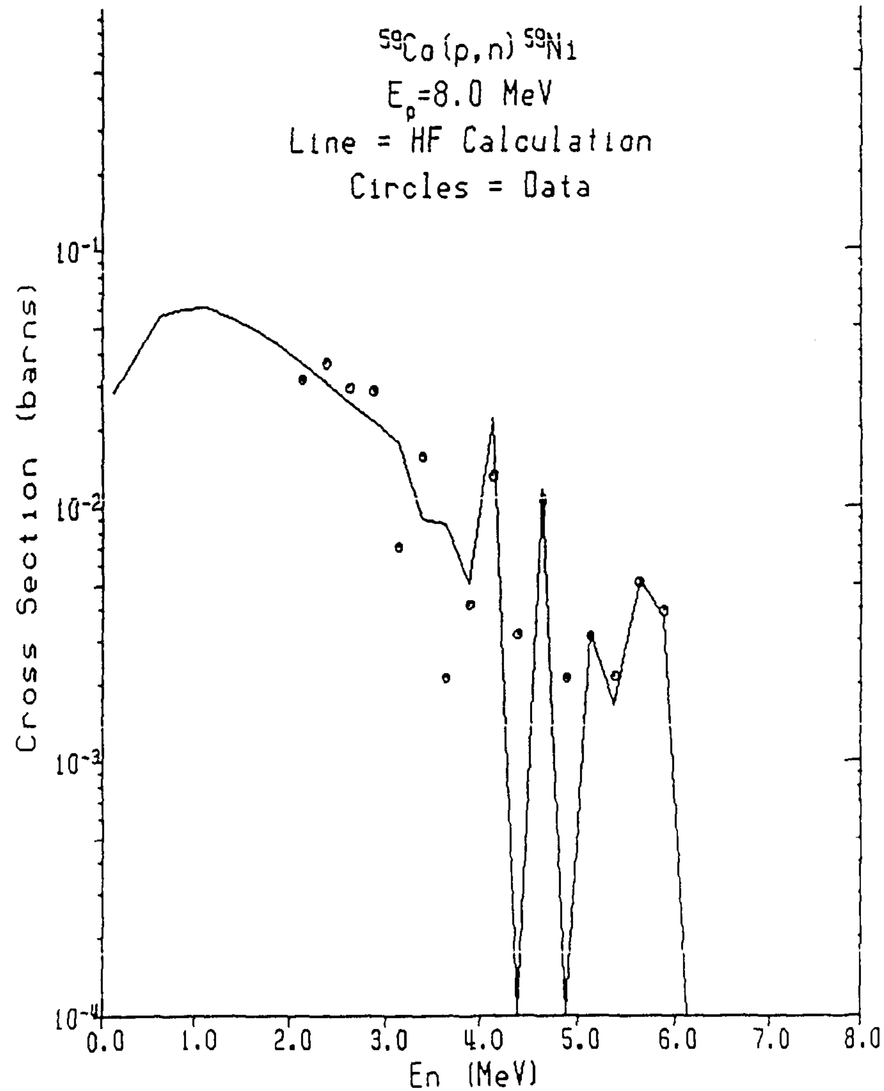

Figure 15

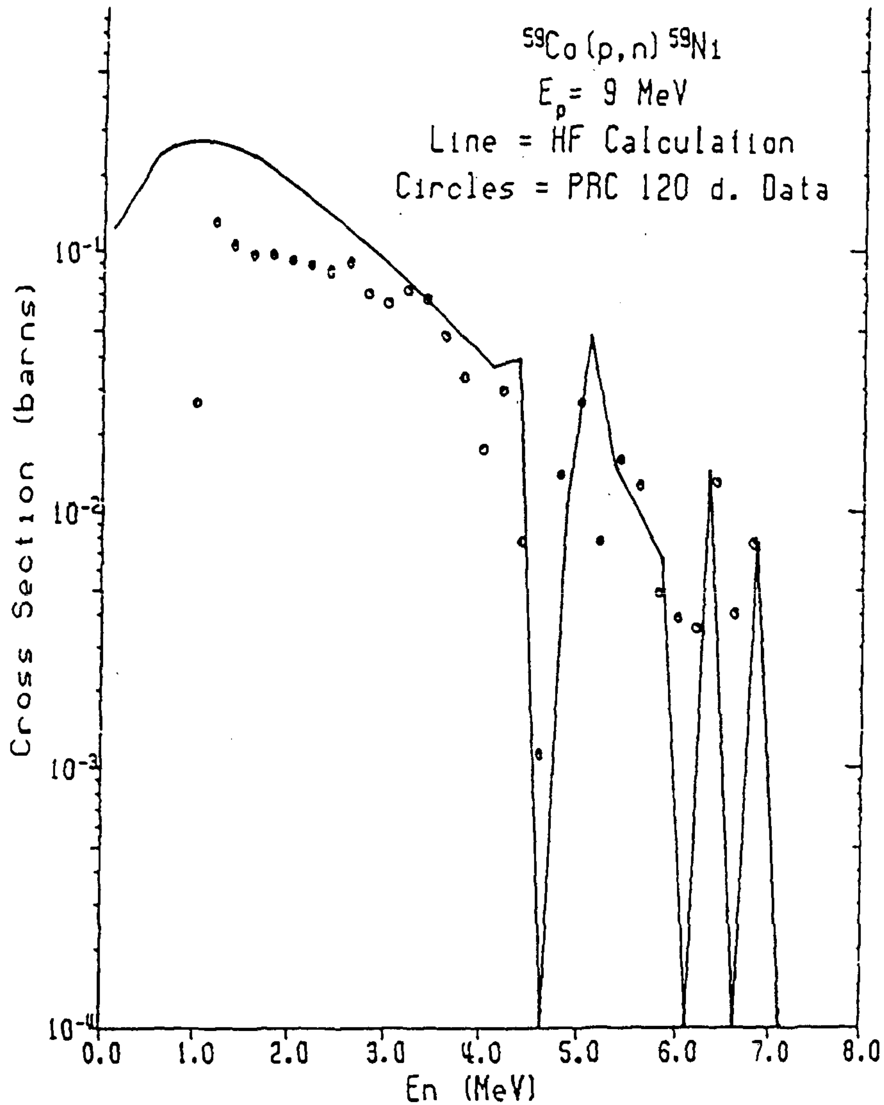

Figure 16

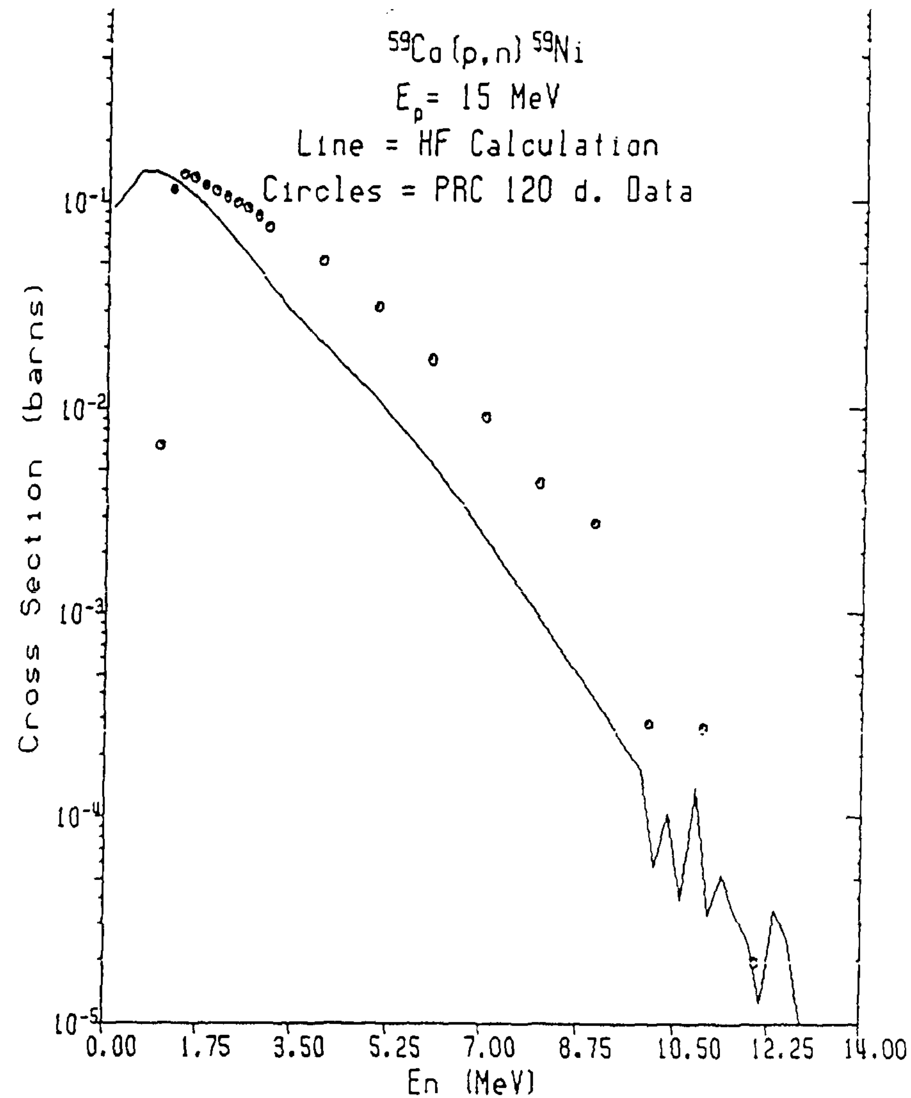

Figure 17

REPORT ON THE IAEA RESEARCH AGREEMENT #4412/CF

P. T. Guenther
Engineering Physics Division
Argonne National Laboratory
Argonne, Illinois 60439
U.S.A.

I. INTRODUCTION

My contribution to this CRP is the provision of double–differential neutron–scattering cross section data on the mono–isotopic (or essentially mono–isotopic) elements Nb, Rh, In, Ho, Ta, Au, and Bi. These data cover the ranges:

Incident neutron energies:	E_{in} = 5–8 Mev,
Angular range:	30–158 degrees,
Excitation energies:	≈ 2 to $E_{in} - 1$ MeV.

In this report I will i) briefly review the original purpose of these measurements, ii) indicate the assumptions and procedures required to obtain the requested cross sections, iii) present the results of this effort, iv) give a few examples of how these results compare to calculations made with relevant nuclear model codes, v) describe the data files that I have prepared for the participants of this CRP, vi) briefly describe sources of error. An appendix contains a short discussion of some experimental concerns.

II. CONCEPTS OF THE EXPERIMENT

The original purpose of these measurements was to explore neutron–emission spectra relevant to an ongoing program of neutron cross–section measurement and evaluation conducted at the Argonne Fast–Neutron Generator. The primary aim was a shape description employing existing scattering apparatus without extensive modifications or optimization. As I have explained more fully in Ref. [1], the common use of the expression $N(E_n) \approx E_n \exp[E_n/T]$ for the description of low–energy emission spectra and the reasonably accurate description of the spontaneous fission neutron spectrum of ^{252}Cf by the Maxwellian form $N(E_n) \approx E^{1/2} \exp[-E_n/T]$, suggested that the requisite temperatures could be deduced from a ratio of these spectra. This method was further justified by the fact that the neutron field of ^{252}Cf is a standard [2] and is used in our laboratory to establish the energy–dependence of our liquid–scintillation neutron detectors [3]. It was expected that for the incident neutron energies and the excitation energies to be increased, the spectra would display no strong angular dependence. Thus, the use of the 10–channel spectrometer amounted to a tenfold overdetermination of the shapes sought, but, nonetheless, afforded an attendant check on the angular distribution. A detailed normalization of the detectors is a time–consuming process (about 20–30% of running time per incident energy) and, since it was not deemed necessary, this time was rather invested in obtaining spectra for an additional sample. Even so, to attain the statistical accuracies of the data provided, approximately 4 months of acceleration time were required.

III. NORMALIZATION

The request by the participants of the CRP for absolute cross sections posed an interesting exercise in compromises. In retrospect, of course, better accuracies could have been achieved with a full, standard normalization procedure. The point to appreciate is that the analysis of these measurements has been pushed beyond the original intent. Two possible normalizations were explored: That with respect to the angle–integrated elastic and that with respect to the inelastic cross section. It was found that the latter was more reliable than the former. The difficulty in using the elastic cross section was twofold.

First, an insufficient number of angles were measured to precisely define the angular distribution. Secondly, even with the use of available shapes of the angular distribution, possible zero–degree shifts (which were not determined) can result in integrated cross section errors of 10% or more. An additional uncertainty arises due to the emphasis in the normalization on the single 30° point whose value depends, moreover, on a very accurate multiple–event correction. In summary, this approach was abandoned primarily because the data could not properly define the dominant forward peak in the elastic angular distribution.

The normalization was effected relative to the continuum cross section for Nb, as given in ENDF/B–V [4]. The onset of this component is given at Q = –2.2. Since the measured spectra were judged reliable to an emitted–neutron energy of ≈ 1 MeV (threshold at ≈ 0.6 MeV) and the temperature distribution for all the samples peaked below this energy, a considerable portion of the cross section had to be obtained by extrapolation of the measured spectra to zero energy (i.e., $E_n = 0$). The extrapolation factors (i.e., the ratio of temperature distribution integral from the continuum onset to the portion observed) amounted to values of ≈ 1.5–2.0 and were subject to two principal uncertainties. First, the value of T used in the expression $N(E_n) \approx E_n \exp[-E_n/T]$, and second, the exact value for the spectrum cutoff. Of these, the former was not particularly critical, but the latter was sensitive to energy scale uncertainties. A reasonable effort was expended to determine the energy scale accuracy to a higher degree necessary than originally anticipated. By carefully matching calculation procedures (e.g., using Q values throughout), it is believed this factor is no more uncertain than 5%. Thus, the overall normalization is dependent on two main sources of error, the file itself and the extrapolation factor.

The elastic angular distributions served as a rough check on the normalization. In Fig. 1, the elastic scattering from In inferred from the present measurement is

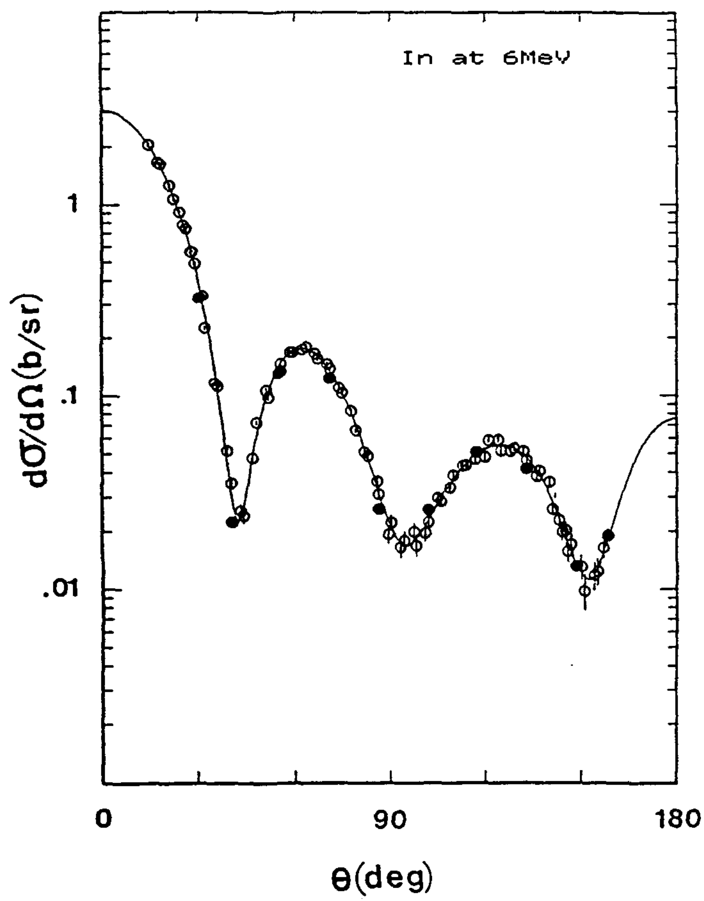

Fig. 1. Elastic angular distribution of elemental indium. The open circles are from current measurements at the ANL FNG. The black circles are from the present work. Both are fully corrected and in the laboratory system.

superimposed (black circles) on a recent and far more detailed elastic scattering distribution obtained with the ten–channel spectrometer.

IV. RESULTS

Since the full reduction of the measurements was only recently completed, the analysis of these data has been minimal. A preliminary slope analysis of the spectral ratios described in Sec. II and such as those shown in Fig. 2 was performed before multiple–event coefficients were available. The results of this survey are indicated in Fig. 3. They are averages over all detectors. As multiple events tend to soften the spectra, a final analysis should increase these temperatures by a few per cent. In Fig. 4, the inelastic–event portion of several TOF spectra of Nb, Ta, and Bi demonstrate varying amounts of "structure." Indium is similar to Nb, evincing a moderate amount of level clustering. Holmium is quite

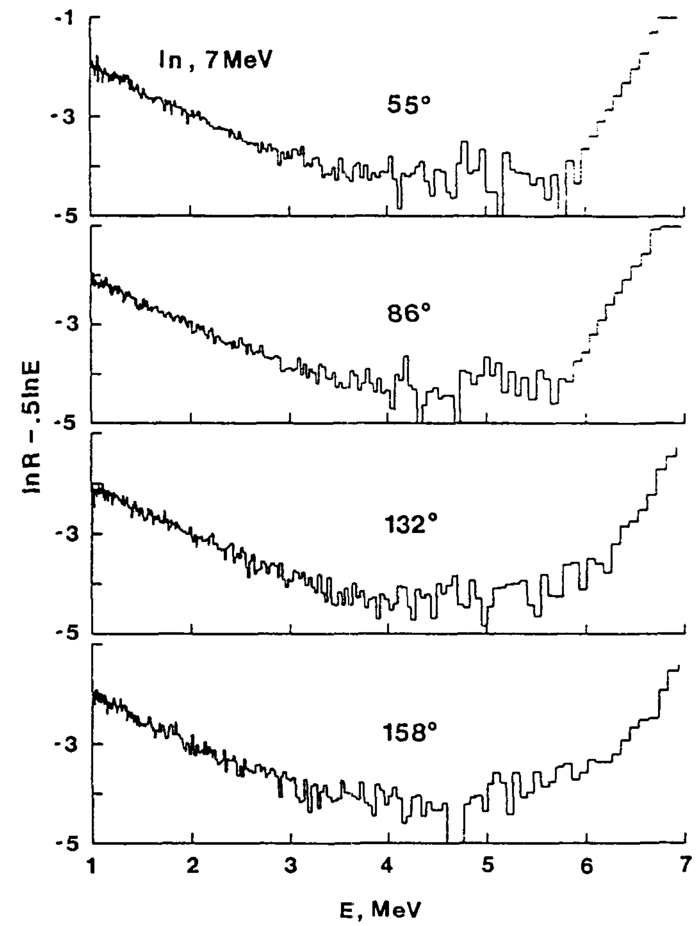

Fig. 2. Ratio of TOF spectra for element indium to those of ^{252}Cf(s.f.). A linear fit of an appropriate low–energy portion of these ratios where used to infer the temperatures given in Fig. 3. These ratios have not been corrected for multiple scattering. Vertical axis arbitrary, horizontal axis emission neutron energies in the lab.

smooth like Ta ("good Nuclei") and Bi near double–shell closure exhibits considerable "structure." The spectra were a guide to choosing the lowest excitation energy groups contained in the files. In Fig. 5, the angular distributions of the full set of half–MeV groups for In is shown at two energies. In Fig. 6, on the other hand, group widths were chosen to include primarily direct and precompound, precompound and compound, and mostly compound contributions to the emission spectrum.

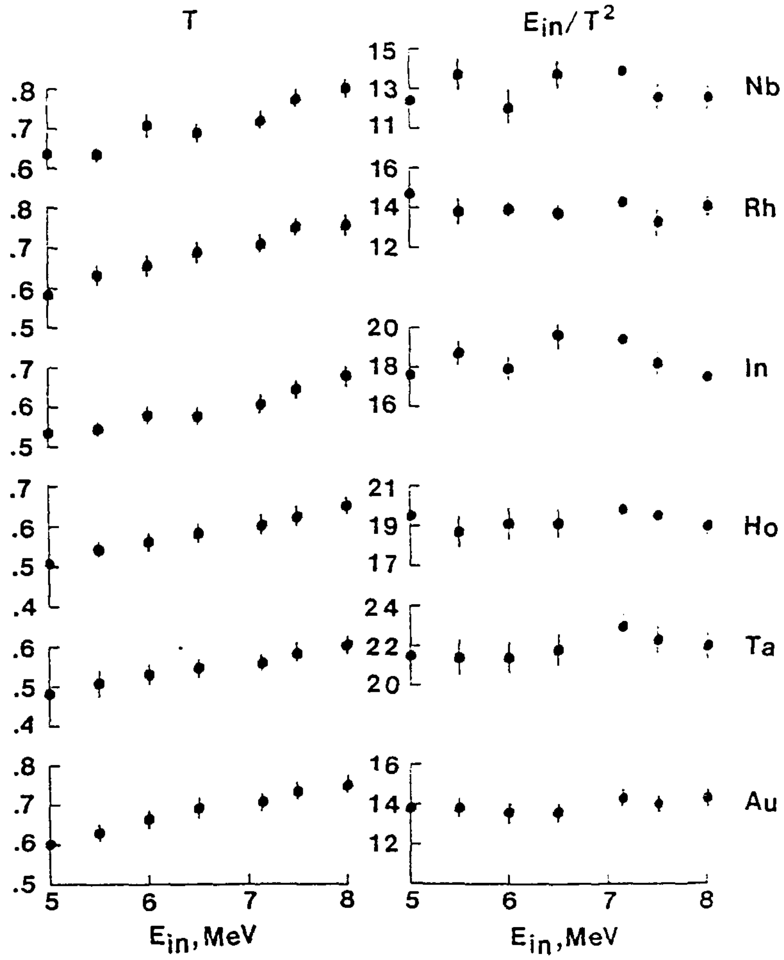

Fig. 3. Preliminary temperatures and E_{in}/T^2 values derived from ratios such as those explained in Fig. 2. Within the errors of the measurement and the limited energy range E_{in}/T^2 appears to be essentially energy independent.

V. SOME MODEL CALCULATIONS

The angle–integrated file for indium is compared to ALICE [5] calculations. For each incident energy in Fig. 7a, the upper curve is computed with the default optical model potential parameters. The lower curves result when the optical model parameters recently determined by our group in connection with a current evaluation effort on In are used. The level density parameter (PLD) was adjusted to reflect the Gilbert and Cameron [6] level density a = 17.4. The calculations for Fig. 7b were identical in all respects, except that PLD was adjusted to reflect the E_{in}/T^2 value of 18.4, an average of the values shown in Fig. 3. There is barely discernible improvement in agreement with the experimental values. The deviation of the two lowest groups at higher energies is well beyond experimental error and may be due to direct interactions.

A second set of calculations were done for us by E. D. Arthur using GNASH [7]. The results for Nb are depicted in Fig. 8a, those for Ta in 8b. Here, the level density was from the Gilbert and Cameron constant temperature model. The experimental Nb cross sections may again evince direct reaction to some extend, whereas these contributions seem to be minimal for Ta. Once again, the calculations do quite well.

VI. DATA FILES

Two types of files have been prepared for the participants, together with a README documentation file. The latter contains an explanation of the files and the

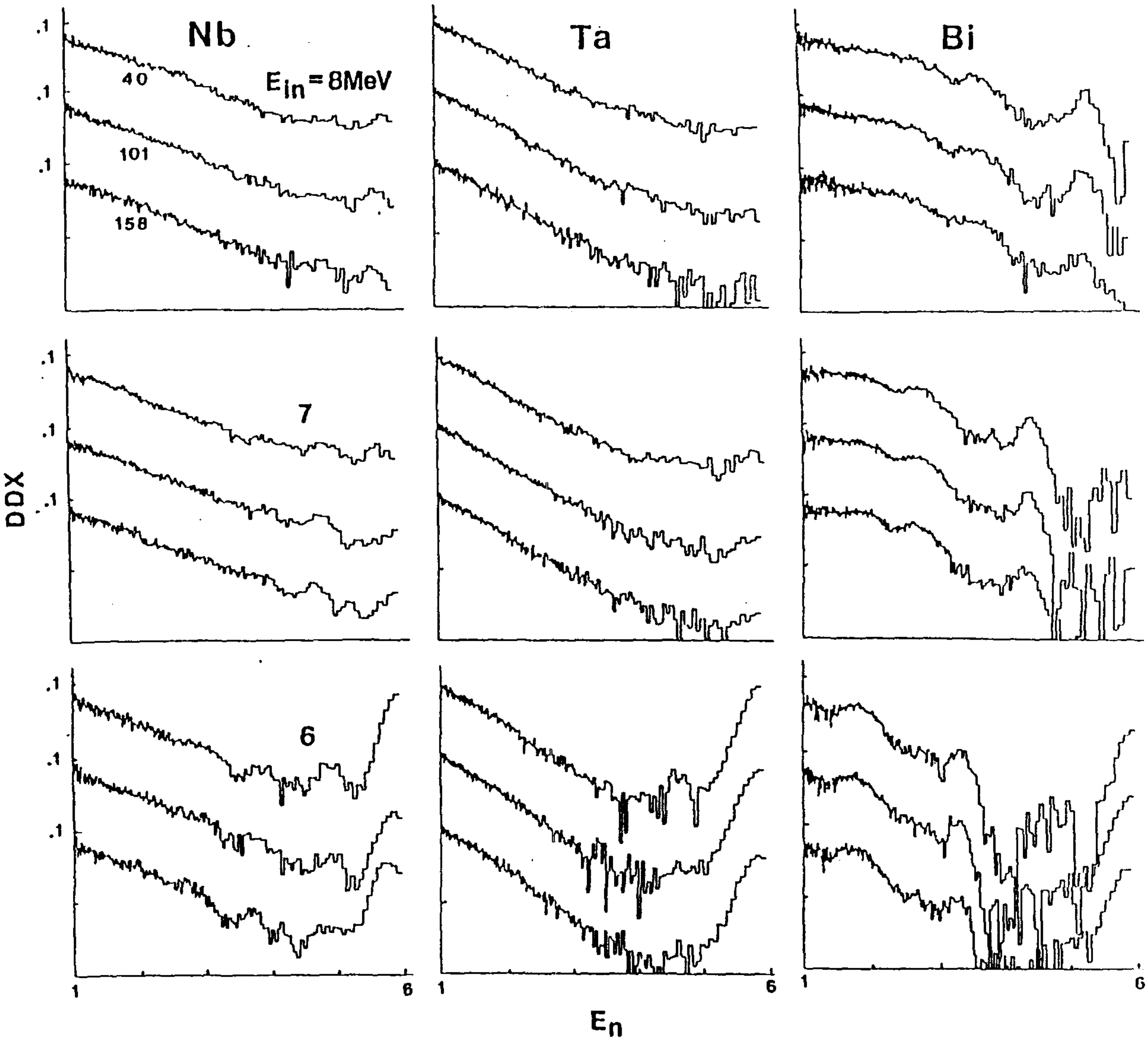

Fig. 4. Continuum emission spectra for Nb, Ta, and Bi at several energies. The vertical axis is in b/MeV. Horizontal axis is in emission neutron energy (MeV)E. The nuclei display varying amounts of "structure". These features were used to establish sum limits for the double–differential entries in the files.

preliminary information on the error analysis. The files do not yet contain data on Rh and Au, as these require further work. Thus, an updated file will be distributed in early 1990.

The files are on 2S/2D 5–1/4" floppy disks and are readable in the IBM/MSDOS environment. The README file is accessible by typing README. It has been reproduced in Fig. 9.

VII. ERROR ANALYSIS

It is intended to include in the updated data file errors, sensitivities, and correlations sufficient to construct a correlation matrix. This approach has been favored by many evaluators, as it better controls the evolution of a given correlation matrix.

Some primary sources of error are summarized below to temporarily assist the data user in assigning rational weights to these quantities in fitting procedures. These error estimates are thought to be conservative. Additional less quantifiable uncertainties connected with experimental performance are discussed in the appendix.

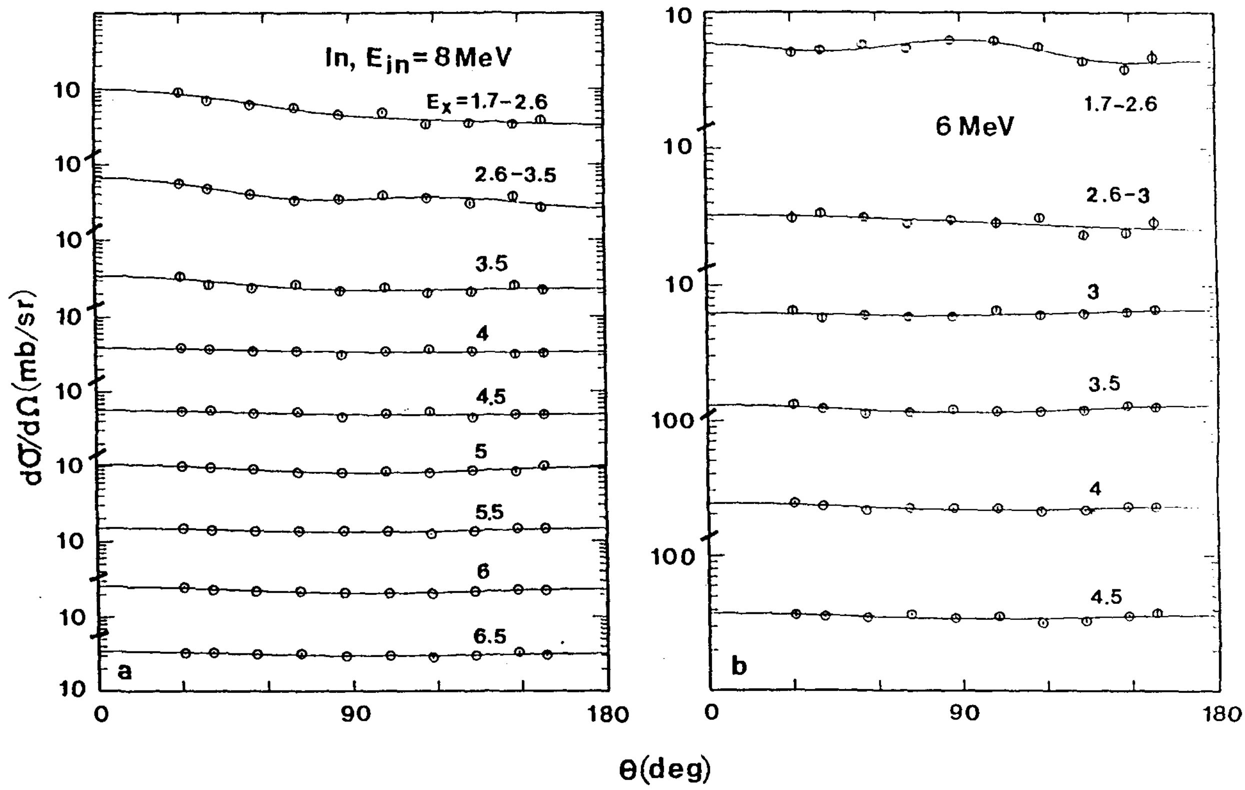

Fig. 5. Complete inelastic angular distributions for In at 8 MeV (a) and 6 MeV (b) incident–neutron energy. The cross sections and angles are in the center of mass coordinates.

A. <u>Energy–Scale Related Uncertainties</u>

i) Accelerator energy calibration was checked with the Q–value of the first–excited state in C–12. The incident energies given in the files account for this. There is less than 1% uncertainty in the incident neutron energy.

ii) Time jitter: For the on–line measurements this is conservatively estimated at $\lesssim 1$ channel (1 nsec). This affects the energy scale most acutely at the bombarding energy and diminishes towards higher excitation energies. The range of uncertainties is 10–50 keV. For the ^{252}Cf spectra, the jitter is somewhat larger ($\lesssim 2$ nsec), and influences ratios and/or efficiencies. The energy dependence for this uncertainty is, of course, similar to the one above. This uncertainty, in the case of elastic scattering at 8 MeV translates into $\approx$ 5% at worst, and into less than the statistical scatter for emission–neutron energies of 4 MeV or less.

iii) Time scale: The time per channel is determined with calibrated delay lines. It has been very stable over the year ($\lesssim$ 0.1%), but may be subject to a systematic error of perhaps 1%.

iv) Flight paths: These are known to 0.1%.

v) Energy resolution: 0.4 to 0.65 keV FWHM. Broad resolution performance was sought.

B. <u>Angular uncertainty $\approx$ 1 degree</u>

There is evidence in comparing the present elastic cross sections with more detailed elastic angular distribution data that there may be a bias of $\approx$ 1 degree towards

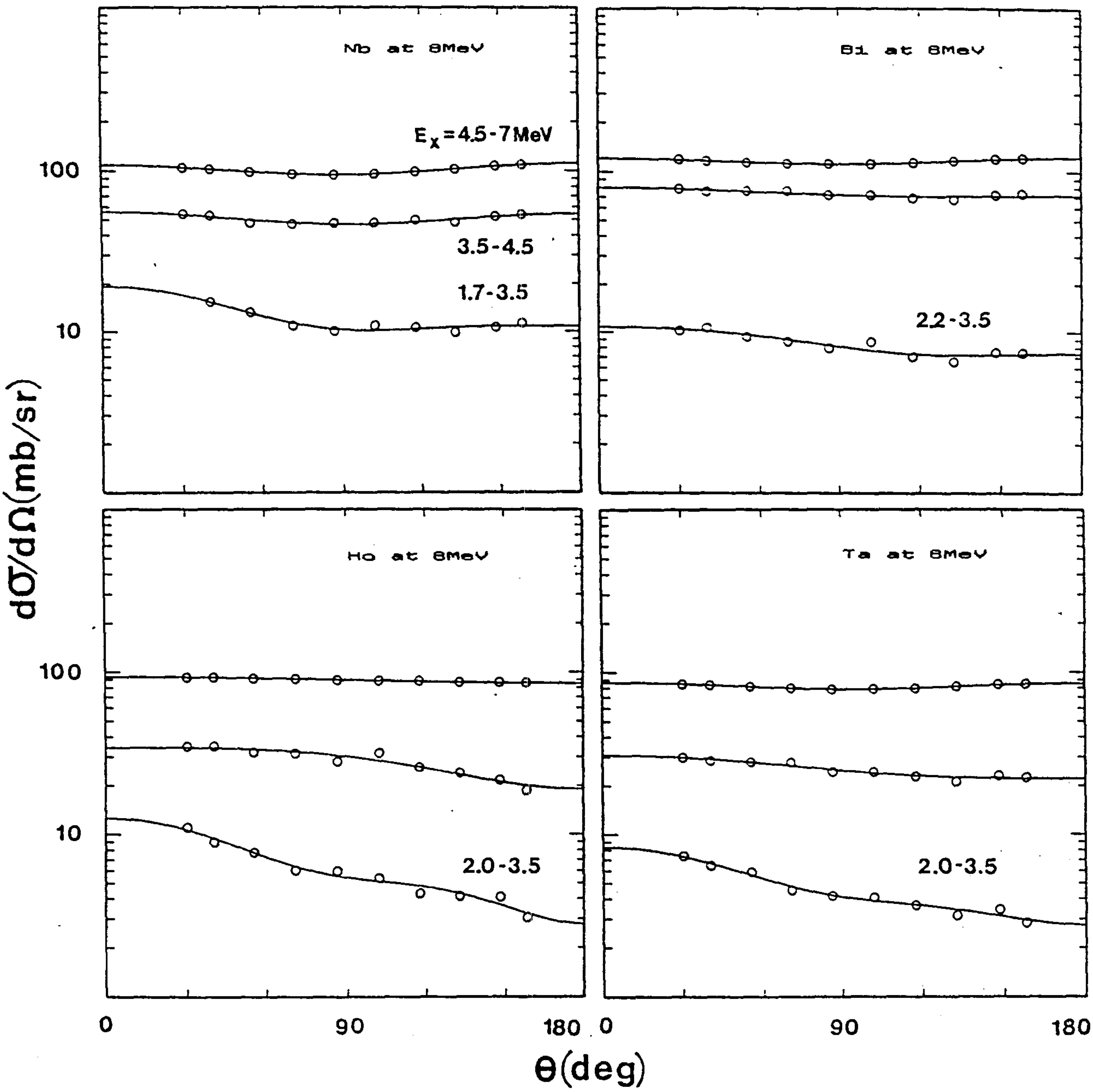

Fig. 6. Schematic indication of the interplay of direct, preequilibrium, and equilibrium contributions to neutron emission spectra. Redundant excitation energies are omitted. Center of mass coordinates.

smaller values. As this is not critical to the accuracy of mildly anisotropic distributions, this deviation has been ignored primarily because the data required for a precise determination of the shift were not available.

C. Normalization of Spectra

A consequence of the ratio method is that the energy dependence of the detector efficiency is folded into the ratio ab initio. To obtain cross sections, a reasonably accurate representation of the Cf spectrum is required. Fröhner [8] has recently fit all available Cf spectrum data in order to demonstrate the superiority of the Watt spectrum representation. The difference between his Watt spectrum and a Maxwellian with T = 1.42 was very small in the equilibrium portion of the

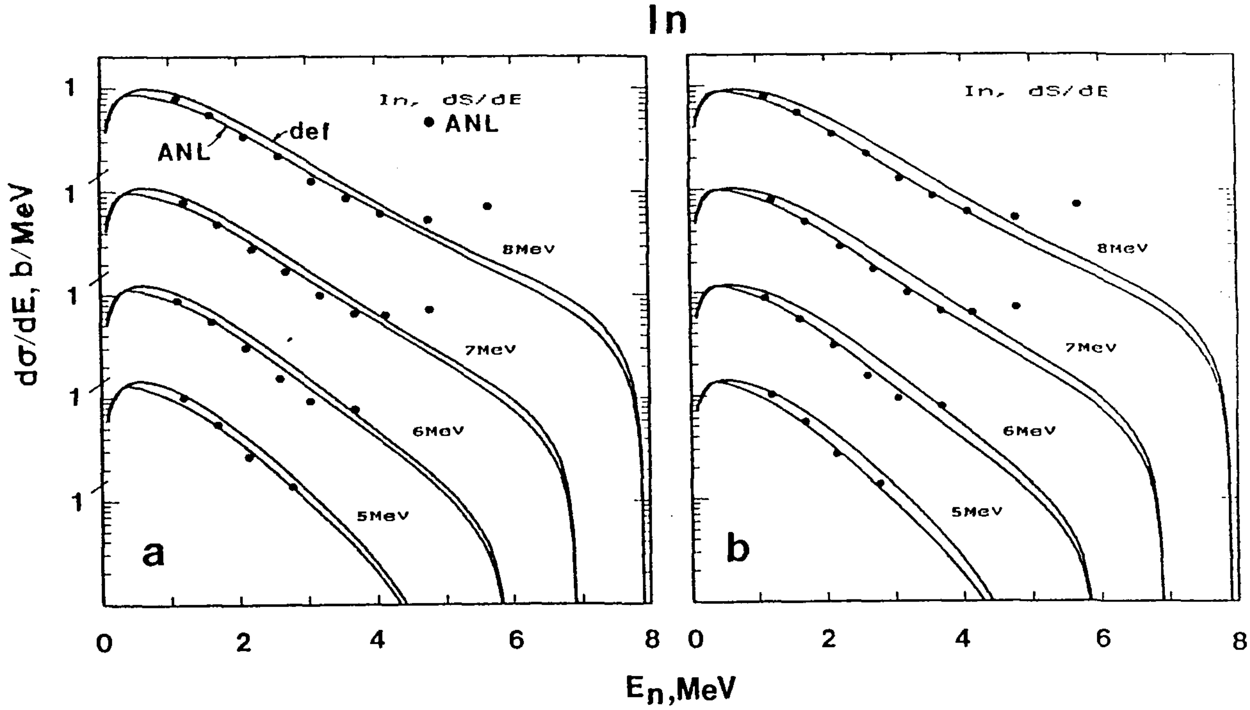

Fig. 7. Comparison of ALICE calculations with present cross sections. In both figures, the upper curves result from the default optical potential, while the lower curve obtains when an elastic–scattering data specific potential is used. The latter was recently deduced in our group. Fig. 7a pertains to the Gilbert and Cameron a value, while Fig. 7b uses the average E_{in}/T^2 value of Fig. 3. The differences are very slight.

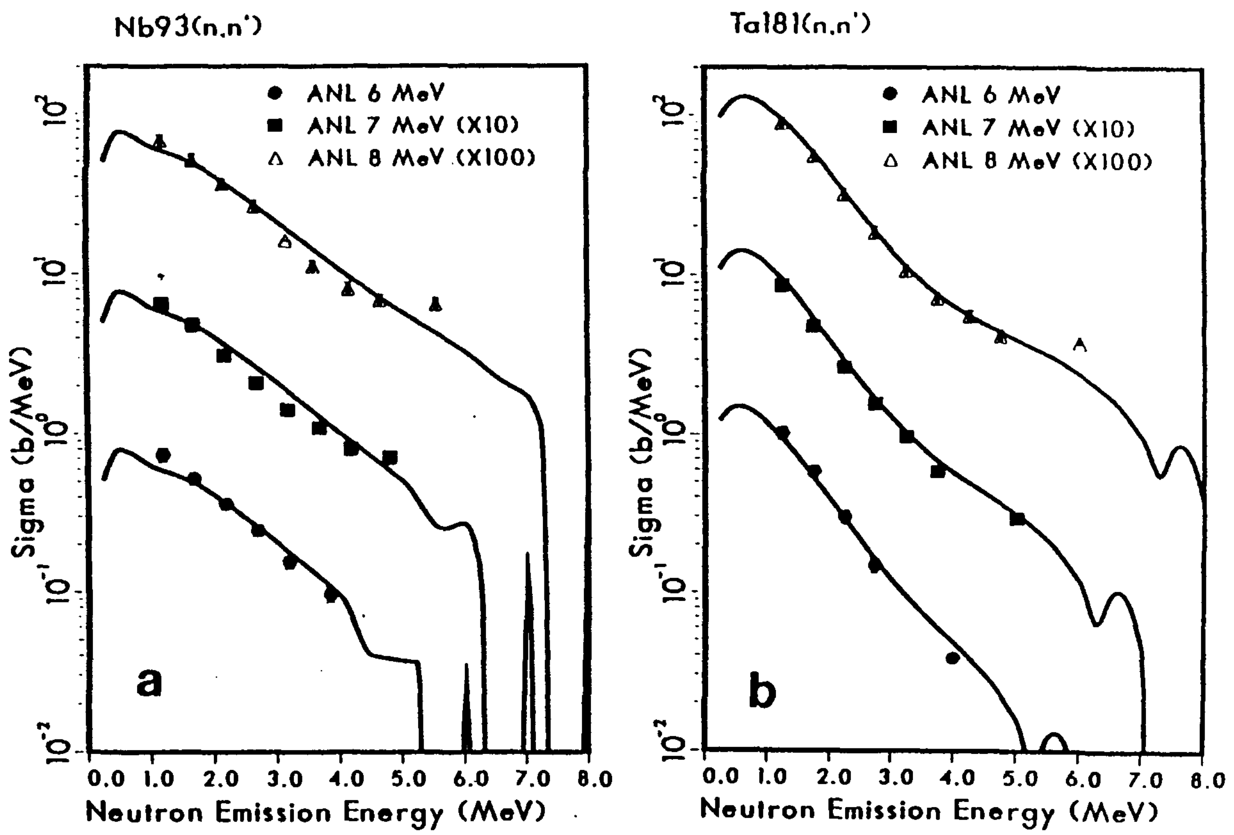

Fig. 8. Comparison of GNASH calculations with present cross sections. For Nb (Fig. 8a), a region OM potential was used. For Ta (Fig. 8b) an OM potential for W was employed. Both calculations demonstrate the consistency with the Gilbert and Cameron constant temperature model.

```
     There are two kinds of data sets in this disk.  One is called *EL.DAT,
the other *EL.INT.  The *EL.DAT contains the angular distribution data,
while *EL.INT contains angle-integrated energy differential data.
(Note:* stands for the element symbol, e.g. NBEL.DAT)

1) *EL.DAT

     This set of data contains angular distribution of inelastic groups
in the center-of-mass system.

     The format of this data set is,

ID, ITOPE, E, dE, Q1, Q2, NA,NF                        FORMAT(1X,A2,I3,4F6.3,2I6)
(XX(1,i),XX(2,i),XX(3,i),i=1,NA)                            FORMAT(1P6E10.3)
(W(j),j=1,NF)                                          FORMAT(1P7E10.3)
COMMENT                                                FORMAT(A60)

where
 ID(A2)      denotes the chemical symbol of the target,
 ITOPE(i3) the atomic number of id, 0 for a natural element,
 E(F6.3)     the incident neutron energy in MeV,
 dE(F6.3)    indicates the energy spread of the incident neutron beam, in
             Half Width at Half Maximum ( = 0.5 * FWHM ),
 Q1(F6.3)    the upper Q-value (MeV) of this inelastic scattering group,
 Q2(F6.3)    the lower Q-value (MeV) of this inelastic scattering group,
 NA(I6)      number of data points in this group,
 NF(I6)      number of Legendre coefficients,
 XX(1,i)     Center-of-mass angle in degree,
 XX(2,i)     Center-of-mass cross section in barn/sr,
 XX(3,i)     error of the cross section in %,
 W(j)        Legendre coefficients, W's.  The cross section is expanded as,
             CS = W(1)/(4pai)x[1 + W(2)P(1)+W(3)P(2) + ... + W(NF)P(NF-1)].
 COMMENT     is a comment.

      An example of the data contained in NBEL.DAT looks like this:

 NB  0 5.000 0.270-1.700-2.500     10     4                              NB500170
 1.583E+02 1.327E-02 4.686E+00 1.484E+02 1.244E-02 4.190E+00             NB500170
 1.331E+02 1.166E-02 3.260E+00 1.177E+02 1.224E-02 3.986E+00             NB500170
 1.023E+02 1.263E-02 3.276E+00 8.681E+01 1.212E-02 3.423E+00             NB500170
 7.127E+01 1.172E-02 3.267E+00 5.567E+01 1.081E-02 3.339E+00             NB500170
 4.052E+01 1.162E-02 3.982E+00 3.041E+01 1.325E-02 3.966E+00             NB500170
 1.522E-01-2.482E-02 6.149E-02 5.205E-02 0.000E+00 0.000E+00 0.000E+00NB500170
   PTG data in CMS.  Date : 11/ 8/1989, Time : 13:56:51                  NB500170

2)*EL.INT

      An example (INEL.INT) of the data in this set is as follows:

  Summary of angle-integrated cross sections

 Element : IN, Energy :  5.000, Q-format :PTG, Date : 11/ 9/1989, Time : 16:29:55

    En(CMS)  X-sect.      Error     Qupper     Qlower
     [MeV]   [b/MeV]       (%)      [MeV]      [MeV]
     2.783 1.371E-01     5.000     -1.700     -2.600
     2.138 2.675E-01     5.000     -2.600     -3.000
     1.692 5.476E-01     5.000     -3.000     -3.500
     1.196 1.012E+00     5.000     -3.500     -4.000

 Element : IN, Energy :  5.500, Q-format :PTG, Date : 11/ 9/1989, Time : 16:29:55

    En(CMS)  X-sect.      Error     Qupper     Qlower
     [MeV]   [b/MeV]       (%)      [MeV]      [MeV]
     3.274 9.600E-02     5.000     -1.700     -2.600
     2.630 1.485E-01     5.000     -2.600     -3.000
     2.184 2.918E-01     5.000     -3.000     -3.500
     1.688 5.764E-01     5.000     -3.500     -4.000
     1.192 9.768E-01     5.000     -4.000     -4.500

      The format here is selfexplanatory.
      The error, 5%, is temporary but typical for these quantities.
```

Fig. 9. A listing of the README.DOC file provided with the data files. It explains the relevant formats and conventions.

spectrum. Hence, for the sake of the slope analysis mentioned above, the simpler Maxwellian form was retained.

Normalization: The primary concerns of this procedure have already been expressed in Sec. III. Some of the uncertainties are difficult to quantify. But for most samples and energies, we were able to reproduce the listed neutron total cross sections to 3–5%. By adding inelastic and inelastic portions of the spectrum. We estimate an overall uncertainty of 7%.

D. <u>Summary of Errors</u>

1. Incident energy uncertainty $\lesssim 1\%$.

2. Energy resolution 0.4 (at 5 MeV) to 6.5 (at 8 MeV).

3. Error in relative energy–dependence of detector calibration $\lesssim 1\%$ from emitted neutron energies of 1–3 MeV, increasing to $\lesssim 5\%$ at 8 MeV.

4. Normalization relative to ENDF/B–V Nb file $\lesssim 5\%$.

5. Miscellaneous:

Multiple event corrections	1–2%.
Sample density	< 1%
Attenuation correction	$\lesssim$ 1%
Q–value bin partitions	≈ 20 keV

REFERENCES

1. P.T. Guenther and A.B. Smith, Proc. International Conference on Nuclear Data for Basic and Applied Science, Santa Fe, NM, Vol. 1, p. 955, (1985.

2. W. Mannhart, "Status of the ^{252}Cf Spectrum as a Standard...Reactor Dosimetry," H. Farrar IV and E.L. Lippincott, eds., ASTM Philadelphia, USA (1989).

3. A. Smith et al., Argonne National Laboratory Report ANL–NDM 21 (1976).

4. Evaluated Nuclear Data File –B Version V (ENDF/B–V), National Neutron Cross Section Center, Brookhaven Natl. Lab. See also A.B. Smith et al., Argonne National Laboratory Report ANL/NDM–105 (1988).

5. M. Blann, Livermore Natl. Lab. Report UCID–20169 (1984).

6. A. Gilbert and A. Cameron, Can. Journal of Physics <u>43</u>, 1446 (1965).

7. P. Young and E. Arthur, "GNASH: A Preequilibrium Statistical Nuclear Model Code," Los Alamos Natl. Lab. Report LA–6747 (1977).

8. F. Fröhner, private communication, 1988.

APPENDIX

Snout Scattering

No particular modifications were attempted to optimize an experimental apparatus that had heretofore been used to determine elastic and discrete inelastic angle–differential cross sections. The important point here is that the shielding could have been more favorably enhanced for this experiment, but at the sacrifice of several detector positions. This option was waived. As a consequence, a substantial background peak must be subtracted in the forward quadrant. This peak arises due to source neutrons striking the front end of the collimators ("snout"). Its position in the spectrum depends on angle. Variations in the pulsed beam profile can therefore result in slight over– or under–subtractions leading to small distortions in the low E_x portions of the spectrum. In the data sets, this will manifest itself as an occasional trade—off of cross section magnitude in neighboring groups, particularly between 90 and 50 degrees.

Glitches

Continuum–neutron measurements are susceptible to unwanted (and often undetected, if they have no recognizable structure) neutron source contaminants (glitches). Sharp peaks in the 30° and 40° detector spectra were identified and were believed to be associated with the $^{14}N(d,n)^{15}N$ stripping reaction. Corrections were made for the two forward detectors for these contaminants which occurred in the groups -6 MeV $< Q < -5$ MeV. No other significant contaminants could be identified. Nevertheless, they may have contributed to the cross section of a given group. It is difficult to estimate these contributions, but they are believed to be no more than 2% and certainly not in all groups.

EXTRACTION OF LEVEL DENSITY FROM EXCITATION FUNCTIONS OF THRESHOLD REACTIONS

O.T. Grudzevich, A.V. Ignatyuk, V.I.Plyaskin, A.V.Zelenetsky
Physics and Power Engineering Institute, Obninsk, USSR.

The method of extraction of level density from excitation functions of threshold reaction is discussed. It is demonstrated that the data obtained are in good agreement both with the results of the evaporation spectra analysis and with systematics of neutron resonance density and resolved levels.

The density of excited levels is one of the most important characteristics in the statistical theory of nuclear reactions. For calculations of the level densities are broadly used the phenomenological models with parameters derived from analysis of i)the neutron resonance densities and ii) the cumulative number of discrete levels . In spite of model improvements [1-3] the problem of testing the energy dependence of the level density is actual. It is important to use the evaporation spectra and excitation functions of the threshold reactions for this purpose.

An efficient method of extraction of the level density from the evaporation spectra was proposed by H. Vonach [4]. The analysis of threshold reaction excitation functions presents supplementarypotential possibilities for examination of the level density. In this paper it is shown that the results of such analysis are in good agreement with both the modern theoretical description of the level density and with the description of evaporation spectra of different particles.

1. Use of statistical model formulas for extraction of level density.

In the framework of the statistical theory of nuclear reactions the differential cross-sections can be written as :

$$\frac{d\sigma_{a,b}(\varepsilon_b)}{d\varepsilon_b}\, d\varepsilon_b = \pi\lambda_a^2 \sum_{ljJ^\pi} g_J \frac{T^{J^\pi}_{alj}(\varepsilon_a) \sum_{l'j'} T^{J^\pi}_{bl'j'}(\varepsilon_b)}{N(E,J^\pi)} \rho_b(U,J)\, d\varepsilon_b \qquad (1)$$

$$N(E,J^\pi) = \sum_{\nu} \sum_{J'} \int_0^{E+B_\nu} d\varepsilon_\nu\, T_{\nu lj} \rho_\nu(E-B_\nu-\varepsilon_\nu, J)$$

where $\varepsilon_a, \varepsilon_b$ are the energes of particles a and b; E is the excitation energy and J is the total spin of compound nucleus; $T_{\nu lj}(\varepsilon_\nu)$ are the transmission coefficients; $\rho_\nu(U,J)$ is the level density of residual nucleus. The whole energy region of compound and residual nuclei can be divided into the discrete part with known scheme of levels and the continuum one where the statistical description in terms of level densites is used.

If transmission coefficients are fixed the energy dependence of particle spectra are defined by the level density . Hence, the absolute value of level density would be extracted from comparison of experimental data with calculated one as

$$\rho_b^{exp}(U) = \rho_b^{calc}(U) \left[\frac{\left(\frac{d\sigma_{a\cdot b}}{d\varepsilon_b}\right)_{exp}}{\left(\frac{d\sigma_{a\cdot b}}{d\varepsilon_b}\right)_{calc}} \right]_{\varepsilon=U_{max}-U} \qquad (2)$$

where $\sigma_{a,b}$ is the cross section of analized reaction, U_{max} is the maximal excitation energy of residual nucleus. The level density obtained does not depend practicaly upon the initial values of $\rho_b^{calc}(U)$, if the description of experimental spectra is rather satisfactory [4].

It should be emphasized that in the analysis of neutron spectra the expression (2) must be used carefully because the extracted value of level density is included also in the denominator of Exp.(1) which define the absolute cross section value. However, in the case of the charged particle spectra (when $N(E,J^\pi)$ are defined mainly by neutron channel) the problem is simplified and the extracted level density depends only on the accuracy of integrated values of neutron cross sections. It is shown in[4] that the hardpart of evaporation spectra in the resolved levels area canbe used for the normalization of the integral probability of compound nucleus decay. Naturally we must be sure that analized spectra are not disturbed by any nonstatistical processes. Apparently the spectra of (p,n), (α,n), (α,p), (n,α) and (n,p) reactions with the projectile energes up to 15 MeV satisfies this requirement in the most extent. This paper is devoted to the analysis of the spectra and excitation functions of these reactions.

The cross section of (a,b) reaction is an integral of differential spectrum (1) in the energy range from 0 to $E_{max}=E_a+Q_{a,b}$, where $Q_{a,b}$ is the reaction energy. In the discrete level area the integration must be substituted by the corresponded summs. Thus cross section can be divided into two parts: the contribution of discrete levels σ_{dis} and the contribution of continuum σ_{cont}. For the fixed transmission coefficients the extraction of level density can be performed into two steps:

i) at the low projectile energies when only discrete levels of residual nucleus are excited the normalization of the denominator of Exp.(1) must be executed as in the case of evaporation spectra [4]. This normalization is connected as a rule with the determination of neutron channel level density at the excitation energy that correspond to the most probable energy of emitted neutrons.

ii) as the projectile energy increases the contribution of the continuum part σ_{cont} is increases too. When this contribution becomes dominant the corresponded level density can be obtained from the comparison of the experimental cross section $\sigma^{exp}(E_a)$ with calculated one:

$$\rho_b^{exp}(U)=\rho_b^{calc}(U)\frac{\sigma^{exp}(E_a) - \sigma^{dis}}{\sigma^{calc}(E_a) - \sigma^{dis}}, \qquad (3)$$

where U is the excitation energy of residual nucleus corresponding to the most probable energy of emitted particle.

With the help of Exp.(3) the energy dependence of level density can be extracted in the region starting from the resolved discrete levels up to the energy where the contribution of the non-compound prosseses in the investigated cross sections will be sufficiently small.

The extraction of level density within described method has great advantage in comparison with usual fitting of the level density parameters in the description of experimental spectra because we can distinguish the situations when the description of spectra must be performed by changing of another components of statistical theory (f.e. the transmission coefficients) rather than correction of the level density [5].

2. Analysis of spectra and excitation functions of (n,p) reactions.

Today great amount of experimental information on excitation functions is accumulated in energy region where statistical processes are predominant . It is interesting to analyse the cases when both the excitation functions and the particle spectra for the same residual nucleus are available.

We will use the proposed method to analyse the level density of ^{56}Mn. The excitation function of ^{56}Fe(n,p) reaction is selected for extraction of level density of ^{56}Mn because i) the consistent experimental data are available near threshold of reaction; ii)the neutron channel dominates the compound nucleus decay. Hence for the energies near threshold when only discrete levels of ^{56}Mn are excited it is possible to normalize denominator of Exp. (1) by changing the level density of ^{56}Fe. Then it is possible to derive the level density of ^{56}Mn from excitation function at the greater energies .

All the data on level density of ^{56}Mn are given in fig.1a. Satisfactory coincidence of different data demonstrates the efficiency of proposed method. Analogous data for level density of ^{54}Mn are given too. One can see that different experimental data are consistet. It should be noted that some difficulties in extracting the data exists in this case. This difficulties are connected with the fact that denominator normalization in (1) for the ^{54}Fe(n,p) cannot be performed correctly as in ^{56}Fe(n,p) case because neutron channel of ^{55}Fe decay is not dominant.

The results of similar analysis for the nuclei ^{58}Co and ^{60}Co are given in fig. 2.

Description of energy dependence of level density of all the discussed nuclei in the frame of generalized superfluid nuclear model with the parameters obtained from systematics of the number of discrete level and neutron resonance density [3] also are given in fig. 1 and 2. This theoretical description is in good

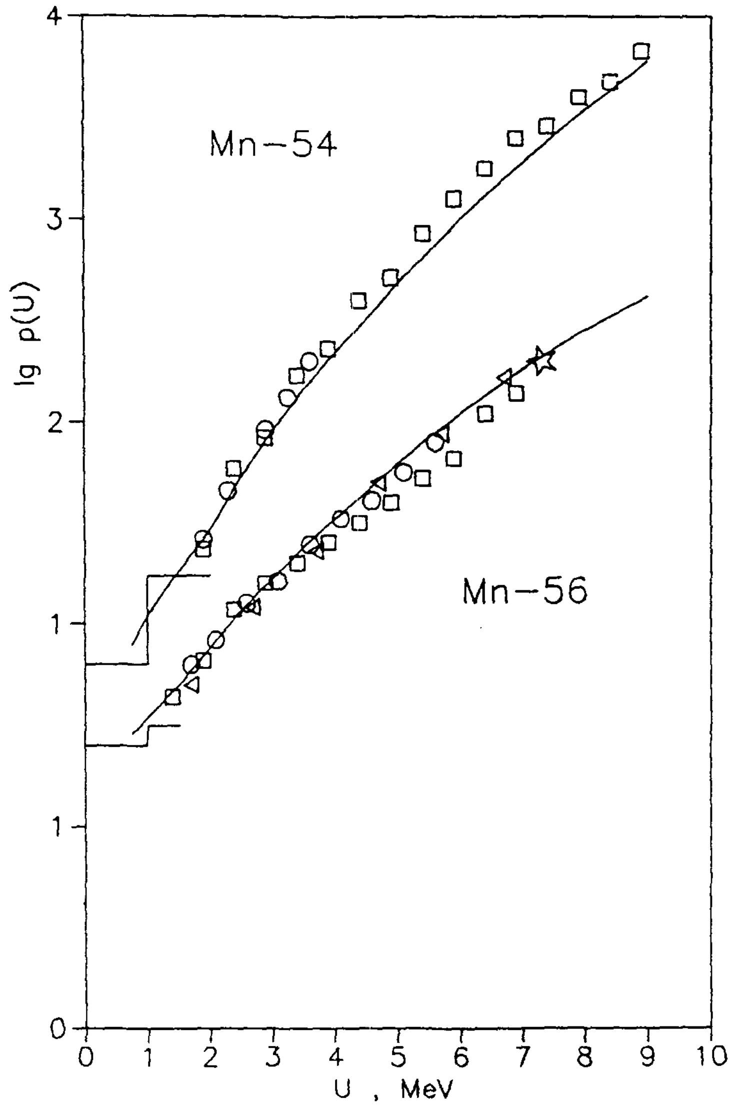

Fig. 1. Level density data for the nuclei ^{56}Mn and ^{54}Mn: □ - results of analysis of spectra of (n,p) reaction at E_n = 15 MeV [7]; Δ - analysis of spectra of (n,α) reaction at E_n = 14.1 MeV [8]; o - analysis of excitation function of ^{56}Fe(n,p) reaction; star is analysis of neutron resonance density; histogram is discrete level density [9]; solid line is calculation based on generalized superfluid nuclear model [3].

consistence with experimental data obtained from the analysis of evaporation spectra and excitation function of threshold reactions.

Summary

The possibility of extraction of the nuclear level densities from excitation function of threshold reactions is shown. Proposed method requires careful analysis of initial experimental data and

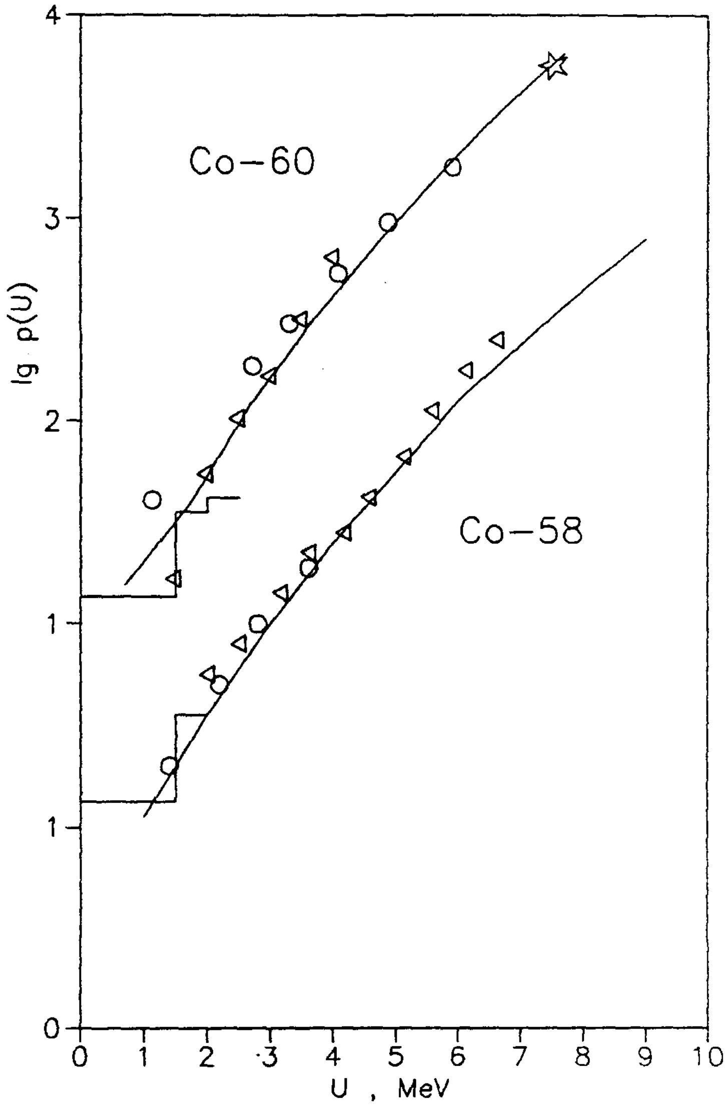

Fig.2. Level density data for ^{58}Co and ^{60}Co . The symbols are the same as in Fig.1.

performing proper statistical calculations of observed cross sections of nuclear reactions. For this reason such approaches are more complicated than thedirect description of neutron resonance density and discrete levels. However the complicated method gives more qualitative information which allows to make a new step in understanding of energy dependence of level density and its theoretical description.

References

1. Ignatyuk A.V. Statistical Property of Excited Atomic Nuclei. (in Russian) Moscow, Energoatomizdat, 1983.

2. Blokchin A.I. Ignatyuk A.V. Shubin Yu.N. Sov. J. Nucl. Phys. v.39, p.369, 1988.

3. Grudzevich O.T. et al., In.: Proc. Intern. Conf. on Nuclear Data for Science and Technology, Mito,Japan,1988.

4. Vonach H., Proc. IAEA Advisory Group Meeting on Basic and Applied Problems of Nuclear Level Densities, New York, 1983, p.247.

5. Bychkov V.M. et al, In: Proc. Int. Conf. "Nuclear Data for Science and Technology", Mito, 1988, p.1221.

6. Bychkov V.M. et al. Cross Sections of Neutron Induced Threshold Reactions, (in Russian) Moscow, Energoizdat, 1982.

7. Grimes S.M. et al. Phys. Rev. 1979, v.C19,p.2127.

8. Fischer R. et al Santa-Fe,1987, p.1651.

9. Lederer C.M., Shirly V.S. Tables of Isotopes, 7 edition, New York, 1978.

10. Graham S.L., Ahmad M., Grimes S.M. e.a. Nucl. Sci. Eng., 1987, v.95, p.60.

11. Grimes S.M. private communication.

NUCLEAR LEVEL DENSITIES FROM PARTICLE YIELDS AND SPECTRA IN PROTON INDUCED REACTIONS ON MOLYBDNUM ISOTOPES

S.K.Kataria, Kiran Kumar,V.S.Ramamurthy and M.Blann#
Nuclear Physics Division, B A R C, Bombay, INDIA
L L N L, Livermore,Ca U.S.A.

ABSTRACT

The inclusive energy and angular distribution of neutrons at 13.13 and 25.6 MeV and of protons and alphas at 18 MeV in several isotopes of Mo(p,x) have been reported recently where x is either a neutron or proton or an alpha particle. In the present work,we have used modified ALICE Code to calculate the energy spectra as well as integral yields of the various particles emitted. This modified ALICE code has a new option to use shell dependent nuclear level density formulla which smoothly goes over to Fermi Gas Model expressions at high excitation energies in a realistic manner. The calculated neutron energy spectra and yields donot depend significantly on the use of either Fermi Gas Model option or the shell dependent option. The calculated yields and the energy spectra of protons and alpha particles does depend on the level density option being used.

INTRODUCTION

Statistical model and pre-equilibrium model codes for the decay of highly excited nuclei are being extensively used in the theoritical calculations of various nuclear reaction yields and the spectra of the outgoing particles. One of the major sources of inaccuracy in these calculations is our lack of reliable and complete information on the nuclear level densities. The main experimental source on the absolute nuclear level density is confined to a narrow band of nuclei around the beta stability line, and almost at one excitation energy equal to neutron binding energy, and low values of spin. Whereas the calculations of the decay widths, energy and angular distribution of the particles involves the knowledge of the nuclear level density of daughter nuclei, after the emission of the particles in a wide range of excitation energy . Such information is not directly available from the experiments ,therefore, one has to rely on the semi-empirical extrapolation into all excitation energy ranges as well as for unknown and unstable nuclei. A number of semi-empirical nuclear level density formullae have been proposed in the literature which take into account shell structure effects and pairing corrections in a realistic manner[1,2,3].

In the present work, the modified ALICE computer code which incorporates the shell dependent nuclear level density due to Kataria Ramamurthy Kapoor (KRK) [1] has been used to calculate the inclusive enrgy spectra and absolute yields of neutrons, protons and alpha particles from various isotopes of Molybdnum (92, 94, 95, 96, 97, 98, 100) in the proton induced reactions at 13.13, 18 and 25.6 MeV proton energies. In the accompanying contribution, the details of the modification of the ALICE computer code are described. To use this optionin ALICE code, only a single entry LDOPT=1 is needed for shell dependent nuclear level density and LDOPT=0 for the use of Fermi gas model nuclear level density.

The predictions of the reaction rates and the spectra on the basis of the statistical model codes depend in a sensitive manner not only on the nuclear level density of the daughter nucleus in a given channel (p,xn), but also on all the other competing channels such as (p,p') and (p,α) over a wide energy range. Therefore it is of interest to compare the predictions of statistical model code ALICE with both the options LDOPT=0 & 1. For the Fermi gas model option, the value of the level density parameter a was taken as $\underline{a}$ = A/9 , whereas for LDOPT=1, the level density parameter was calculated as given in the modified ALICE Code.

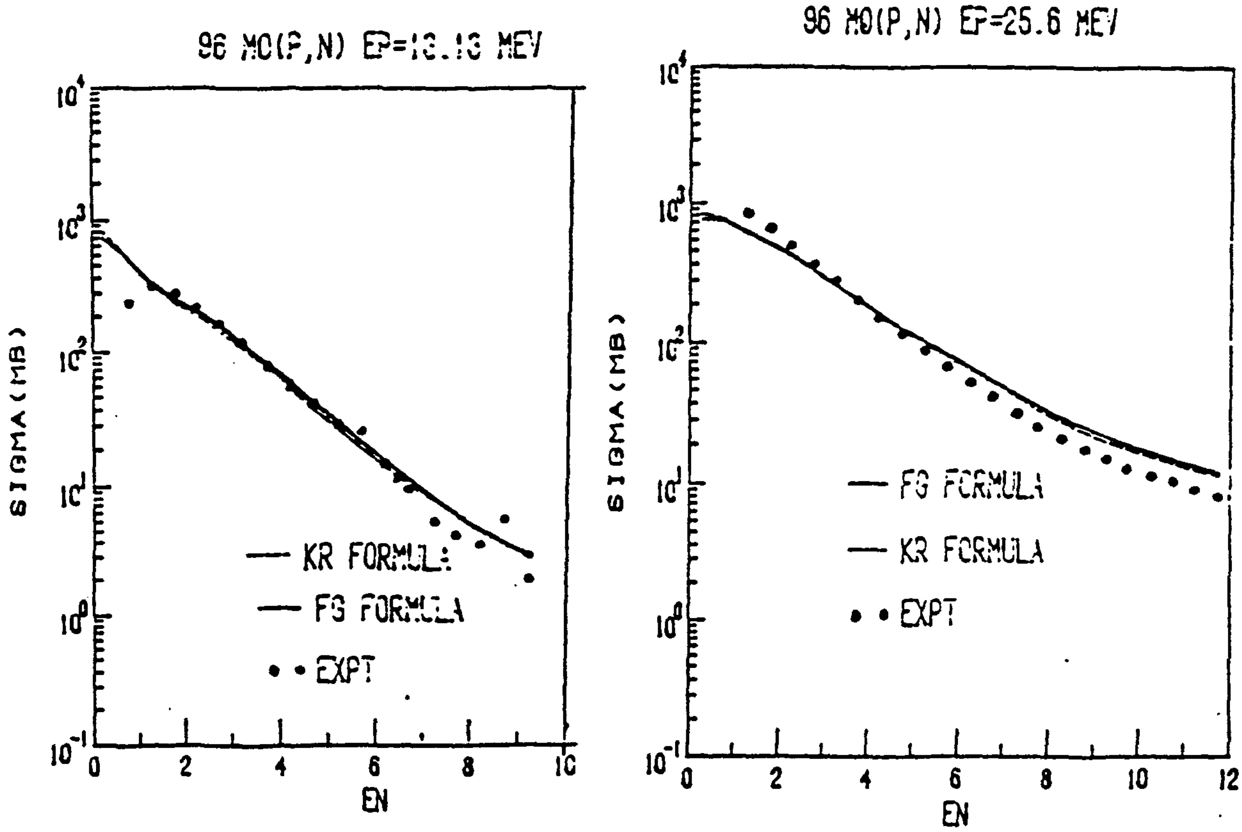

1. The energy spectra of neutrons from ^{96}Mo(p,xn) at 13.13 MeV and 25.6 MeV for LDOPT=1 (- - -) and LDOPT=0 (———) options compared with experiment (•••••••)

RESULTS

Fig. 1 shows typical calculated neutron energy spectra for ^{96}Mo(p,xn) at 13.13 and 25.6 MeV energy, where tha spectral shape and their yields are found to be similiar for both the options LDOPT=0 & 1 for nuclear level density . The calculated neutron energy spectra for all the Mo isotopes in (p,xn) reactions at 13.13 MeV are in good agreement with the experimental angle integrated energy spectra in centre of mass system. Whereas the calculated neutron energy spectra at 25.6 MeV beam energy for all the isotopes of Mo isotopes show significantly lower slopes as compared to the experimental measurements. The calculated total integral neutron yields differ from the experimental values upto a maximum of about 20 percent only. One of the possible ways to attribute this difference in slope is to introduce an energy dependent level density parameter $\underline{a}$. However, at present we have only carried out a simplified least squares fits to the slopes of

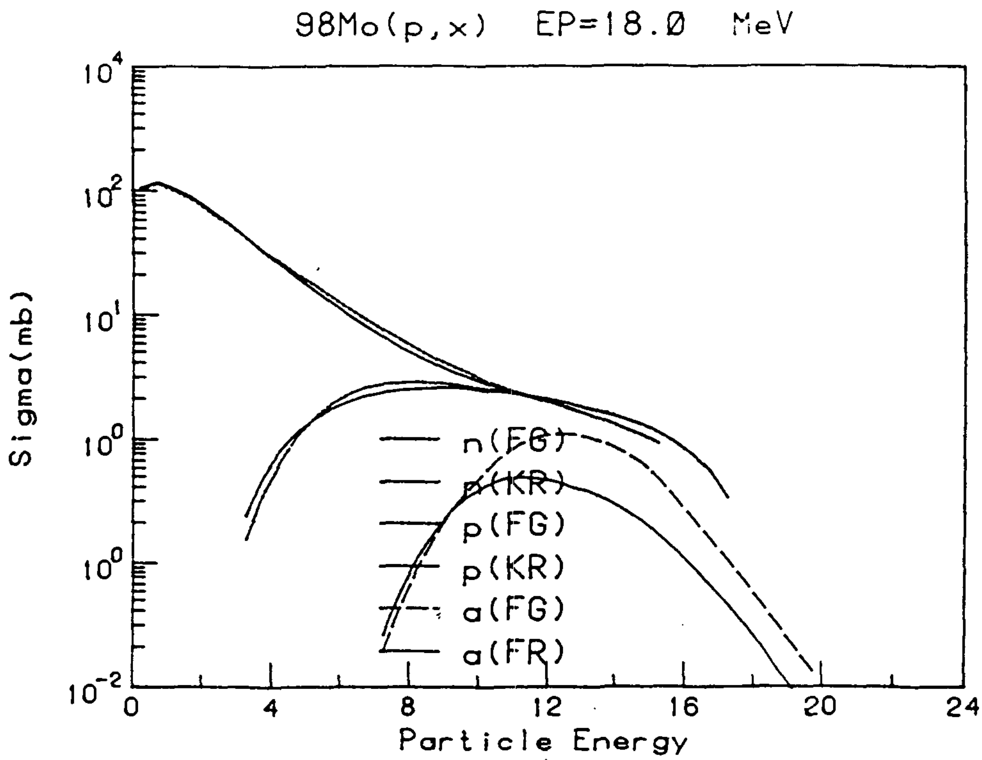

2 The calculated neutron, proton and alpha particle spectra from ^{98}Mo(p,x) reactions at 18.0 MeV for LDOPT = 1 (———) and LDOPT = 0 (- - - - - for neutrons, — — — — for protons — — — — for alpha particles)

the calculated neutron energy spectra by varying the level density parameter α from 1/5 to 1/25 (a $= \alpha A$) in an energy independent way. The best fits to the data were obtained for α = 1/7 at 25.6 MeV and for α = 1/9 at 13.13 MeV for all the Mo isotopes. From these one can conclude that the semi-empirical nuclear level densities derived from thermal neutron resonance spacings are reasonably accurate for use at low excitation energy . Whereas at higher excitation energy produced with 25.6 MeV incident protons, one may have to use an effectively larger value of level density parameter a.

Fig.2 shows the calculated energy spectra for neutrons, protons and alpha particles for the ^{98}Mo(p,xn) at 18.0 MeV proton energy using the two options LDOPT=0 & 1 . The calculated integral proton and alpha spectra and absolute yields are significantly different under the two options; the deviations being larger for alpha particles. the magnitude of deviations between the two options depend sensitively on the particular Mo isotope and thereby implying the influence of shell structure effects and pairing correlation effects on the charged particle emission as given in table 1.

Further, the calculated integral energy spectra of protons and alpha particles at 18 MeV donot show any systematic dependence on the level density parameter a as these are rather governed by the relative emission probabilities from different contributing channels. In other words, from the slope of the integral energy spectra of charged particles one cannot deduce the relevant level density parameter, whereas the charged particles decay widths are sensitively dependent on the level density parameter a .

Table 1

cross-section in millibarns	KRK neutron	KRK proton	KRK alphas	FGM neutron	FGM proton	FGM alphas
^{92}Mo	798	956	28.1	474	1310	8.38
^{94}Mo	1750	251	34.0	1650	250	86.6
^{95}Mo	1740	279	92.3	1810	235	73.9
^{96}Mo	2010	94.0	16.4	1960	104	34.1
^{97}Mo	1980	136.0	43.4	2030	110	25.2
^{98}Mo	2130	68.6	5.48	2110	73	13.2
^{100}Mo	2200	57.9	1.42	2190	61	5.05

Therefore, a simulataneous fit to all the three neutron, proton and alpha particles channels and also to their respective excitation functions will provide a unambiguous test of nuclear level densities in the region of Mo isotopes. Unfortunately, the experimental data are not available for charged particles yields at 13.13 and 25.6 MeV where exhaustive experimental integral neutron energy spectral measurements have been reported.[5,6].

At 18.0 MeV, the experimental data on charged particles emission have been reported[7,8], but no neutron measurements have been carried out. Using the shell dependent option LDOPT=1, the calculated proton and alpha energy spectra are in good agreement with experimental data for Mo (94, 95, 100) isotopes, whereas for other isotopes, the disagreement is large upto a factor of 2 for alpha particles and smaller for protons upto a factor of 1.2 only.

Work is in progress to analyse integral energy spectra for neutron, proton and alpha particles observed at different angles and also to include the shell dependent nuclear level density in other statistical model code which calculate the angular distributions of the emitted particles.

REFERENCES

1. Kataria S.K., Ramamurthy V.S., and Kapoor S.S. Phys. Rev. C18 (1978) 549.
2. Ignatyuk A.V., Smirenkin G.N. and Tishin A.S., Sov. J. Nucl. Phys. 21 (1975) 255.
3. Jensen A.S. and Sandberg J., Phys.Scripta. 17 (1978) 107.
4. Kataria.S.K., Ramamurthy V.S.,Blann M. and Komoto T.T. submitted to Nuclear Instruments and Methods
5. Scobel W.,Blann M., Komoto T.T., Trabandt M., Grimes S.M.,Hansen L.F., Wong C. and Pohl B.A. Phys.Rev. C30 (1984) 1480
6. Modhurst E., Trabandt M., Kaminsky A., Krause H., Scobel W., Bonetti R., Crespi F., Phys. Rev. C34 (1986) 103
7. Kumabe I., Mito Y., Hyakutake M., Koori N., Sakai H. and Watanbe Y., Phys.Rev. C35 (1987) 467.
8. Watanabe Y. Kumabe I., Hyakutake M., Koori N., Ogawa K., Orito K., Akagi K., Oda N. Phys. Rev. C36 (1987) 1325.

"CONTAMINATION" OF NEUTRON EVAPORATION SPECTRA BY DIRECT AND PRE-EQUILIBRIUM PROCESSES

H. Kalka, H. Märten, and D. Seeliger

Technische Universität Dresden, GDR

Abstract

Contributions of direct and pre-equilibrium processes to secondary-neutron spectra in (n,n') and (p,n) reactions are analysed in the framework of the SMD/SMC theory. Specifically, statistical multistep-compound reactions (SMC) based on the closed solution of the Pauli master equation are shown to be a superposition of equilibrium and pre-equlibrium contributions. Results are presented for the reactions ^{93}Nb(n,n') and ^{109}Ag(p,n).

1. Introduction

According to a new SMD/SMC approach[1,2] the secondary-neutron spectra in nucleon-induced reactions are understood as a superposition of different mechanisms:

<table>
<tr><td colspan="2">Statistical Multistep Compound
SMC</td><td colspan="3">Statistical Multistep Direct
SMD</td></tr>
<tr><td rowspan="2">equilibrium emission
$\sigma^{(eq)}$</td><td rowspan="2">pre-equilibrium emission
$\sigma^{(pre)}$</td><td colspan="2">single-step
$\sigma^{(1)}$</td><td rowspan="2">two-step etc.
$\sigma^{(2)}+\sigma^{(3)}+\ldots$
(exex)
(exvib)
(vibex)
(vibvib)
...</td></tr>
<tr><td>collective excitations (vibrations)
$\sigma^{(vib)}$</td><td>non-collective excitations (excitons)
$\sigma^{(ex)}$</td></tr>
<tr><td>EVAPORATION SPECTRUM</td><td colspan="4">"CONTAMINATION"</td></tr>
</table>

Hence, neutron evaporation spectra are contamined by different SMD contributions as well as a pre-equilibrium SMC part to be specified in this work. We consider nucleon-induced reactions $A(\alpha,\beta)B$ with ε (ε') as the energy of the incoming (outgoing) nucleon $\alpha(\beta)$; $\alpha,\beta = \nu$ or π(neutron or proton).

Differential cross sections are splitted into the SMD and SMC parts:

$$\frac{d\sigma_{\alpha\beta}}{d\varepsilon'}(\varepsilon) = \frac{d\sigma_{\alpha\beta}^{SMD}}{d\varepsilon'}(\varepsilon) + \frac{d\sigma_{\alpha\beta}^{SMC}}{d\varepsilon'}(\varepsilon) \qquad (1)$$

2. SMD processes

Within the SMD approach, the most important one-step processes, i.e. direct excitations of (non-collective) particle-hole states (excitons) and collective modes (vibrations) are superposed:

$$\frac{d\sigma_{\alpha\beta}^{(1)}}{d\varepsilon'}(\varepsilon) = \frac{d\sigma_{\alpha\beta}^{(ex)}}{d\varepsilon'}(\varepsilon) + \frac{d\sigma_{\alpha\beta}^{(vib)}}{d\varepsilon'}(\varepsilon) \qquad (2)$$

To avoid complicated DWBA calculations the following ansatzes for both contributions have been deduced[1,2]:

$$\frac{d\sigma_{\alpha\beta}^{(ex)}}{d\varepsilon'}(\varepsilon) = R_{\alpha\beta}\left(\frac{m V_N}{2\pi\hbar^2}\right)^2 \cdot 4\pi \cdot (2s+1) \cdot \overline{I^2} \cdot \left(\frac{g}{2}\right)^2 \cdot$$

$$\cdot \left(\varepsilon - \varepsilon' + B_\alpha - B_\beta\right) \cdot \left(\frac{\varepsilon'}{\varepsilon}\right)^{\frac{1}{2}} \cdot P_\alpha(\varepsilon) \cdot P_\beta(\varepsilon'), \qquad (3)$$

where $R_{\alpha\beta}$ - combinatorical factor,

m - neutron rest mass,

V_N - nucleus volume,

$B_{\alpha(\beta)}$ - separation energy of particle $\alpha(\beta)$

$P_{\alpha(\beta)}$ - penetration probability of particle $\alpha(\beta)$ (=1 for neutrons).

The single-particle state density g is assumed to be A/13. for non-magic nuclei. Based on the approximation of the total multistep contribution in relation to the optical model (OM) reaction cross section the average matrix element I^2 can be fairly described[2] by

$$\overline{I^2} = \overline{I^2}(\varepsilon) \approx 1800 \cdot A^{-3} \cdot \varepsilon^{-1} \tag{4}$$

for $\varepsilon \gtrsim 5$ MeV. The single-step cross section for the excitation of collective modes λ has the form

$$\frac{d\sigma_{\alpha\beta}^{(vib)}}{d\varepsilon'}(\varepsilon) = \left(\frac{m \cdot V_{surf}}{2\pi\hbar^2}\right)^2 \cdot \left(\frac{1}{2}\right)^2 \cdot \delta_{\alpha\beta} \cdot P_\alpha(\varepsilon) \cdot P_\beta(\varepsilon') \cdot \sum_\lambda \beta_\lambda^2 \cdot V_0^2 \cdot \delta(\varepsilon - \varepsilon' - \omega_\lambda) \cdot \left(\frac{\varepsilon'}{\varepsilon}\right)^{\frac{1}{2}}, \tag{5}$$

where $V_{surf} \approx 4 \cdot \pi \cdot aR^2$ - volume at the surface of the nucleus,
a - difuseness parameter,
R - nucleus radius,
β_λ - deformation parameter of mode λ,
ω_λ - energy of the collective excitation,
V_0 - real OM potential depth.

Higher-order SMD contributions are described as in the theory of Feshbach, Kerman, and Koonin[3]. They are less important in the cases studied in this work (see below).

3. SMC processes

The SMC model including the basic equation

$$\frac{d\sigma_{\alpha\beta}^{SMC}}{d\varepsilon'}(\varepsilon) = \sigma_\alpha^{SMC}(\varepsilon) \cdot \sum_{n=n_0}^{N} \frac{\tau_n}{\hbar} \cdot \left[\Gamma_{n\beta}^{(0)\uparrow}(\varepsilon') + \Gamma_{n\beta}^{(-)\uparrow}(\varepsilon')\right]$$
$$= \frac{d\sigma_{\alpha\beta}^{(pre)}}{d\varepsilon'}(\varepsilon) + \frac{d\sigma_{\alpha\beta}^{(eq)}}{d\varepsilon'}(\varepsilon) \tag{6}$$

represents a superposition of both pre-equilibrium and equilibrium emission in a unique description due to the solution of the Pauli master equation from time $T = 0$ to $T = \infty$:

$$\frac{dP_n}{dt} = -\sum_m P_m \cdot A_{mn} \tag{7}$$

with the dynamical matrix

$$A_{nn'} = (\Gamma_n^{\downarrow} + \Gamma_n^{\uparrow})\delta_{nn'} - \Gamma_{nn'}^{\downarrow} \tag{8}$$

The inverse of this three-diagonal matrix is easily solved by the iterative relation

$$-\hbar\delta_{nn_0} = \Gamma_{n-2}^{(+)\downarrow}\tau_{n-2} + \Gamma_{n+2}^{(-)\downarrow}\tau_{n+2} - (\Gamma_n^{(+)\downarrow} + \Gamma_n^{(-)\downarrow} + \Gamma_n^{\uparrow})\tau_n \tag{9}$$

for the mean life time τ_n and $n_0 \leqq n \lesssim N$.
Exciton number changes $\Delta n = -2,0,+2$ are denoted by (-), (0), and (+), respectively. P_n is the occupation probability of exciton state n. The damping and escape widths $\Gamma_n^{\downarrow}$ and $\Gamma_n^{\uparrow}$, respectively, are related to the mean square matrix elements $\overline{I^2}$ as

$$\Gamma_n^{(\Delta n)\downarrow} = 2\pi \cdot \overline{I^2} \cdot \rho_n^{(\Delta n)} \quad \text{for } \Delta n = 2,-2; \tag{10a}$$

$$\Gamma_{n\beta}^{(\Delta n)\uparrow}(\varepsilon') = 2\pi \cdot (2s+1) \cdot \overline{I^2} \cdot \rho(\varepsilon') \cdot \rho_{n\beta}^{(\Delta n)}(u) \quad \text{for } \Delta n = 0,-2. \tag{10b}$$

The total escape width is

$$\Gamma_n^{\uparrow}(\varepsilon') = \sum_{\beta=\pi,\nu} \left[\Gamma_{n\beta}^{(0)\uparrow}(\varepsilon') + \Gamma_{n\beta}^{(-)\uparrow}(\varepsilon')\right]. \tag{11}$$

For the appropriate final state densities $\rho_n^{(\Delta n)}$, $\rho_{n\beta}^{(\Delta n)}$, we refer to /1/. Since we have

$$\sum_{n=n_0}^{N} \frac{\tau_n}{\hbar} \cdot \Gamma_n^{\uparrow} = 1 \tag{12}$$

the quantity $\sigma_\alpha^{SMC}(\varepsilon)$ in eq. (6) is a normalization constant obtained from the OM reaction cross section $\sigma_\alpha(\varepsilon)$ by the use of

$$\sigma_\alpha^{SMC}(\varepsilon) = \sigma_\alpha(\varepsilon) - \sum_{\beta=\pi,\nu} \sigma_{\alpha\beta}^{SMD}(\varepsilon) \tag{13}$$

(flux conservation).

Note that both $\Gamma_n^{\uparrow}$ and τ_n^{-1} are proportional to $\overline{I^2}$. Consequently, all $\overline{I^2}$ cancel exactly within the sum of eq. (6). The shape of the SMC emission cross section, which becomes independent of $\overline{I^2}$, is mostly determined by the final single-particle state density (g) and the consideration of the Pauli exclusion principle reducing the average exciton number $\bar{n}$ for equilibrium considerably (cf. ref. 4). In first order, the damping width description rather than escape width description affects the shape of SMC cross sections. The main difference between (n,n') and (p,n) SMC emission spectra is due to the OM reaction cross section $\sigma_\alpha(\varepsilon)$, whereas the shape for both reaction types are almost identical.

Finally, we define the pre-equilibrium part of the SMC cross section

$$\frac{d\sigma^{pre}_{\alpha\beta}}{d\varepsilon'}(\varepsilon) = \sigma_\alpha(\varepsilon)\cdot\sum_{n=n_0}^{\tilde{n}} \frac{\tau_n}{\hbar}\cdot\Gamma_n^{\uparrow} \qquad (14)$$

with $\tilde{n}$ as a summation limit strongly depending on ε (see below).

4. Results

The SMD/SMC model approach has been applied to the reactions $^{109}Ag(p,n)$ and $^{93}Nb(n,n')$ to study both direct and pre-equilibrium contributions to secondary-neutron spectra ($\beta \equiv \nu$). The total SMC emission probabilities $\Gamma_n^{\uparrow}\cdot\tau_n/\hbar$ from all exciton states (n = p + h = 2p +1 in the present cases) are represented in the figs. 1,2 for selected ε. Obviously, equilibrium emission corresponds to Gaussian-shaped emission distributions. The tail at low exciton number has to be attributed to non-equilibrium neutron emission. For both reactions considered we find $\tilde{n} \approx 0.4\cdot\varepsilon$/MeV/ approximatively. Note that the distinction between σ^{pre} and σ^{eq} is somewhat artificial since the SMC emission cross sections are described in a unique manner.

Concerning SMD contributions, there are remarkable differences between (p,n) and (n,n') reactions. For $\alpha = \pi$, direct excitations of collective modes cancel (cf. eq. 5). The contributions from direct particle-hole (ex) excitations are comparable for both reaction types. We assume $\overline{I^2_{\nu\nu'}} = \overline{I^2_{\pi\nu}}$.
As described in refs. 1,2 in more detail, collective excitations

of 2^- and 3^+ modes (vibrations) are taken into account in the calculations for ^{93}Nb(n,n'). The delta functions $\delta(\varepsilon - \varepsilon' - \omega_\lambda)$ are replaced by Gaussians of 1 MeV width.
The results of the calculations show:

(i) the predominance of $\frac{d\sigma^{eq}_{\alpha\beta}}{d\varepsilon'}$ at low ε' generally ($\approx$ 99 %),

(ii) the predominance of $\frac{d\sigma^{(1)}_{\alpha\beta}}{d\varepsilon'}$ at high ε' (more pronounced in (n,n') reactions and at high ε),

(iii) the increasing influence of SMC pre-equilibrium contributions with increasing ε.

Consequently, the differences between the total emission cross section and the equilibrium part are rapidly increasing with ε. The "contamination" of the equilibrium spectra by direct and pre-equilibrium processes can only be understood as a "correction" for low incidence energy (especially for (p,n) reactions).

5. Conclusions

The present analysis in the framework of the SMD/SMC model has shown that secondary-neutron spectra from (p,n) and (n,n') reactions can be well reproduced in a physically consistent way without parameter adjustment. Specifically, the "contamination" of equilibrium spectra by direct and pre-equilibrium contributions has been deduced. Thus, previous treatments based on non-complete considerations of the reaction mechanisms (evaporation + direct, evaporation + pre-equilibrium) have been generalized. The theoretical method proposed in this work indicates the possibility to deduce pure neutron equilibrium spectra from measured complex secondary-neutron spectra by correcting for all "contamination"[5] contributions. Uncertainties can be estimated from results presented in §4.

References

1 - H. Kàlka, F.A. Zhivopistsev, D. Seeliger, Z. Phys. A, in print

2 - H. Kalka, Proc. XVIIth Int. Symp. Nucl. Phys. - Nuclear Reactions - , Gaussig, 1987, in print

3 - H. Feshbach, A. Kerman, S. Koonin, Ann. Phys. 125(1980)429

4 - Zhang Jing Shang, Yang Xian Jun, Proc. IAEA Advisory Group Meeting on Nuclear Theory for Fast Neutron Nuclear Data Evaluation, Beijing, 1987, in print

5 - H. Vonach, Proc. IAEA Advisory Group Meeting on Basic and Applied Problems of Nuclear Level Densities, Brookhaven National Laboratory, 1983, BNL-NCS-51694 (1983)247

6 - W. Pilz, D. Schmidt, D. Seeliger, A.I. Vdovin, Yad. Fiz. 33(1981)885

7 - M. Adel-Fawzy, H. Förtsch, S. Mittag, D. Schmidt, D. Seeliger, T. Streil, EXFOR 32001, IAEA(NDS)-1982

8 - A. Takahashi et al., OKTAVIAN report A 83-01(1983)

Figures

Fig. 1 The total SMC emission probability $\Gamma_n^{\uparrow} \cdot \tau_n / \hbar$ from exciton state n as a function of particle number p = (n+1)/2 calculated for 109-Ag(p,n) at selected incidence energies.

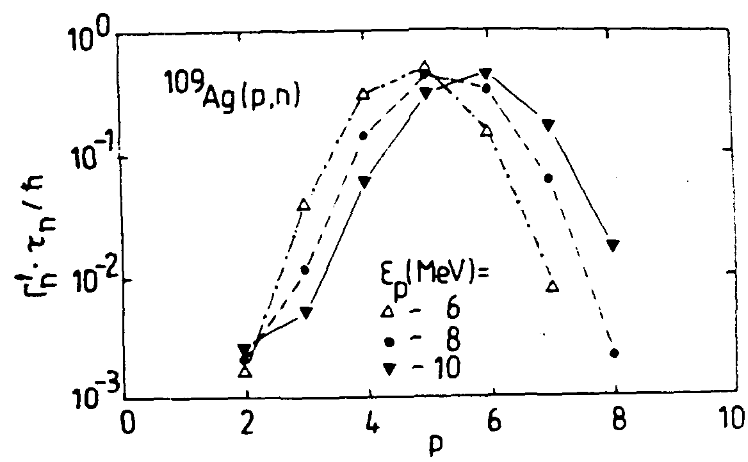

Fig. 2 As for fig. 1, but for 93-Nb(n,n')

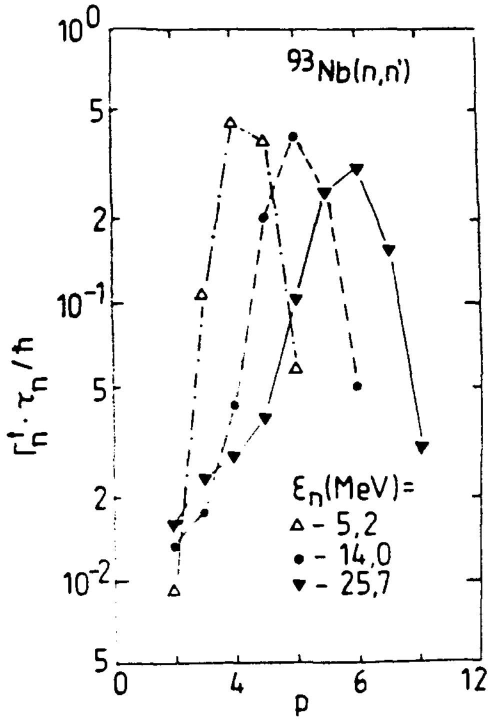

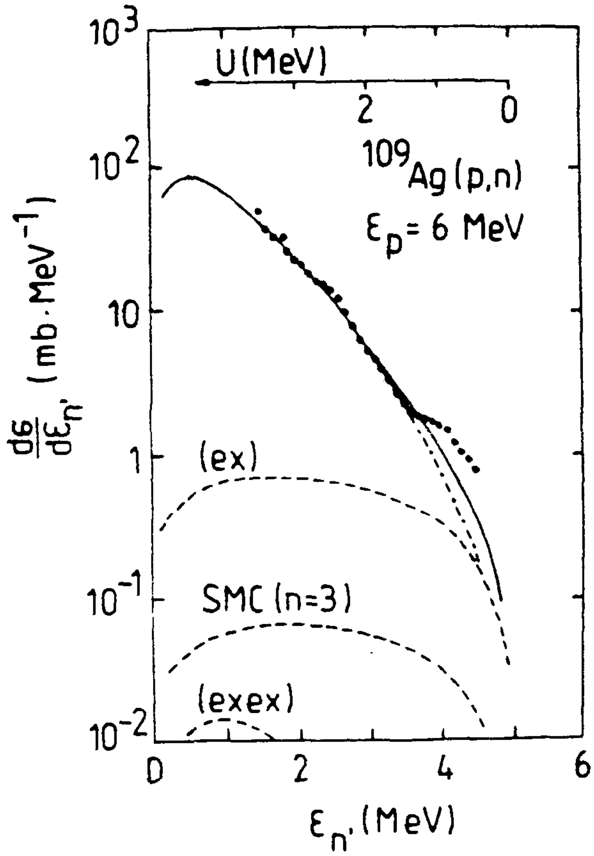

Fig. 3 The emission cross section of neutrons from 109-Ag(p,n) reaction at 6 MeV proton energy (dots - experimental points from ref. 6, dashed lines - SMD contributions as specified, dashed-dotted line - pure equilibrium part, full line - total SMD/SMC spectrum)

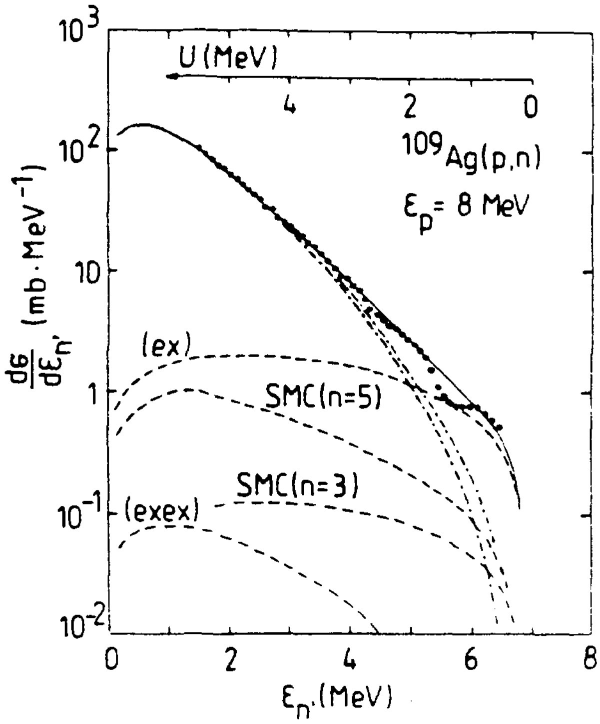

Fig. 4 As for fig. 3, but for 8 MeV proton energy. The upper (lower) dashed-dotted line represents the equilibrium spectrum without (with) consideration of the SMC(n=5) contribution.

Fig. 5 Emission cross section of neutrons from 93-Nb(n,n') reaction at 5.2, 7.2, and 9.0 MeV incidence energy (experimental data from ref. 7, dotted line - equilibrium part, full line - total SMD/SMC spectrum)

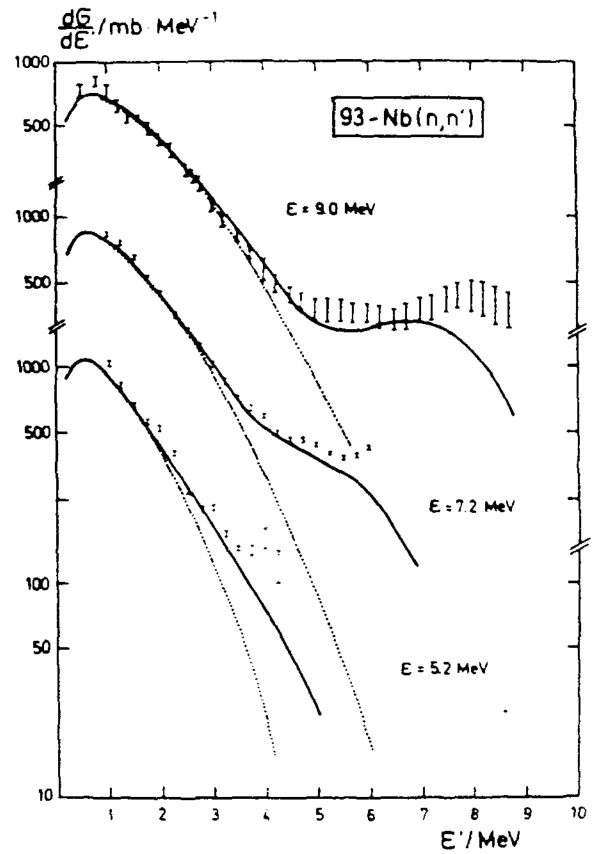

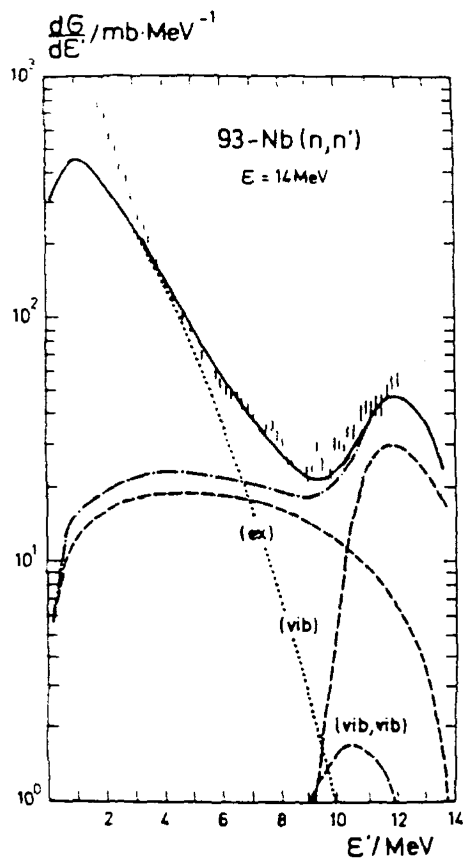

Fig. 6 As for fig. 5, but for 14 MeV incidence neutron energy (dashed lines - SMD contributions, dashed-dotted line - total SMD spectrum). Experimental data were taken from ref. 8. The total SMD/SMC spectrum doesn't include (n,2n) contributions.

INTEGRAL TEST OF LEVEL DENSITY DESCRIPTIONS IN THE FRAMEWORK OF FISSION NEUTRON THEORY

H. Märten, D. Seeliger, and K. Arnold

Technische Universität Dresden, GDR

Abstract

Several methods for the semi-empirical description of nuclear level density have been tested within the complex cascade evaporation model (CEM). The standard neutron spectrum from spontaneous fission of ^{252}Cf can be well reproduced if taking into account shell and pairing effects in a reliable manner.

Several semi-empirical formulae have been proposed for the calculation of nuclear level density $\rho(U,J)$, which take into consideration nuclear shell, pairing, and (partly) collective effects (see, for example, ref. 1).
The aim of this work is to test the methods for global $\rho(U,J)$ descriptions presented in refs. 2-4 within fission neutron theory, i.e. use of necessary model parameters for neutron-enriched nuclei in the 70-170 mass number range.
The CEM[5-7] based on an extended Weisskopf-Ewing ansatz accounts for

- a complex fragment distribution in mass number, charge number, kinetic energy, excitation energy, and angular momentum;
- cascade emission;
- neutron-γ-competition of prompt fragment de-excitation;
- emission anisotropy in the centre-of-mass system (CMS) due to fragment angular momentum;
- optical-model cross section for compound-nucleus formation calculated on the basis of a global optical potential;
- exact transformation of CMS spectra into lab. frame.

The CEM has been successfully applied to reproduce energy and angular distributions of $^{252}Cf(sf)$ neutrons in a wide range[6,7] on the basis of the semi-empirical $\varrho(U)$ formula of Schmidt et al.[2]. In addition, the results of further CEM calculations based on the semi-empirical methods proposed by Ignatyuk et al.[3] and Ramamurthy et al.[4] are presented in this work in comparison with the earlier results. All these calculations have been performed by using the Holmqvist potential[8] for calculating inverse cross sections of compound-nucleus formation in the mass number range specified above.

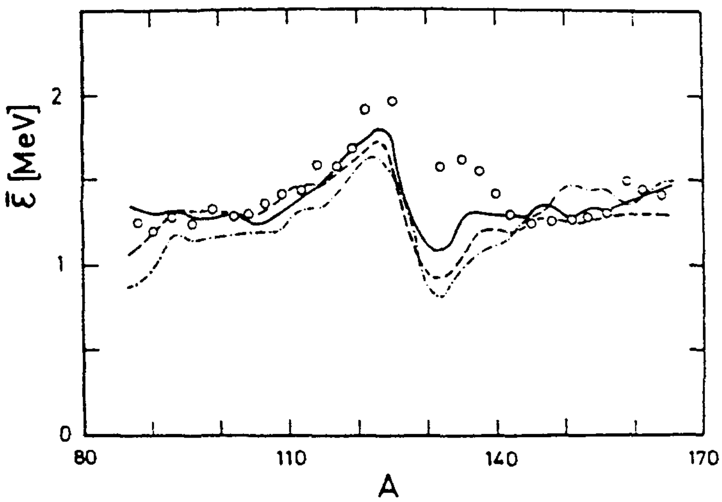

Fig. 1 Average CMS emission energies of 252-Cf(sf) neutrons as a function of fragment mass number A (o - data deduced from experiment, ref. 9, curves - CEM calculations based on the level density formulae by Schmidt et al., ref. 2 (———), Ramamurthy et al., ref. 4 (----), and Ignatyuk et al., ref. 3 (-.-.-))

The average CMS emission energies as a function of fragment mass number A, which are rather sensitive to the choice of the level density description, exhibit small differences between the calculations. They are in agreement with experimental data[9] with exception of the region around the double-magic fragment with A = 132 (cf. ref. 6).
The integral neutron spectrum (nuclear standard) is well described if applying the $\varrho(U)$ formulae of Schmidt et al. and Ramamurthy et al. Considerable deviations appear if using the previous method of Ignatyuk et al. including a rough pairing correction (constant energy scale shift). Here, calculated CMS spectra are characterized by too small neutron emission probabilities at the upper neutron energy limit depending on fragment excitation energy.

As pointed out by Ignatyuk et al. themselves, their formula fails to reproduce nuclear level densities below neutron binding energy.

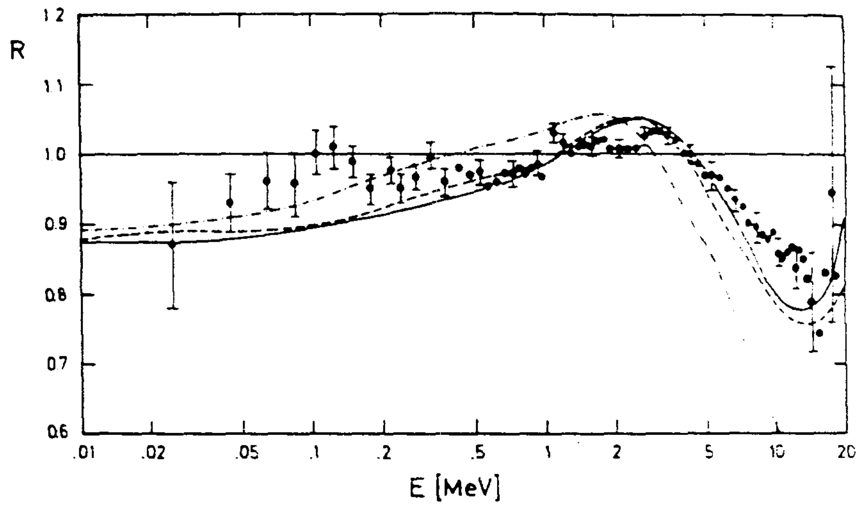

Fig. 2 The 252-Cf(sf) neutron spectrum represented as ratio to a Maxwellian distribution with a 1.42 MeV T-parameter. Points represent evaluated data of Mannhart, ref. 10. The meaning of CEM curves is as in fig. 1.

The present analysis has shown that semi-empirical methods of $\rho(U,J)$ description including microscopic effects are suitable for fission neutron spectrum calculations.

References

1 - V.S. Ramamurthy et al., Proc. IAEA Advisory Group Meeting on Basic and Applied Problems of Nuclear Level Densities, Brookhaven National Laboratory, 1983, BNL-NCS-51694(1983)187

2 - K.H. Schmidt et al., Z. Phys. A 308(1982)215

3 - A.V. Ignatyuk et al., Yad. Fiz. 21(1975)485

4 - V.S. Ramamurthy et al., Proc. IAEA Consultants' Meeting on the Use of Nuclear Theory in Neutron Nuclear Data Evaluation, Trieste, 1975, IAEA-190, II(1976)117

5 - H. Märten, D. Seeliger, J. Phys. G 10(1984)349

6 - H. Märten et al., Proc. Int. Conf. on Neutron Physics, Kiev, 1987, in print

7 - H. Märten, Proc. IAEA Advisory Group Meeting on Nuclear Theory for Fast Neutron Nuclear Data Evaluation, Beijing, 1987, in print

8 - B. Holmqvist, Arkiv Fysik 38(1968)403

9 - H.R. Bowman et al., Phys. Rev. 126(1962)2120

10 - W. Mannhart, Proc. IAEA Advisory Group Meeting on Properties of Neutron Sources, Leningrad, 1986, IAEA-TECDOC-410(1987)158

Double Differential Cross Sections for the (p,n) Reactions of 13.1 MeV Protons with $^{94,95,96,97,98,100}Mo$

T. Bröer, E. Mordhorst, S. Stamer, M. Trabandt and W. Scobel

Abstract

Cross sections for the inclusive production of neutrons of 13.13±0.15 MeV protons with all stable Molybdenum isotopes (with the exception of ^{92}Mo) have been measured with time-of-flight techniques for 22 angles ranging from 3° to 177°. After a short presentation of the motivations for this work, the experimental set up and the tables of double differential and angle integrated cross sections are presented.

1. Introduction

The data presented in this report have been taken as a contribution to the Coordinated Research Program of the IAEA on "Measurement and Analysis of Double-Differential Neutron Emission Spectra in (p,n) and (α,n) Reactions". The main objectives of this CRP are:

(i) to extract systematic information about nuclear level densities as function of excitation energy by analyzing the neutron emission spectra from (p,n) and (α,n) reactions on properly selected targets and bombarding energy range, and

(ii) to parameterize this information into appropriate phenomenological models to enable reliable extrapolation for general use of level density information in basic and applied nuclear physics related problems.

The participants from the University of Hamburg have taken over the task to study the inclusive neutron production from proton induced reactions on Molybdenum isotopes with the time-of-flight facility at the Hamburg Isochrochronous Cyclotron.

In a first series of measurements we have determined the double differential cross sections for 25.6 MeV protons on all stable isotopes, i.e. ^{92,94,95,96,97,98,100}Mo. The experiment and its results has been discussed with emphasis on the experimental set up and the systematic and/or statistical uncertainties pertinent to that work in [1]. Interpretations of the results in terms of preequilibrium reaction mechanism have been published, too [2,10,11].

In a second series of measurements we have determined the double differential (p,xn) cross sections for E_p = 13.1 MeV. The target ^{92}Mo has been excluded because of its highly negative Q-value, cf. Table II. The experimental set up is essentially the same as that one described in [1]; in order to make this paper selfcontained, we repeat it here and all the modifications necessary in the conduct of the 13.1 MeV measurements.

2. Apparatus and Measurements

2.1 Experimental set up

The experiment has been performed with the 13.1±0.15 MeV proton beam of the Hamburg Isochronous Cyclotron. The energy spread includes the effect of the target thickness. The 13.81 MHz repetition rate (cyclotron RF) was scaled down with an external deflection system [3] by a factor of 12 to allow for neutron time-of-flight (TOF) spectroscopy with flight paths of at most 8 m and neutron energies between 1 MeV and 13 MeV without ambiguities due to overlapping bursts.

The geometry of the neutron TOF area is shown in Fig. 1. The set up consists of 8 detectors and is designed for low background and large angular range performance [4]. For this purpose the proton beam is bent with two dipole magnets by 2 × 17° out of the

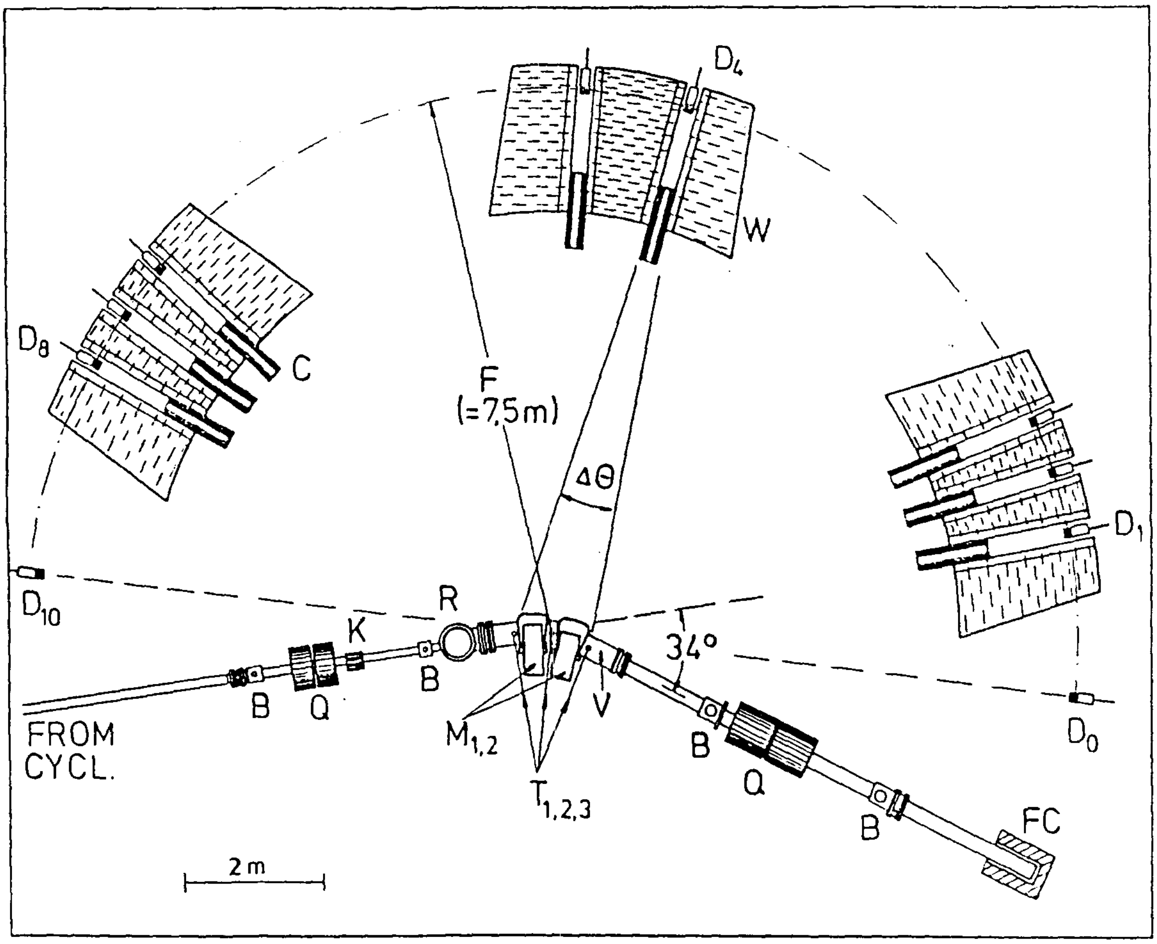

Fig. 1: Layout of the neutron TOF facility (from [4]).

0° direction and then dumped into a heavily shielded (water, paraffine, lead) Faraday Cup. The yokes of the magnets are of C type with a gap width of 10 cm. The reaction chamber inserted into this gap has a shape corresponding to a 34° segment of a circle. It has three remotely controlled target positions in front of, between and behind the two magnets. The integrated Faraday Cup current was recorded for absolute cross section determination.

Reaction neutrons from the target position in operation enter flight paths of (7.5±0.5) m length through a thin exit window (0.13 mm Kapton foil) towards the neutron detectors. The detectors consist of cylindrical 4"ϕ x 2" cells filled with liquid scintillator NE213 and coupled to photomultipliers VALVO XP2-041. They are viewing the targets through collimator tubes traversing a water shielding of more than 1 m thickness. Conical polyethylene throats at the front ends of the collimator tubes supplement the efficient shielding against time correlated and stray neutrons. The collimator tubes can be aligned towards any of the three optional target positions such that the set up covers an internal of reaction angles θ ranging from 3° to 177° with 24 fixed positions and increments of 6.5° for small and large, and 10.5° for intermediate angles, respectively.

The targets were self-supporting, isotopically enriched metallic foils of 12 mm effective diameter and nominal thicknesses ranging from 3.0 to 4.9 mm/cm² (see Table I). Their thicknesses were determined by weighting. The effective thickness in the region of the beam spot of about 4 mm diameter was controlled with the energy loss [5] of ^{241}Am α-particles; these values agreed within 5% with those of Table I (exception: ^{94}Mo, + 12%).

Table I: Target foils and isotopic composition

Target	thickness mg/cm²	isotopic costituents (%)						
		92	94	95	96	97	98	100
^{94}Mo	2.64	0.87	94.60	2.50	0.98	0.32	0.55	0.18
^{95}Mo	4.18	0.14	0.32	97.43	1.38	0.25	0.38	0.09
^{96}Mo	4.31	0.13	0.16	0.52	97.67	0.79	0.62	0.11
^{97}Mo	4.65	0.22	0.24	0.59	1.34	94.25	3.07	0.30
^{98}Mo	4.16	0.10	0.07	0.16	0.23	0.33	98.78	0.33
^{100}Mo	4.15	0.12	0.16	0.27	0.38	0.28	0.84	97.95

The electronics of a single neutron TOF detector were conventional. The block diagram of the combined electronics of all 8 detectors is shown in Fig. 2. A linear bias was set individually for each detector at a pulse height corresponding to a proton energy $E_{thr} \approx 1.0$ MeV. The exact positions were determined [4] with the Compton edges of sources (^{22}Na, ^{88}Y, ^{137}Cs, ^{207}Bi). The photomultiplier signals were stabilized [6] with respect to a

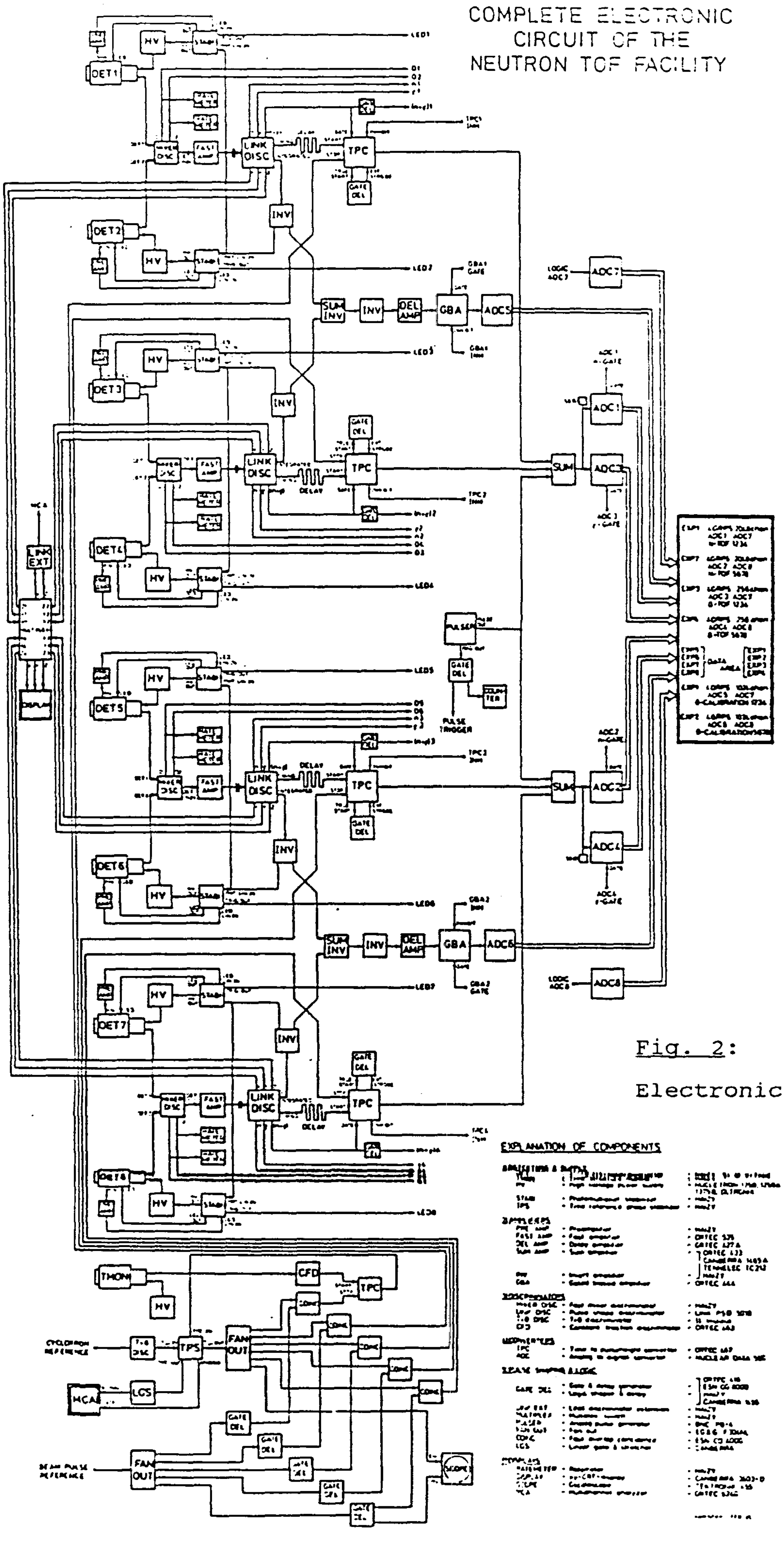

Fig. 2:

Electronics diagram.

stabilized LED. The radiation was effectively suppressed by pulse shape discrimination [7].

The TOF stop signal was derived from the cyclotron radio frequency. The TOF data for neutrons as well as for particles were routed via 8 ADC's into an ND4420 multichannel analyzer. The overall time resolution obtained was ≤ 2.5 ns (FWHM) corresponding to a neutron energy resolution of up to 100 keV (270 keV) for $E_n = 5$ MeV (10 MeV).

2.2. Measurements and data reduction

The measurements were performed with proton beam intensities of typically 80 nA. For each target and target position a total charge Q_{FC} of about 1.5 mC was accumulated in the Faraday Cup. Each run was followed by a shorter ($Q_{FC} \approx 0.5$ mC) background run with shadow bars being placed in the flight paths about midway between target and detectors. The shadow bars are truncated polyethylene cones of 80 cm length (corresponding to 7 attenuation lengths λ for 15 MeV neutrons). However, for the extreme reaction angles 3° and 177°, respectively, carefully aligned shadow bars made out of copper (length: 50 cm, attenuation length for $E_n = 15$ MeV $\approx 10\,\lambda$), that were designed for mounting close to the target, were used instead to account for the worse background conditions due to the upstream beam line and the Faraday Cup, respectively.

The background subtraction represented at most a 10% correction of the integral yield in the physical region $E_{thr} \leq E_n \leq E_{n,max}$ and was substantial ($\leq 20\%$) only for the extreme angles and the high neutron energies. The energy scale is deduced from the position of the target γ peak and the time calibration of the system. In any case, the background spectra do not exhibit individual structures nor do they reflect the structures in the corresponding target in runs and therefore cannot be responsible for structures in the spectra, which remain after background subtraction. Further experimental details have been reported elsewhere [4,8].

After background subtraction, the TOF spectra were converted with relativistic kinematics into center-of-mass energy spectra of bin size ΔE_n = 100 keV with the detector efficiencies as described in [9] and under the assumption of single nucleon emission. The Q-values and additional reaction data are listed in

Table II: Reaction data. Maximum kinetic energies (in MeV) $E_{n,max}$ of the neutrons refer to the c.m.s. The uncertainty $\Delta E_{n,max}$ is ± 200 keV.

Reaction	I_{Target}	$Q(p,n_0)$	$Q(p,n_1)$	$E_{n,max}$
$^{92}Mo(p,n)^{92}Tc$	0^+	-8.65	-8.86	4.13
$^{94}Mo(p,n)^{94}Tc$	0^+	-5.04	-5.12	7.87
$^{95}Mo(p,n)^{95}Tc$	$5/2^+$	-2.48	-2.52	10.40
$^{96}Mo(p,n)^{96}Tc$	0^+	-3.76	-3.79	9.14
$^{97}Mo(p,n)^{97}Tc$	$5/2^+$	-1.10	-1.20	11.77
$^{98}Mo(p,n)^{98}Tc$	0^+	-2.46	-2.48	10.43
$^{100}Mo(p,n)^{100}Tc$	0^+	-0.95	-1.12	11.93

Table II. The shifts E_n for neutrons actually resulting from second or third chance emission are at most equal to the recoil correction for the highest possible nucleon energy of ≈ 10 MeV (secondary emission), i.e. $|\pm E_n| \leq 40$ keV. The rare events of neutrons following α particle emission are neglected.

Having determined the sets of 22 energy spectra for all 6 Molybdenum targets with known isotopic composition (Table I), one can calculate for each bin the double differential cross sections for isotopically pure material from a system of 6 linear equations. All cross sections presented furtheron are unfolded this way.

For one target (^{96}Mo), the measurements under $\theta_{lab} = 95°$ and 147° failed. Therefore no data are given for any target under these two angles (indicated by values 0.0 in the tables). However, the data for all targets but ^{96}Mo are available upon request for these angles, too, but without correction for isotopic impurities.

Angle integrated neutron energy spectra were calculated as

$$\frac{d\sigma}{dE_n} = \sum_{\nu=1}^{22} \frac{d^2\sigma}{dE_n d\Omega} \cdot (\Theta_\nu, E_n) \cdot \omega(\Theta_\nu) \qquad (1)$$

with the solid angle weighting for $2 \le \nu \le 21$:

$$\omega(\Theta_\nu) = 2\pi \cdot \left[\cos\frac{\Theta_\nu + \Theta_{\nu-1}}{2} - \cos\frac{\Theta_{\nu+1} - \Theta_\nu}{2}\right] \qquad (2)$$

and for $\nu = 1$ or 22:

$$\omega(\Theta_\nu) = 2\pi \cdot \left[1 - \cos\frac{\Theta_\nu + \Theta_{\nu'}}{2}\right] \qquad (3)$$

where $\nu' = 21$ (or 2) for $\nu = 22$ (or 1).

The resulting set of angle integrated neutron energy spectra is shown in Fig. 3.

For a first orientation, the double differential as well as the angle integrated spectra $N(E_n)$ have been analyzed in terms of the logarithmic plot, viz.

$$\ln \frac{E^2 \cdot N(E_n)}{E_n \cdot \sigma_{inv}(E_n)} \quad \text{vs.} \quad \sqrt{E}$$

where E denotes the excitation energy in the residual nucleus. The level density parameter a was then obtained from a least squares fit in the range 2 MeV $\le$ E $\le$ 5 MeV, cf. Fig. 4a. It turned out that within $\Delta a = \pm\ 0.6\ \mathrm{MeV}^{-1}$ the values obtained this way from the angle differential spectra agreed with the one from the angle integrated spectrum. The resulting a-parameters are shown in Fig. 4b as a function of the mass number A of the residual nucleus. They roughly follow the dependence $a \sim A/8.5\ \mathrm{MeV}^{-1}$ for odd odd nuclei, whereas for the two odd mass nuclei a systematic excess in

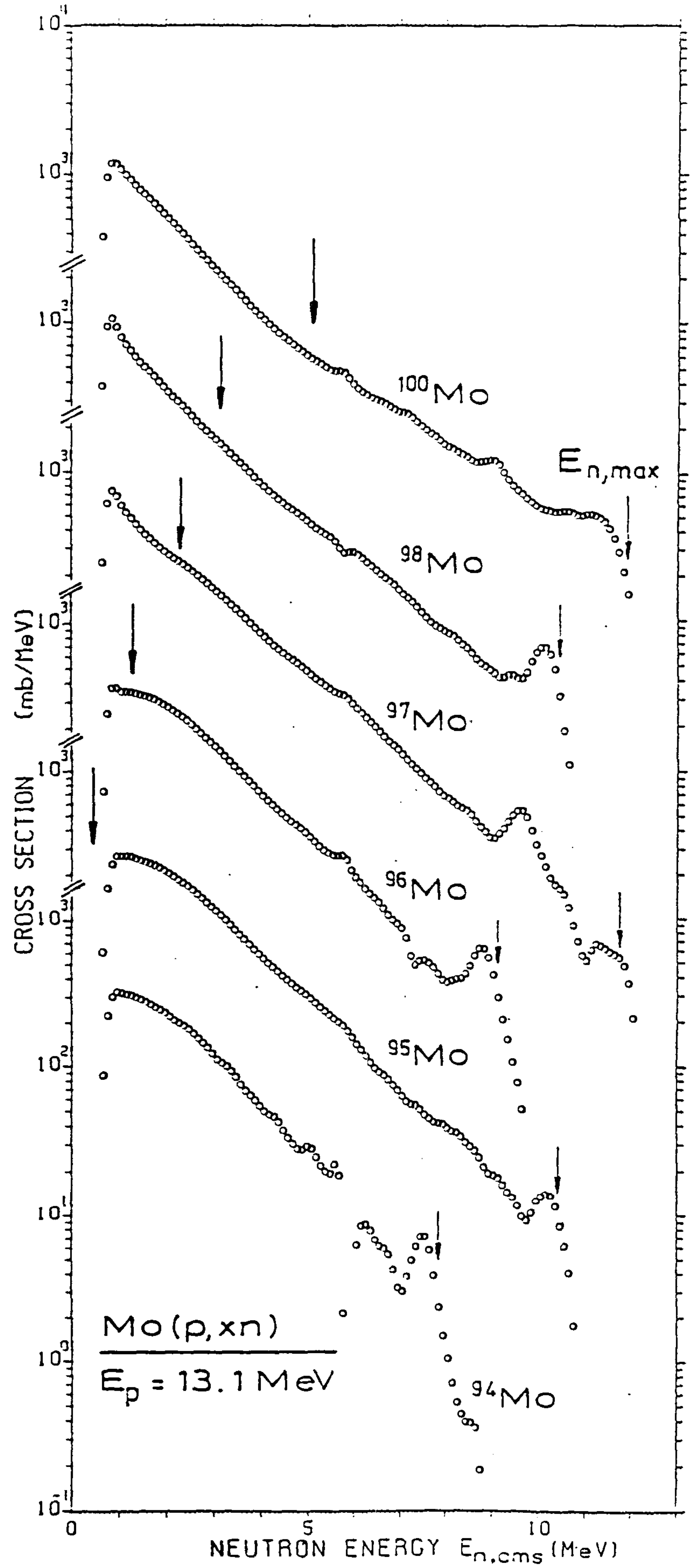

Fig. 3: Angle integrated spectra. The arrows indicate the maximum energies of neutrons from the (p,n) and (p,2n) reaction, respectively.

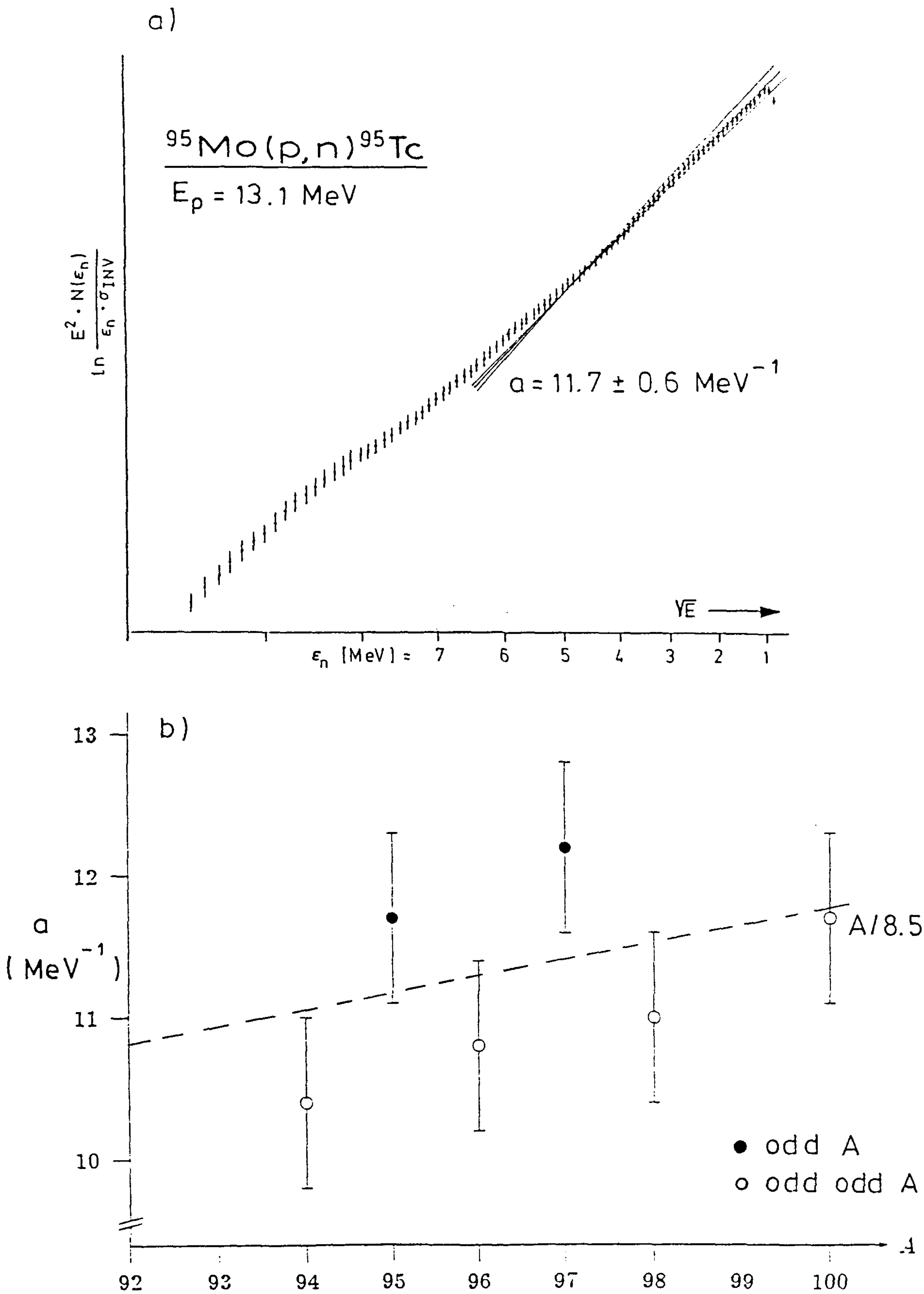

Fig. 4: a) Angle integrated spectrum for $^{95}Mo(p,xn)$ reduced to a logarithmic plot.
b) Resulting slope parameters a.

the order of 1 MeV is observed that reflects the neglect of any pairing corrections.

2.3. Uncertainty estimates and explanation of tables

The main uncertainty sources and their estimates are:

(1) Neutron detector efficiency	5%
(2) Effective target thickness (due to inhomogeneities and uncertainties of the range-energy tables)	5%
(3) Inconsistencies in the background treatment	5%
(4) Statistical uncertainties (< 1% for $E_n \le 6$ MeV; < 10% for $E_n \le 13$ MeV; < 10% for $E_n \le 20$ MeV)	< 10%
(5) Incomplete beam current integration	3%

The estimated relative uncertainties between neutron spectra obtained in different runs are due to (2)-(5) and should not exceed 10% for all angles and all but the highest neutron energies. Absolute uncertainties are slightly higher due to contribution (1). Therefore we claim absolute uncertainties ≤ 12% for most of the double differential and all angle integrated cross sections.

The uncertainties given in the tables in the columns labelled PE are given in absolute units and include only the statistical contributions (including background subtraction).

References

[1] E. Mordhorst, M. Trabandt, F. Binasch, A. Kaminsky, H. Krause, R. Langkau, W. Scobel and M. Strecker
Report INDC(GER)-31/GX and Internal Report HH86-10

[2] E. Mordhorst, M. Trabandt, A. Kaminsky, H. Krause, W. Scobel, R. Bonetti and F. Crespi
Phys. Rev. C34(1986)103

[3] H. Krause, R. Langkau and N. Schirm
Nucl. Instr. and Meth. 134(1976)15

[4] Y. Holler, A. Kaminsky, B. Scharlemann, H. Krause, R. Langkau, W. Peters, G. Poppe, N. Schirm, W. Scobel and R. Wien
Nucl. Instr. and Meth. A235(1985)123

[5] J.F. Ziegler: Helium Stopping Powers and Ranges in All Elemental Matter (Pergamon Press, 1977)

[6] Y. Holler, J. Koch and A. Naini
Nucl. Instr. and Meth. 204(1983)485

[7] J.M. Adams and G. White
Nucl. Instr. and Meth. 156(1978)459

[8] Y. Holler, A. Kaminsky, R. Langkau, W. Scobel, M. Trabandt and R. Bonetti
Nucl. Phys. A442(1985)79

[9] G. Dietze and H. Klein
Report PTB-ND-22 (Braunschweig, 1982)

[10] I. Kumabe and Y. Watanabe
Phys. Rev. C36(1987)543

[11] I. Kumabe and Y. Watanabe
Phys. Rev. C40(1989)535

APPENDIX A

Contains the double differential cross sections for $^{94,95,96,97,98,100}Mo(p,xn)$ in ΔE_n = 100 keV increments. It is not included in this report, but it is available upon request.

APPENDIX B

Angle integrated neutron energy spectra.

MeV	+ 0.000	+ 0.100	+ 0.200	+ 0.300	+ 0.400
0.050	0.000	0.000	0.000	0.000	0.000
0.550	1.034	74.200	198.389	273.975	295.379
1.050	288.075	281.641	275.788	266.994	259.612
1.550	251.493	241.035	230.226	220.483	210.896
2.050	198.722	187.288	179.470	171.874	161.960
2.550	150.613	140.419	130.963	121.711	110.165
3.050	99.015	94.314	90.534	83.951	76.311
3.550	67.914	61.246	57.015	52.949	48.656
4.050	44.837	42.821	41.342	37.814	33.383
4.550	29.823	27.232	25.152	24.822	25.993
5.050	25.203	22.132	19.492	17.925	17.577
5.550	20.660	17.334	0.681	-9.136	-2.490
6.050	5.264	7.569	7.787	7.076	6.101
6.550	5.505	5.336	4.867	3.834	2.849
7.050	2.659	3.405	4.464	5.570	5.547
7.550	6.551	5.300	3.532	2.103	1.344
8.050	0.952	0.670	0.511	0.434	0.411
8.550	0.419	0.373	0.192	0.081	0.118
9.050	-0.002	-0.126	-0.111	-0.102	-0.096
9.550	-0.088	-0.080	-0.075	-0.078	-0.084
10.050	-0.086	-0.085	-0.079	-0.067	-0.050
10.550	-0.037	-0.028	-0.019	-0.013	-0.011
11.050	-0.010	-0.010	-0.009	-0.010	-0.010
11.550	-0.009	-0.008	-0.006	-0.005	-0.003
12.050	-0.002	-0.001	-0.001	-0.001	0.000
12.550	0.000	0.000	0.000	0.000	0.000

Cross section $d\sigma/dE_n$ in mb/MeV

MeV	+ 0.000	+ 0.100	+ 0.200	+ 0.300	+ 0.400
0.050	0.000	0.000	0.000	0.000	0.000
0.550	0.070	2.429	4.078	3.927	2.483
1.050	1.428	0.903	0.634	0.465	0.354
1.550	0.291	0.245	0.204	0.177	0.159
2.050	0.140	0.122	0.111	0.100	0.089
2.550	0.079	0.071	0.062	0.055	0.051
3.050	0.048	0.046	0.044	0.041	0.036
3.550	0.032	0.029	0.028	0.026	0.025
4.050	0.023	0.024	0.025	0.025	0.023
4.550	0.020	0.016	0.014	0.015	0.020
5.050	0.025	0.027	0.028	0.028	0.030
5.550	0.036	0.036	0.031	0.029	0.030
6.050	0.031	0.032	0.032	0.033	0.034
6.550	0.033	0.029	0.025	0.024	0.025
7.050	0.024	0.020	0.019	0.021	0.022
7.550	0.022	0.022	0.023	0.025	0.027
8.050	0.032	0.024	0.021	0.013	0.020
8.550	0.038	0.024	0.113	0.036	0.040
9.050	0.030	0.000	0.000	0.000	0.000
9.550	0.000	0.000	0.000	0.000	0.000
10.050	0.000	0.000	0.000	0.000	0.000
10.550	0.000	0.000	0.000	0.000	0.000
11.050	0.000	0.000	0.000	0.000	0.000
11.550	0.000	0.000	0.000	0.000	0.000
12.050	0.000	0.000	0.000	0.000	0.000
12.550	0.000	0.000	0.000	0.000	0.000

Uncertainty $\Delta(d\sigma/dE_n)$ in mb/MeV

^{95}Mo

MeV	+ 0.000	+ 0.100	+ 0.200	+ 0.300	+ 0.400
0.050	0.000	0.000	0.000	0.000	0.000
0.550	1.008	53.743	150.813	223.863	252.086
1.050	250.978	249.693	246.953	240.429	234.513
1.550	229.420	223.736	216.856	209.038	200.869
2.050	192.180	182.988	173.985	165.485	156.740
2.550	147.448	138.604	130.262	121.616	113.459
3.050	106.196	99.423	92.654	85.824	79.573
3.550	73.790	68.360	63.075	58.188	54.257
4.050	50.636	47.057	43.922	41.000	38.319
4.550	36.114	33.989	31.930	30.193	28.569
5.050	26.860	25.046	23.425	21.985	20.636
5.550	19.430	18.464	17.479	16.080	14.522
6.050	13.020	11.871	10.797	9.743	8.936
6.550	8.435	8.090	7.503	6.892	6.366
7.050	5.846	5.391	5.189	5.116	4.774
7.550	4.417	4.163	3.934	3.896	3.846
8.050	3.598	3.439	3.370	3.160	2.899
8.550	2.733	2.546	2.283	1.986	1.816
9.050	1.796	1.721	1.529	1.364	1.276
9.550	1.110	0.934	0.868	0.975	1.177
10.050	1.275	1.316	1.286	1.079	0.787
10.550	0.554	0.361	0.148	0.013	-0.023
11.050	-0.027	-0.034	-0.031	-0.006	0.007
11.550	-0.002	-0.004	-0.004	-0.003	-0.002
12.050	-0.001	-0.001	0.000	0.000	0.000
12.550	0.000	0.000	0.000	0.000	0.000

Cross section $d\sigma/dE_n$ in mb/MeV

MeV	+ 0.000	+ 0.100	+ 0.200	+ 0.300	+ 0.400
0.050	0.000	0.000	0.000	0.000	0.000
0.550	0.067	1.679	2.974	3.003	2.007
1.050	1.208	0.786	0.562	0.415	0.317
1.550	0.263	0.224	0.190	0.166	0.150
2.050	0.133	0.118	0.106	0.095	0.084
2.550	0.075	0.067	0.060	0.053	0.049
3.050	0.046	0.042	0.039	0.035	0.031
3.550	0.028	0.026	0.024	0.021	0.019
4.050	0.018	0.017	0.016	0.016	0.015
4.550	0.014	0.013	0.012	0.012	0.012
5.050	0.012	0.012	0.012	0.013	0.014
5.550	0.016	0.017	0.017	0.016	0.015
6.050	0.014	0.013	0.012	0.012	0.011
6.550	0.010	0.010	0.011	0.012	0.012
7.050	0.013	0.015	0.019	0.021	0.022
7.550	0.023	0.024	0.024	0.024	0.025
8.050	0.024	0.021	0.020	0.021	0.024
8.550	0.026	0.026	0.027	0.025	0.022
9.050	0.021	0.022	0.025	0.027	0.028
9.550	0.030	0.031	0.030	0.029	0.028
10.050	0.028	0.026	0.026	0.026	0.024
10.550	0.020	0.020	0.017	0.015	0.014
11.050	0.015	0.023	0.020	0.021	0.017
11.550	0.007	0.000	0.000	0.000	0.000
12.050	0.000	0.000	0.000	0.000	0.000
12.550	0.000	0.000	0.000	0.000	0.000

Uncertainty $\Delta(d\sigma/dE_n)$ in mb/MeV

MeV	+ 0.000	+ 0.100	+ 0.200	+ 0.300	+ 0.400
0.050	0.000	0.000	0.000	0.000	0.000
0.550	1.798	69.529	235.568	350.497	345.527
1.050	320.450	315.594	313.088	306.284	299.768
1.550	294.566	287.764	278.591	268.341	257.869
2.050	247.069	235.458	223.514	211.964	200.589
2.550	188.525	176.670	165.840	155.052	144.394
3.050	134.955	126.064	116.956	108.181	99.938
3.550	92.189	85.175	78.999	73.388	67.938
4.050	62.955	58.394	54.215	50.715	47.557
4.550	44.598	42.029	39.808	37.593	35.260
5.050	32.945	30.640	28.410	26.676	25.447
5.550	24.750	24.774	25.222	23.428	19.755
6.050	17.499	16.049	14.618	13.509	12.721
6.550	11.885	10.763	9.655	8.986	8.497
7.050	7.925	6.904	5.425	4.752	4.833
7.550	4.798	4.600	4.298	3.884	3.513
8.050	3.385	3.497	3.593	3.637	3.903
8.550	4.434	5.171	5.796	5.770	5.012
9.050	3.835	2.669	1.873	1.381	0.985
9.550	0.720	0.475	0.277	0.183	0.113
10.050	0.049	-0.014	0.025	0.017	-0.038
10.550	-0.029	-0.022	-0.016	-0.012	-0.010
11.050	-0.009	-0.009	-0.009	-0.009	-0.009
11.550	-0.009	-0.008	-0.007	-0.006	-0.004
12.050	-0.002	-0.001	-0.001	0.000	0.001
12.550	0.001	0.001	0.001	0.001	0.000

Cross section $d\sigma/dE_n$ in mb/MeV

MeV	+ 0.000	+ 0.100	+ 0.200	+ 0.300	+ 0.400
0.050	0.000	0.000	0.000	0.000	0.000
0.550	0.116	2.208	5.821	6.244	3.478
1.050	1.695	1.034	0.725	0.531	0.405
1.550	0.336	0.286	0.242	0.212	0.191
2.050	0.169	0.150	0.134	0.119	0.106
2.550	0.095	0.084	0.074	0.066	0.061
3.050	0.056	0.052	0.048	0.043	0.038
3.550	0.034	0.032	0.029	0.026	0.023
4.050	0.021	0.020	0.019	0.018	0.017
4.550	0.017	0.018	0.018	0.018	0.016
5.050	0.015	0.015	0.015	0.015	0.015
5.550	0.016	0.017	0.019	0.018	0.016
6.050	0.014	0.013	0.011	0.010	0.012
6.550	0.015	0.017	0.017	0.018	0.019
7.050	0.021	0.022	0.022	0.020	0.019
7.550	0.018	0.017	0.016	0.015	0.015
8.050	0.016	0.018	0.021	0.022	0.023
8.550	0.024	0.028	0.031	0.034	0.038
9.050	0.039	0.038	0.037	0.037	0.036
9.550	0.034	0.033	0.019	0.028	0.018
10.050	0.019	0.009	0.095	0.031	0.000
10.550	0.000	0.000	0.000	0.000	0.000
11.050	0.000	0.000	0.000	0.000	0.000
11.550	0.000	0.000	0.000	0.000	0.000
12.050	0.000	0.000	0.000	0.000	0.000
12.550	0.000	0.000	0.000	0.000	0.000

Uncertainty $\Delta(d\sigma/dE_n)$ in mb/MeV

MeV	+ 0.000	+ 0.100	+ 0.200	+ 0.300	+ 0.400
0.050	0.000	0.000	0.000	0.000	0.000
0.550	2.674	221.866	582.418	725.011	667.667
1.050	572.250	510.981	468.046	427.011	392.843
1.550	365.517	340.305	316.661	295.945	279.010
2.050	264.289	251.000	238.880	227.308	215.856
2.550	203.567	191.675	180.647	169.294	158.143
3.050	148.425	139.809	130.646	121.662	113.561
3.550	105.588	98.152	91.419	84.997	79.217
4.050	74.024	69.006	64.535	60.978	57.692
4.550	54.458	51.723	49.091	46.525	44.004
5.050	41.337	39.069	37.090	35.021	33.289
5.550	31.822	31.105	30.529	28.858	26.680
6.050	24.722	23.109	21.565	20.164	18.911
6.550	17.527	16.179	15.097	14.250	13.436
7.050	12.474	11.526	10.697	9.999	9.316
7.550	8.650	8.151	7.656	7.062	6.600
8.050	6.354	6.016	5.670	5.483	5.279
8.550	4.929	4.441	4.076	3.796	3.467
9.050	3.432	3.675	3.984	4.449	4.943
9.550	5.306	5.320	4.763	3.884	3.115
10.050	2.614	2.201	1.836	1.639	1.528
10.550	1.388	1.135	0.855	0.669	0.537
11.050	0.496	0.586	0.644	0.624	0.599
11.550	0.569	0.546	0.524	0.462	0.350
12.050	0.203	0.078	-0.009	-0.083	-0.144
12.550	-0.173	-0.148	-0.102	-0.089	-0.048

Cross section $d\sigma/dE_n$ in mb/MeV

MeV	+ 0.000	+ 0.100	+ 0.200	+ 0.300	+ 0.400
0.050	0.000	0.000	0.000	0.000	0.000
0.550	0.174	9.116	14.545	12.983	6.935
1.050	3.193	1.749	1.124	0.768	0.547
1.550	0.428	0.348	0.282	0.239	0.212
2.050	0.186	0.164	0.147	0.131	0.117
2.550	0.105	0.094	0.084	0.076	0.071
3.050	0.066	0.062	0.058	0.054	0.049
3.550	0.045	0.043	0.041	0.038	0.036
4.050	0.034	0.033	0.032	0.032	0.032
4.550	0.031	0.031	0.032	0.032	0.032
5.050	0.033	0.033	0.033	0.034	0.036
5.550	0.036	0.036	0.035	0.034	0.034
6.050	0.034	0.034	0.035	0.037	0.039
6.550	0.040	0.043	0.047	0.049	0.050
7.050	0.049	0.048	0.048	0.046	0.043
7.550	0.041	0.039	0.038	0.039	0.039
8.050	0.040	0.040	0.043	0.045	0.046
8.550	0.046	0.046	0.044	0.044	0.043
9.050	0.041	0.037	0.033	0.032	0.032
9.550	0.033	0.031	0.030	0.031	0.032
10.050	0.031	0.030	0.031	0.044	0.025
10.550	0.028	0.028	0.028	0.031	0.030
11.050	0.029	0.028	0.032	0.033	0.029
11.550	0.027	0.029	0.034	0.033	0.032
12.050	0.029	0.017	0.012	0.010	0.009
12.550	0.009	0.009	0.010	0.016	0.013

Uncertainty $\Delta(d\sigma/dE_n)$ in mb/MeV

MeV	+ 0.000	+ 0.100	+ 0.200	+ 0.300	+ 0.400
0.050	0.000	0.000	0.000	0.000	0.000
0.550	3.365	330.684	857.509	1005.388	871.415
1.050	741.550	662.681	605.931	553.078	509.746
1.550	473.838	441.626	410.078	379.125	351.042
2.050	325.285	301.396	280.726	261.592	242.696
2.550	224.364	206.840	191.457	178.131	165.887
3.050	155.227	145.393	135.564	126.014	116.765
3.550	108.414	101.015	94.014	87.094	80.675
4.050	74.999	69.798	65.435	61.672	58.056
4.550	54.797	51.928	49.155	46.488	43.898
5.050	41.174	38.738	36.749	35.151	33.739
5.550	31.369	28.059	26.056	26.449	26.504
6.050	25.347	24.126	22.763	21.490	20.098
6.550	18.840	17.787	16.938	16.084	14.912
7.050	13.891	13.114	12.265	11.376	10.497
7.550	9.697	9.020	8.524	8.166	7.835
8.050	7.572	7.323	6.868	6.422	6.073
8.550	5.607	5.090	4.785	4.583	4.368
9.050	4.140	3.875	3.893	4.050	4.058
9.550	3.881	3.831	4.179	4.916	5.694
10.050	6.163	6.150	5.501	4.364	2.911
10.550	1.711	1.023	0.615	0.360	0.169
11.050	0.056	-0.020	-0.049	-0.034	0.017
11.550	0.072	0.040	-0.011	-0.008	-0.006
12.050	-0.004	-0.002	-0.002	-0.001	0.000
12.550	0.000	0.000	0.000	0.000	0.000

Cross section $d\sigma/dE_n$ in mb/MeV

MeV	+ 0.000	+ 0.100	+ 0.200	+ 0.300	+ 0.400
0.050	0.000	0.000	0.000	0.000	0.000
0.550	0.213	12.068	18.393	15.805	8.277
1.050	3.833	2.147	1.392	0.956	0.687
1.550	0.541	0.440	0.357	0.300	0.262
2.050	0.225	0.193	0.170	0.149	0.129
2.550	0.114	0.100	0.086	0.077	0.070
3.050	0.066	0.061	0.056	0.052	0.045
3.550	0.041	0.038	0.036	0.034	0.031
4.050	0.029	0.028	0.027	0.027	0.025
4.550	0.022	0.018	0.017	0.017	0.018
5.050	0.019	0.019	0.020	0.021	0.022
5.550	0.022	0.022	0.021	0.022	0.023
6.050	0.023	0.022	0.021	0.021	0.021
6.550	0.021	0.019	0.017	0.016	0.016
7.050	0.016	0.016	0.017	0.017	0.017
7.550	0.017	0.017	0.016	0.017	0.019
8.050	0.021	0.022	0.023	0.023	0.022
8.550	0.022	0.022	0.022	0.020	0.019
9.050	0.017	0.017	0.019	0.019	0.019
9.550	0.021	0.022	0.022	0.022	0.023
10.050	0.023	0.024	0.024	0.025	0.025
10.550	0.024	0.022	0.024	0.026	0.012
11.050	0.017	0.026	0.027	0.029	0.024
11.550	0.020	0.027	0.000	0.000	0.000
12.050	0.000	0.000	0.000	0.000	0.000
12.550	0.000	0.000	0.000	0.000	0.000

Uncertainty $\Delta(d\sigma/dE_n)$ in mb/MeV

MeV	+ 0.000	+ 0.100	+ 0.200	+ 0.300	+ 0.400
0.050	0.000	0.000	0.000	0.000	0.000
0.550	4.919	376.622	944.070	1169.305	1153.462
1.050	1060.407	975.789	907.862	838.307	779.286
1.550	729.957	681.246	633.027	587.742	545.941
2.050	505.261	465.981	429.897	397.661	367.130
2.550	337.694	311.046	286.477	263.658	243.166
3.050	225.371	209.532	193.872	179.028	165.598
3.550	152.829	140.994	130.110	120.384	112.011
4.050	104.489	97.343	90.969	85.361	80.544
4.550	76.122	71.726	67.833	64.384	61.039
5.050	57.915	55.389	53.004	50.469	48.399
5.550	47.805	48.060	46.421	42.739	39.189
6.050	36.664	34.847	33.397	31.980	30.856
6.550	30.120	29.093	27.900	26.788	25.907
7.050	25.448	24.881	23.626	22.091	20.782
7.550	19.591	18.544	17.621	16.573	15.615
8.050	14.996	14.585	14.003	13.369	12.858
8.550	12.222	11.867	11.969	12.142	12.237
9.050	12.162	11.409	10.128	9.052	8.252
9.550	7.697	7.219	6.743	6.350	6.011
10.050	5.764	5.626	5.504	5.404	5.425
10.550	5.452	5.439	5.313	5.100	5.090
11.050	5.198	5.198	5.081	4.895	4.611
11.550	4.131	3.539	2.851	2.110	1.485
12.050	1.011	0.719	0.570	0.416	0.228
12.550	0.108	0.082	0.110	0.109	0.043

Cross section $d\sigma/dE_n$ in mb/MeV

MeV	+ 0.000	+ 0.100	+ 0.200	+ 0.300	+ 0.400
0.050	0.000	0.000	0.000	0.000	0.000
0.550	0.309	12.689	17.526	14.323	8.863
1.050	5.129	3.062	2.047	1.437	1.046
1.550	0.831	0.679	0.550	0.464	0.405
2.050	0.348	0.298	0.260	0.225	0.195
2.550	0.171	0.149	0.129	0.114	0.103
3.050	0.095	0.087	0.080	0.073	0.064
3.550	0.057	0.053	0.048	0.043	0.039
4.050	0.036	0.033	0.032	0.030	0.029
4.550	0.027	0.027	0.026	0.026	0.025
5.050	0.025	0.025	0.024	0.025	0.027
5.550	0.030	0.033	0.035	0.036	0.038
6.050	0.040	0.042	0.043	0.044	0.047
6.550	0.051	0.052	0.052	0.052	0.053
7.050	0.053	0.051	0.050	0.049	0.047
7.550	0.047	0.047	0.046	0.045	0.046
8.050	0.048	0.047	0.046	0.049	0.054
8.550	0.056	0.055	0.055	0.056	0.056
9.050	0.056	0.055	0.054	0.053	0.053
9.550	0.054	0.053	0.050	0.047	0.046
10.050	0.046	0.046	0.045	0.043	0.043
10.550	0.043	0.042	0.041	0.040	0.041
11.050	0.042	0.041	0.042	0.043	0.045
11.550	0.046	0.047	0.048	0.048	0.046
12.050	0.039	0.035	0.044	0.043	0.038
12.550	0.037	0.036	0.035	0.040	0.034

Uncertainty $\Delta(d\sigma/dE_n)$ in mb/MeV

DOUBLE DIFFERENTIAL NEUTRON EMISSION CROSS SECTIONS OF (p,n) REACTIONS ON Co-59 AND Mo ISOTOPES

Zhou Zuying, Tang Hongqing, Sa Jun, Sui Qingchang
Qi Bujia, Yu Chunying and Shen Guanren
Neutron Physics Laboratory
Institute of Atomic Energy, Beijing, China

1. Experimental arrangement

Neutron emission spectra from (p,n) reactions on Co-59 and Mo-95, Mo-96, Mo-97, Mo-98, Mo-100 in the incident energy range 9 to 15 MeV were measured by means of TOF technique at the HI-13 tandem Van de Graaff accelerator in the Institute of Atomic Energy, Beijing, China. The spectrometer was described elsewhere(1). The experimental arrangement is shown in fig.1. The pulsed proton beam with a repeatition rate of 2 MHz and beam width of about 1 ns was focused on the target. The beam pick off signal was taken out right in the front of the target chamber. The neutron target chamber is an aluminium cylinder with a diameter of 44 cm, a height of 45 cm and a thin wall of 3 mm. In the center of the chamber is a target holder on which five targets can be mounted. The target holder can move vertically to keep one of the five targets in the beam line at a time. The target is so positioned that the proton beam impinges the target surface perpendicularly.

The neutron emitted from (p,n) reactions were detected by a three detector TOF spectrometer. The neutron detector is composed of a liquid scintillator (Φ105x50 mm) and a photomultiplier tube. It was massive shielded and well collimated. The neutron flight path is 5.21 m, 6.55 m and 5.17 m respectively for detector No.1, No.2 and No.3. The detector bias is about 0.85 MeV. To reduce r-ray background, a CANBERRA 2160A modular was used. The detector efficiency is shown in fig.2. Fig.3 shows the electronics block diagram.

2. Measurement

Before the measurement, one piece of thin quartz plate (for checking beam size and beam position) and three targets to be measured were mounted on the target holder, and the other target position was kept vacant for background measurement. The dimention, thickness and isotopic abundance of the targets are listed in table 1 (2). For each incident energy and each target, two neutron spectra(with and without target) were measured at one angle in the range 20 degree to 160 degrees with 10 degree steps.. To ensure the whole beam is in the middle of the target and much smaller than the target size, the beam was carefully adjusted. Usually, the beam spot is less than 4 mm in diameter and positioned in

Table I Properties of the targets

Target	Diameter of the target (mm)	Thickness of the target (mg/cm^2)	Equivalent energy loss for 10 MeV proton (KeV)	Abundance (%)
Co-59	12	5.11	148	100
Mo-95	12	4.18	100	97.43
Mo-96	12	4.31	103	97.67
Mo-97	12	4.65	112	94.25
Mo-98	12	5.95	142	91.60
Mo-100	12	4.15	100	97.95

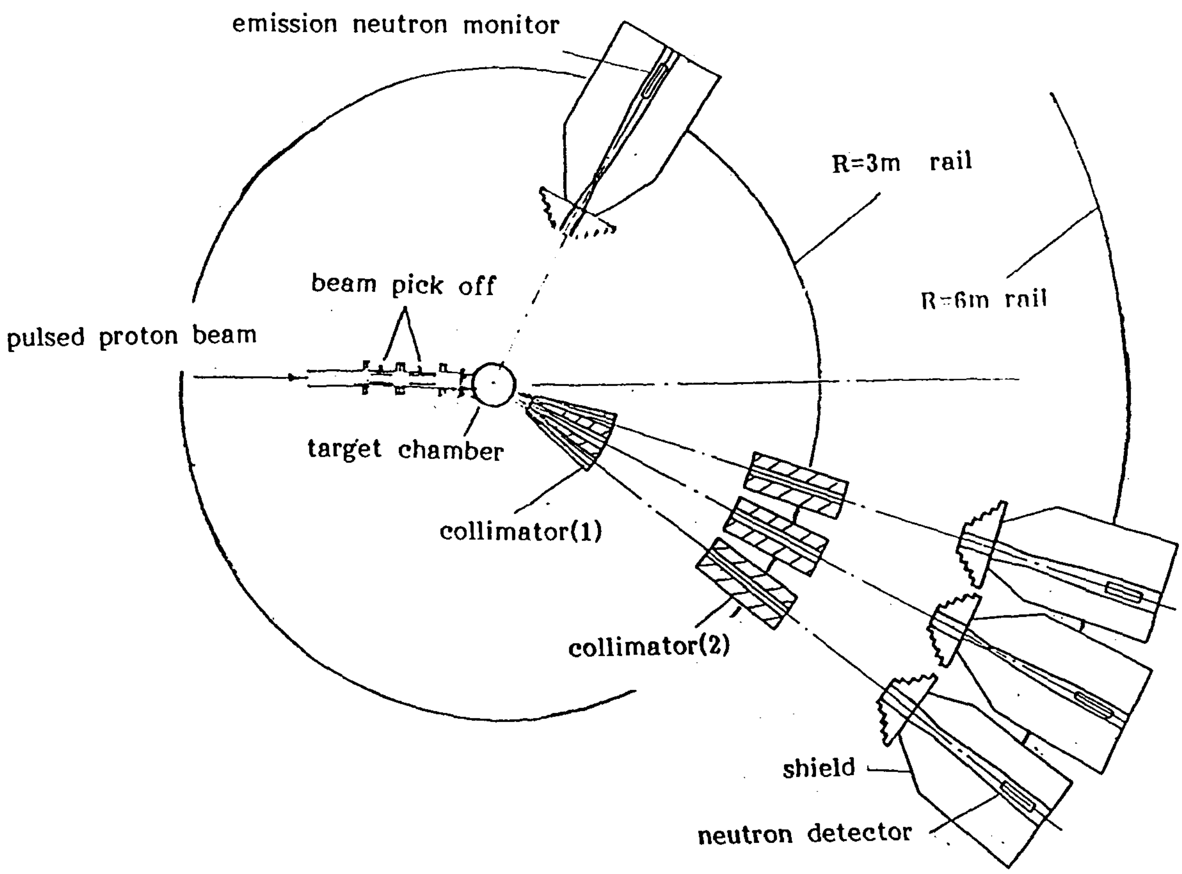

Fig. 1 Three-detector fast neutron TOF spectrometer at the HI-13 tandem accelerator

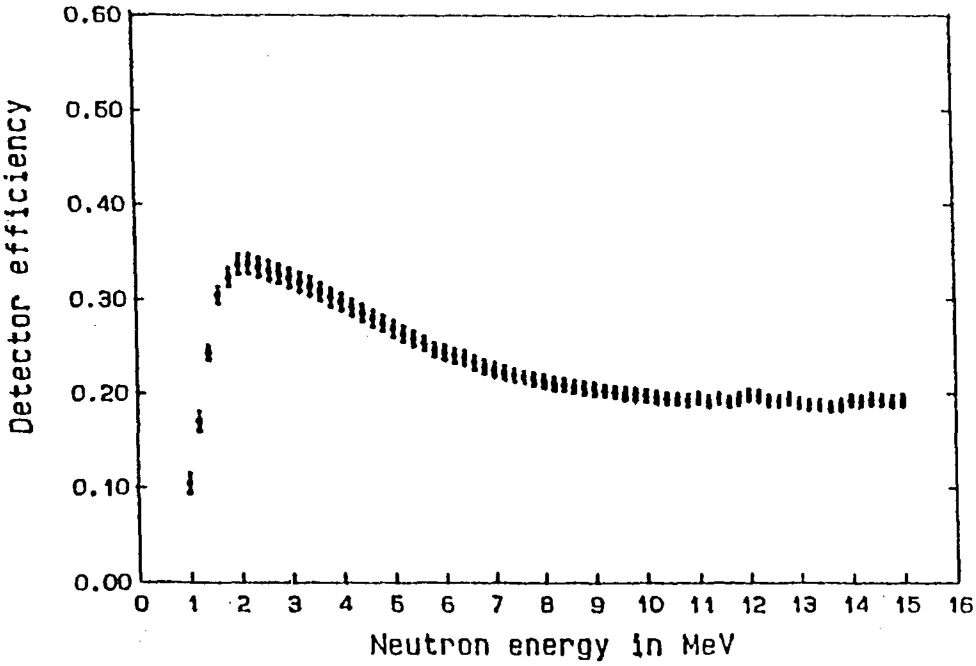

Fig.2 Neutron detector efficiency

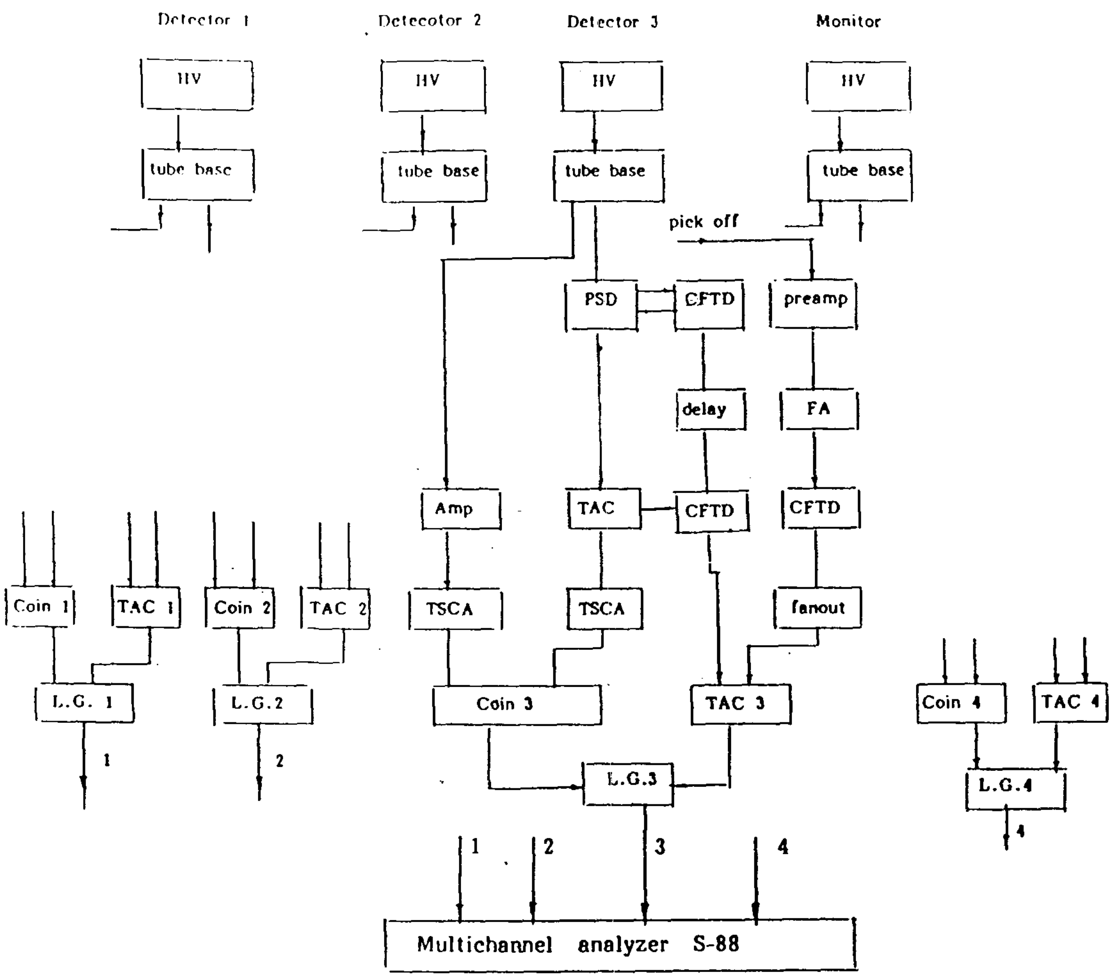

Fig. 3. Electronics block diagram
HV-- high voltage power suplly, tube base--photomultiplier tube base, Amp--amplifier
PSD --pulse shape discriminator, preamp--fast preamplifier, CFTD--constant fraction timing discriminator,
FA--fast amplifier, TAC--time to amplitude convertor, Delay --nanosecond delay,
TSCA--timing scaler, Coin-- coincidance circuit, L.G.-- linear gate

in the center of the target. The average proton beam current is about 100 na and recorded by a digital current integrator. For each spectrum about 500 micro-Coulumb of incident particle charge was accumulated. In addition, annother TOF spectrometer with a shorter flight path of 3 m was used to monitor emission neutrons from the target. For a certain target and a certain proton energy, if the integral number of the emission neutrons of the (p,n) reaction over the spectrum region is in coincidance with accumulated electric charge of the beam current integrator, the data are adopted. If they are in discrepancy, the data should be dropped.

3. Results

Typical neutron TOF spectra of (p,n) reactions on Mo-97 at 9 MeV and Mo-95 at 13 MeV are shown in figs. 4 to 7. After subtraction of corresponding back-ground spectrum and considering the corrections of detector efficiency, dead time ...... and normalization to the numbers of incident particles and target nuclei, the neutron TOF spectrum was converted into double differential neutron emission cross sections as a function of neutron energy in the center of mass system and angle in the laboratory system. Typical neutron emission spectra (in center of mass system) are shown in figs.8 and 9. Some angular distributions (in laboratory system) with an energy bin of 0.2 MeV are given in figs. 10 11 and 12.

The reliable lower energy limit in the spectrum is about 1.4 MeV.

4. Error and error sources

Besides the statistical error, the following errors i.e. neutron detector eficicency, consistance of different neutron detectors, count of beam current integrator, number of target nuclei, dead time of the detector and electronics, should be considered, which are listed in table 2.

Table II Errors and error sources

Error source	Error (%)
Statistics	1-5 (typically, depending on neutron energy in the spectrum)
Neutron detector efficiency	3 (En greater than 1.4 MeV)
Consistance of neutron detectors	3
Number of target nuclei	5
Dead time	negligible
Total	7-8.5 (En greater than 1.4 MeV)

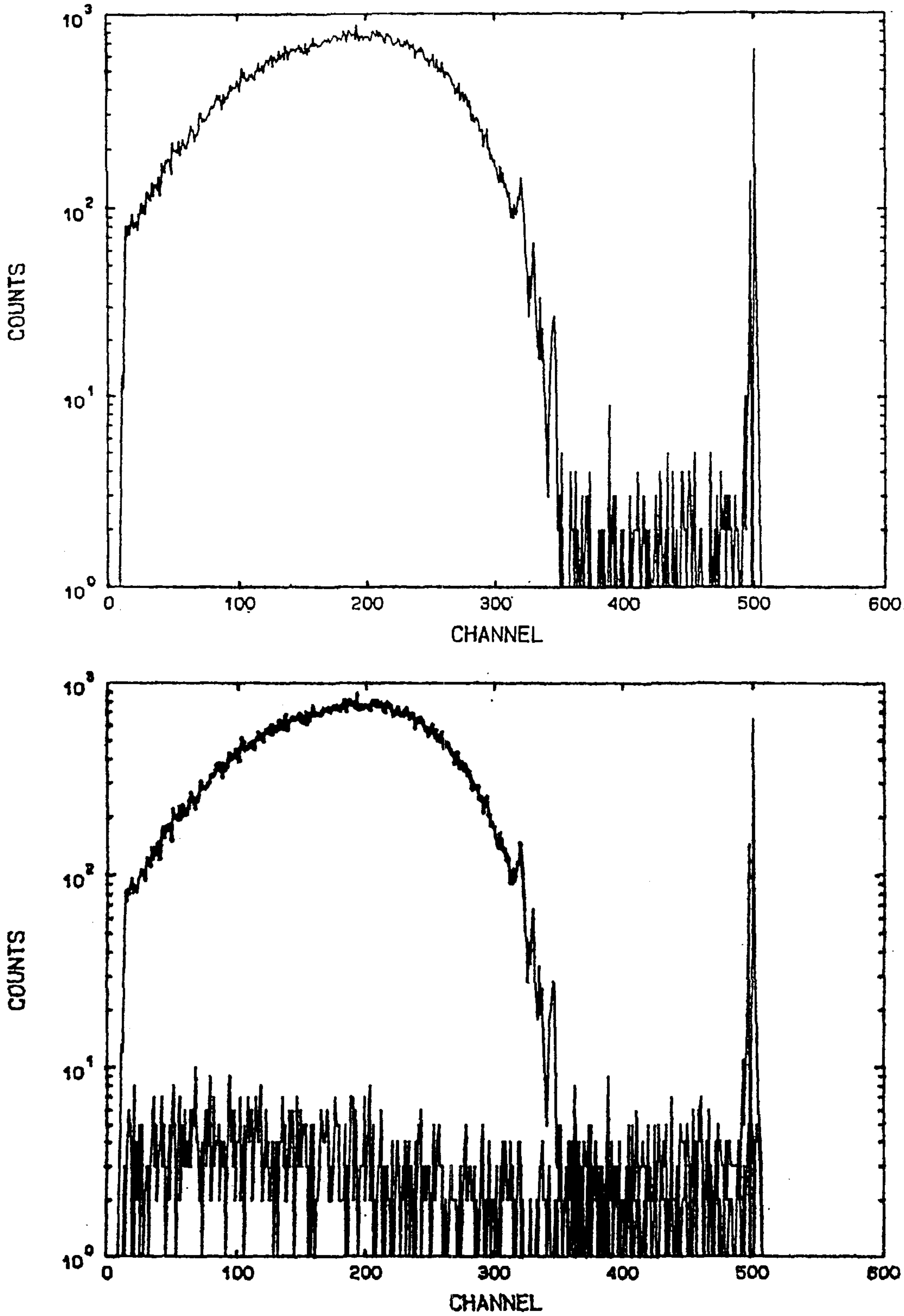

Fig.4 TOF Spectrum of Mo97(p,n)Tc97
Ep=9 MeV at 20 deg.
Top: Background subtracted
Bottom: with and without sample

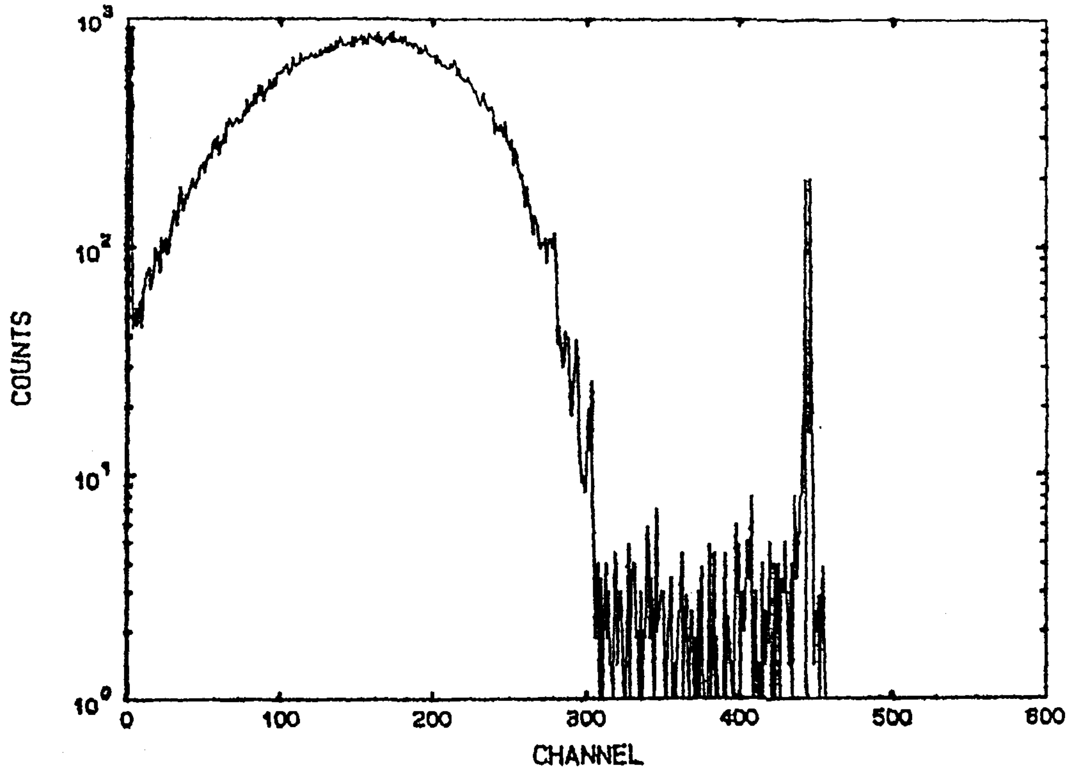

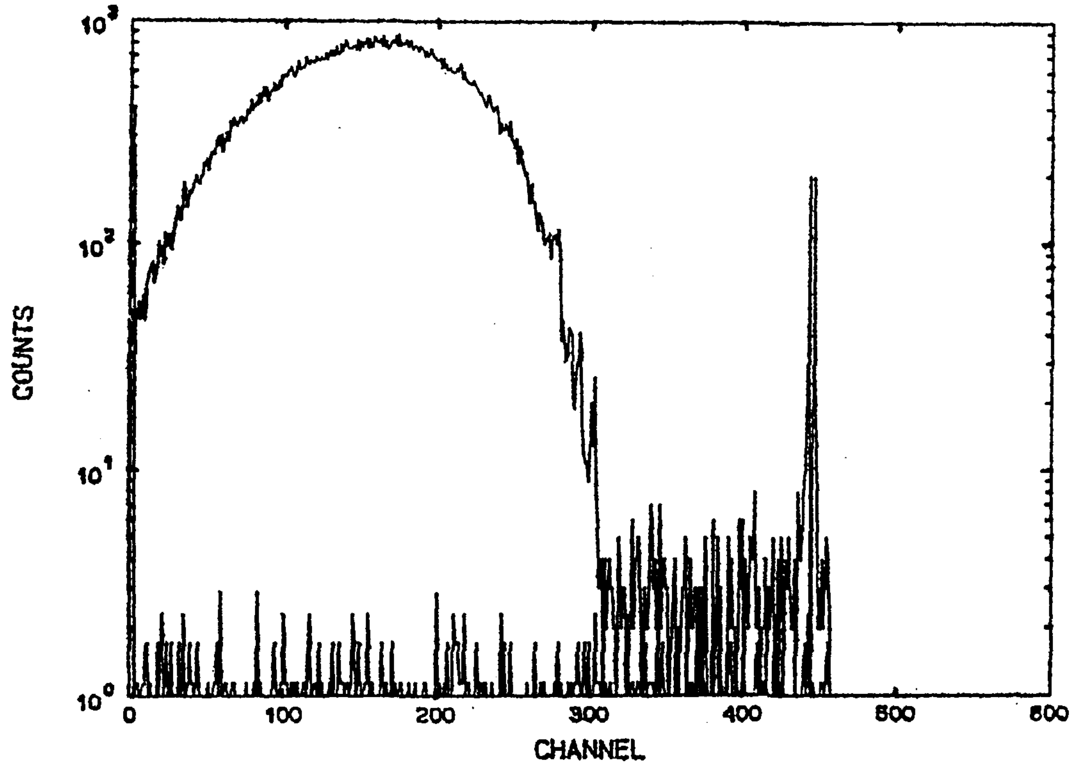

Fig.5 TOF Spectrum of Mo97(p, n) Tc97
Ep=9MeV at 100 deg.
Top: Background subtracted
Bottom: with and without target

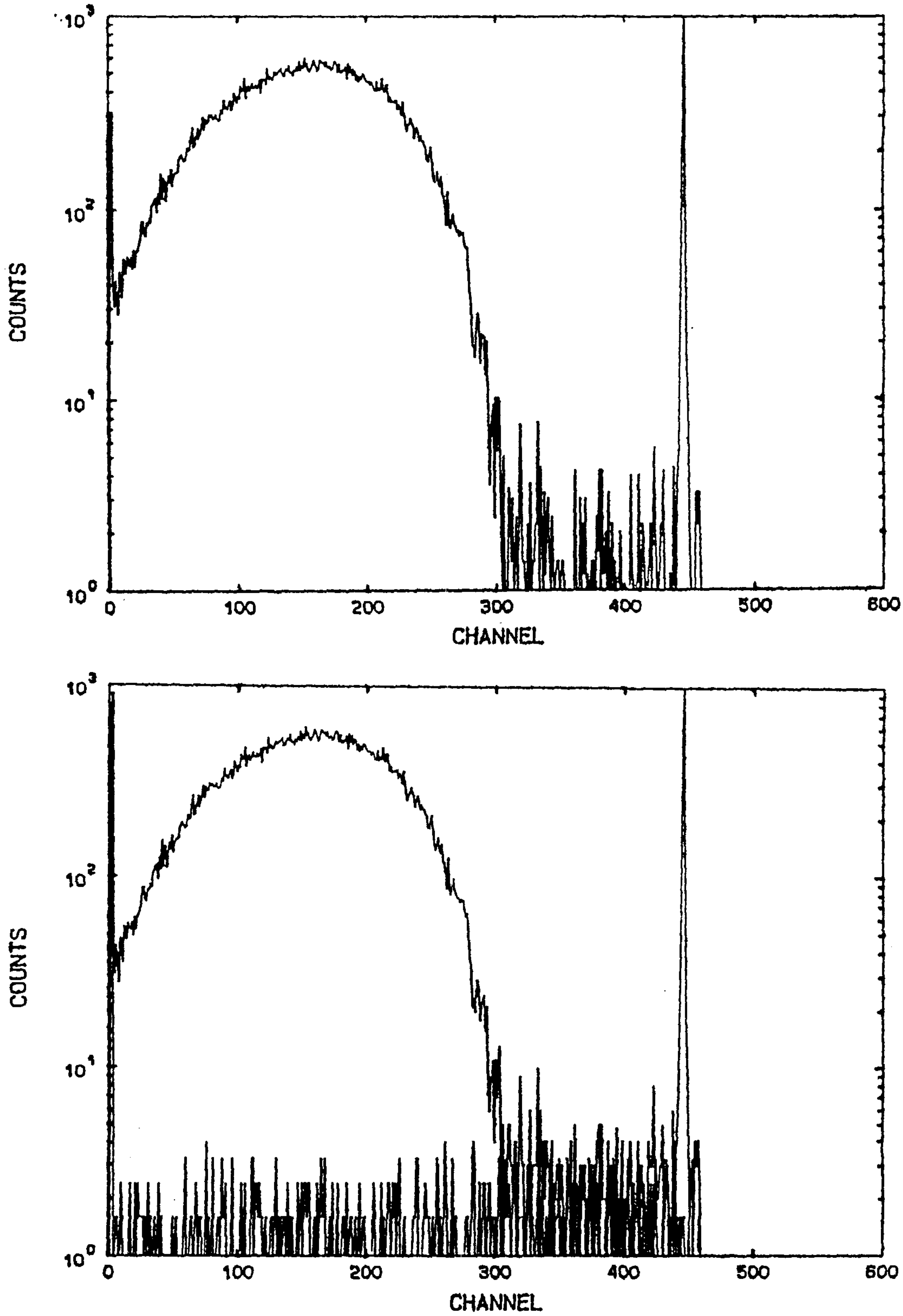

Fig.6 TOF Spectrum of Mo97(p, n) Tc97
Ep=9 MeV at 160 deg.
Top: Background subtracted
Bottom: with and without target

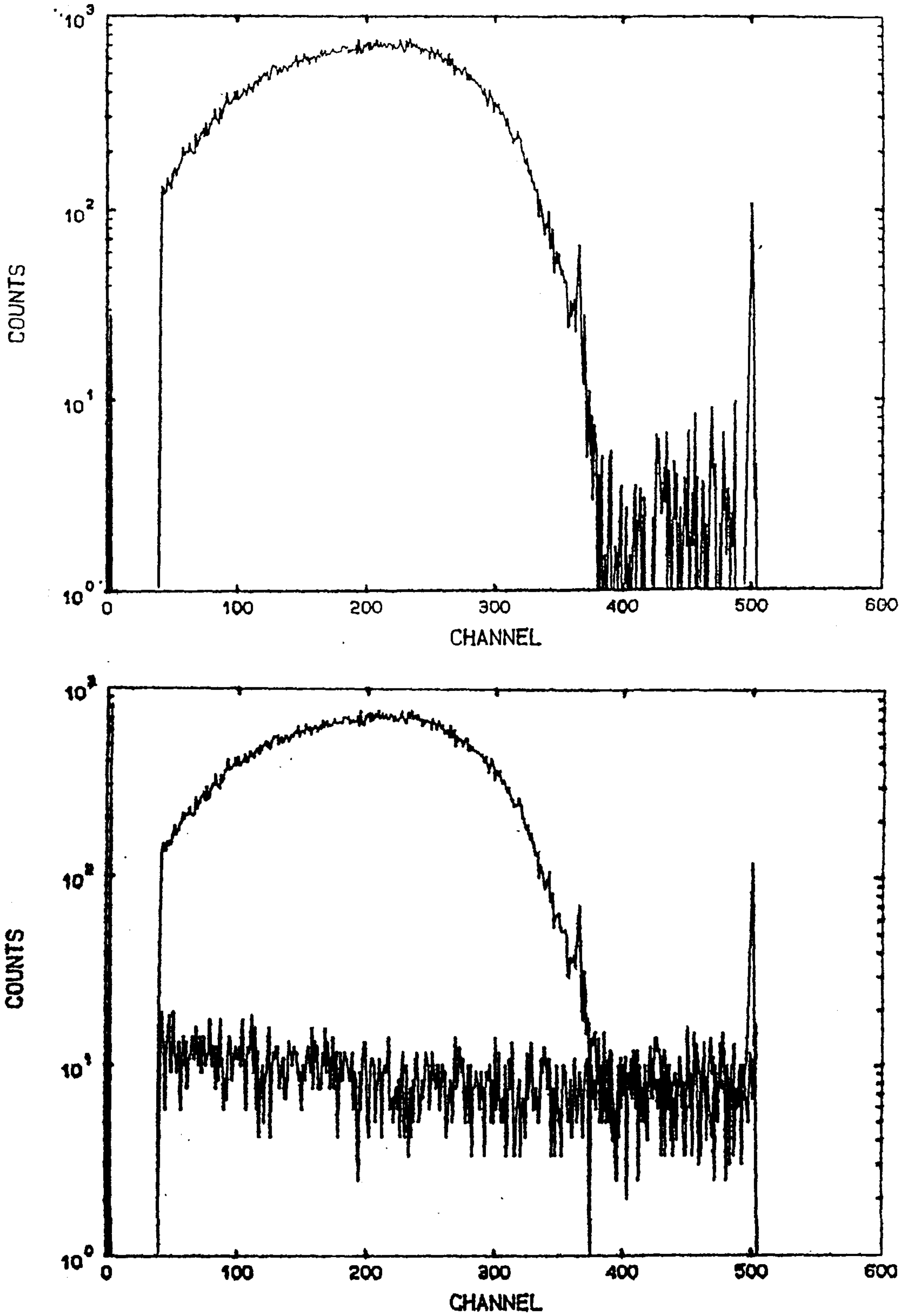

Fig.7 TOF Spectrum of Mo95(p, n)Tc95
Ep=13 MeV at 80 deg.
Top: Background subtracted
Bottom: With and without target

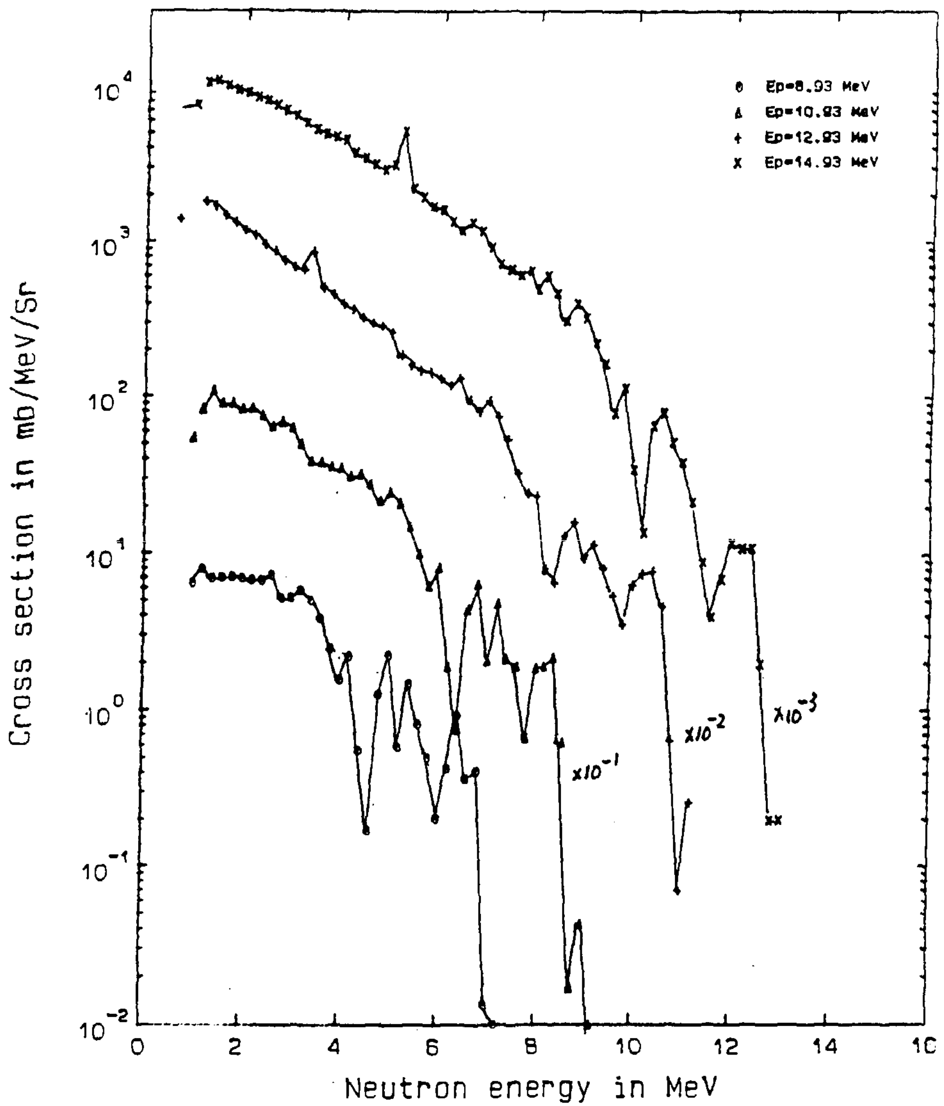

Fig.8 Neutron Spectrum of Co59(p,n)Ni59

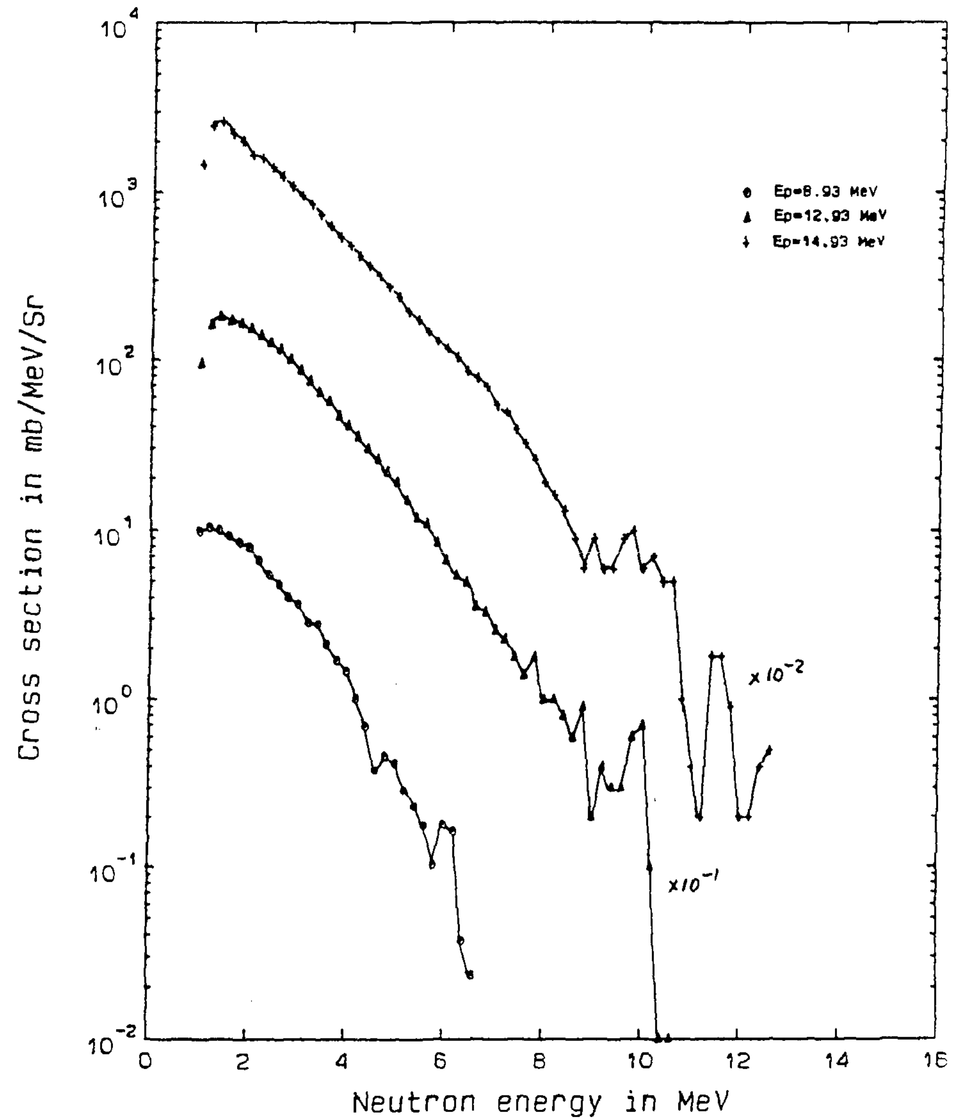

Fig.9 Neutron Spectrum of Mo95(p,n)Tc95

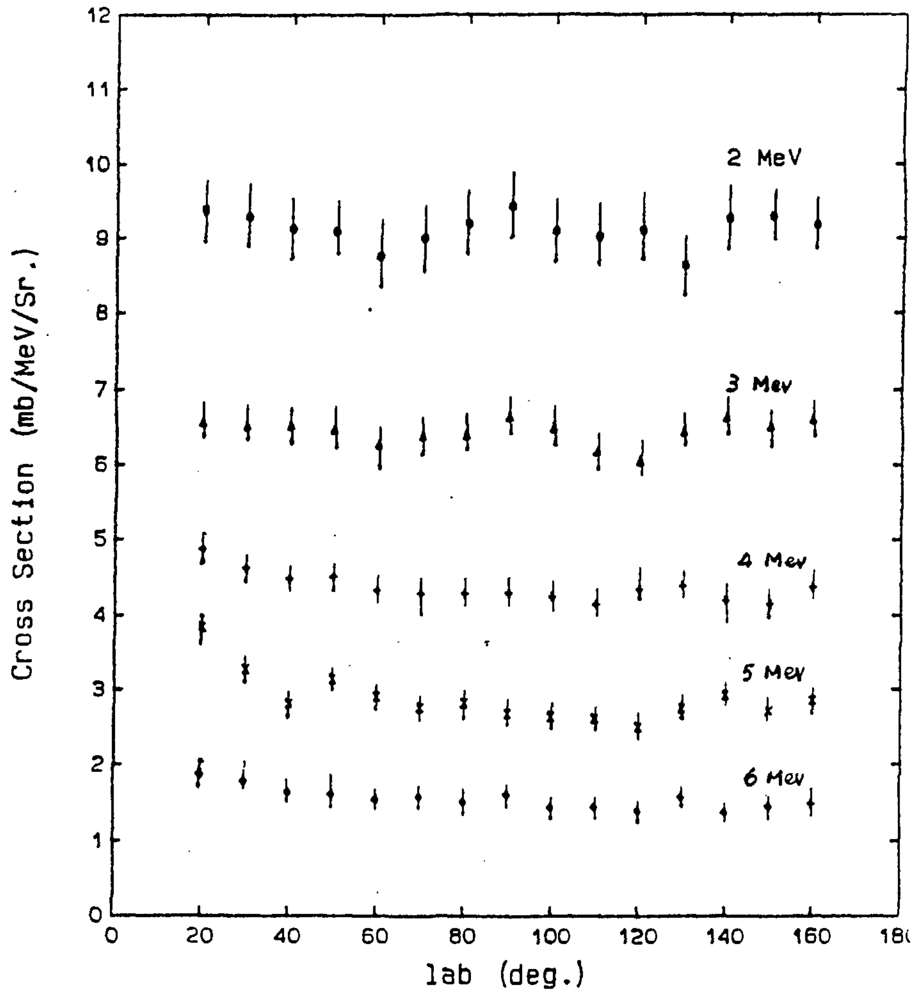

Fig.10 Angular Distribution of
Co59(p,n)Ni59 at 15 MeV

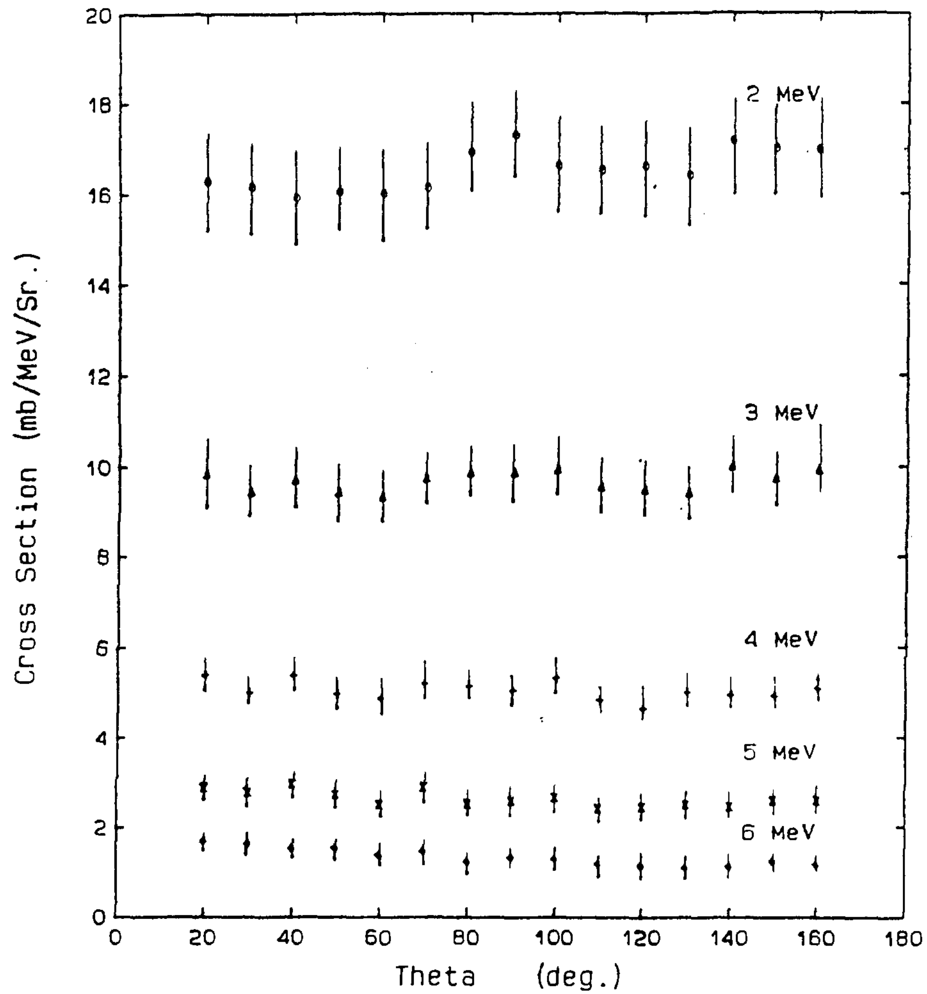

Fig.11 Angular Distribution of
Mo95(p,n)Tc95 at 15 MeV

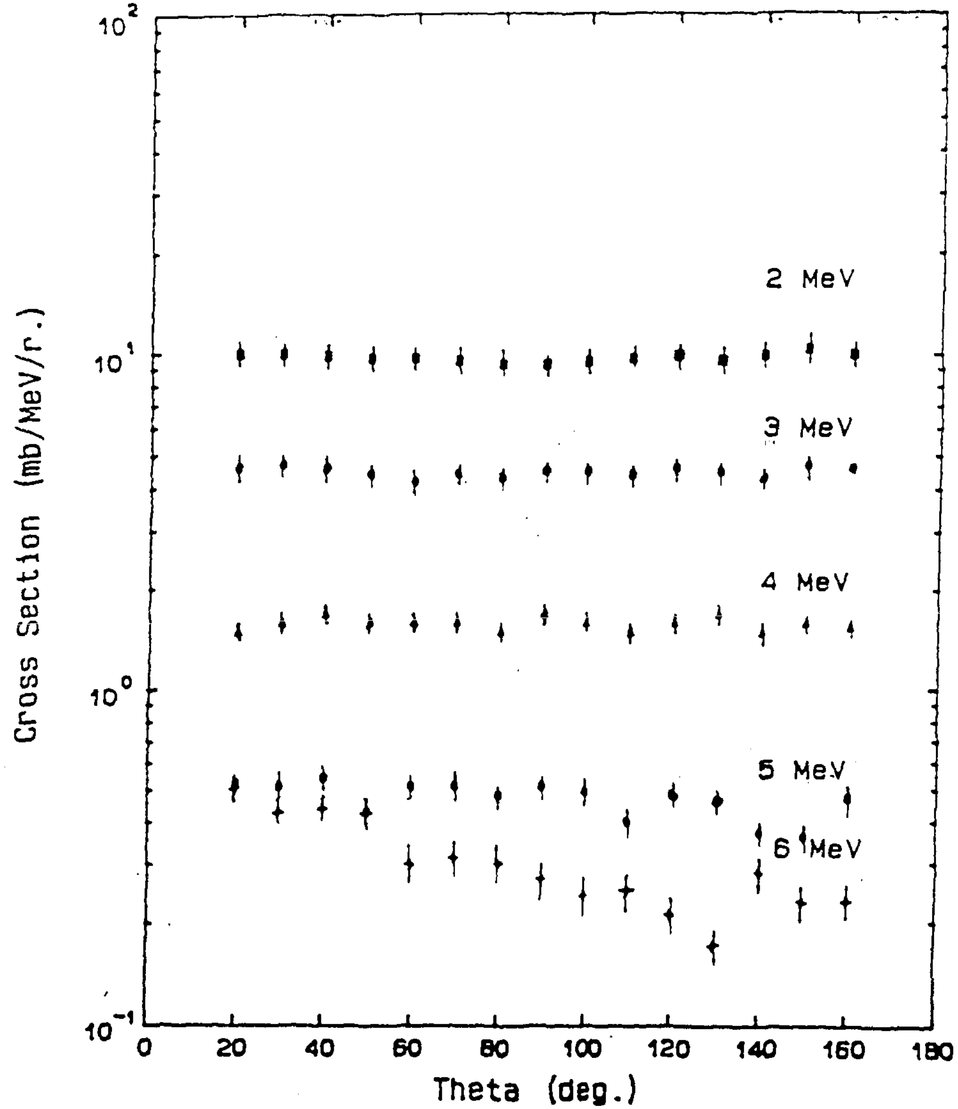

Fig.12 Angular Distribution of Mo100(p,n)Tc100 at 9 MeV

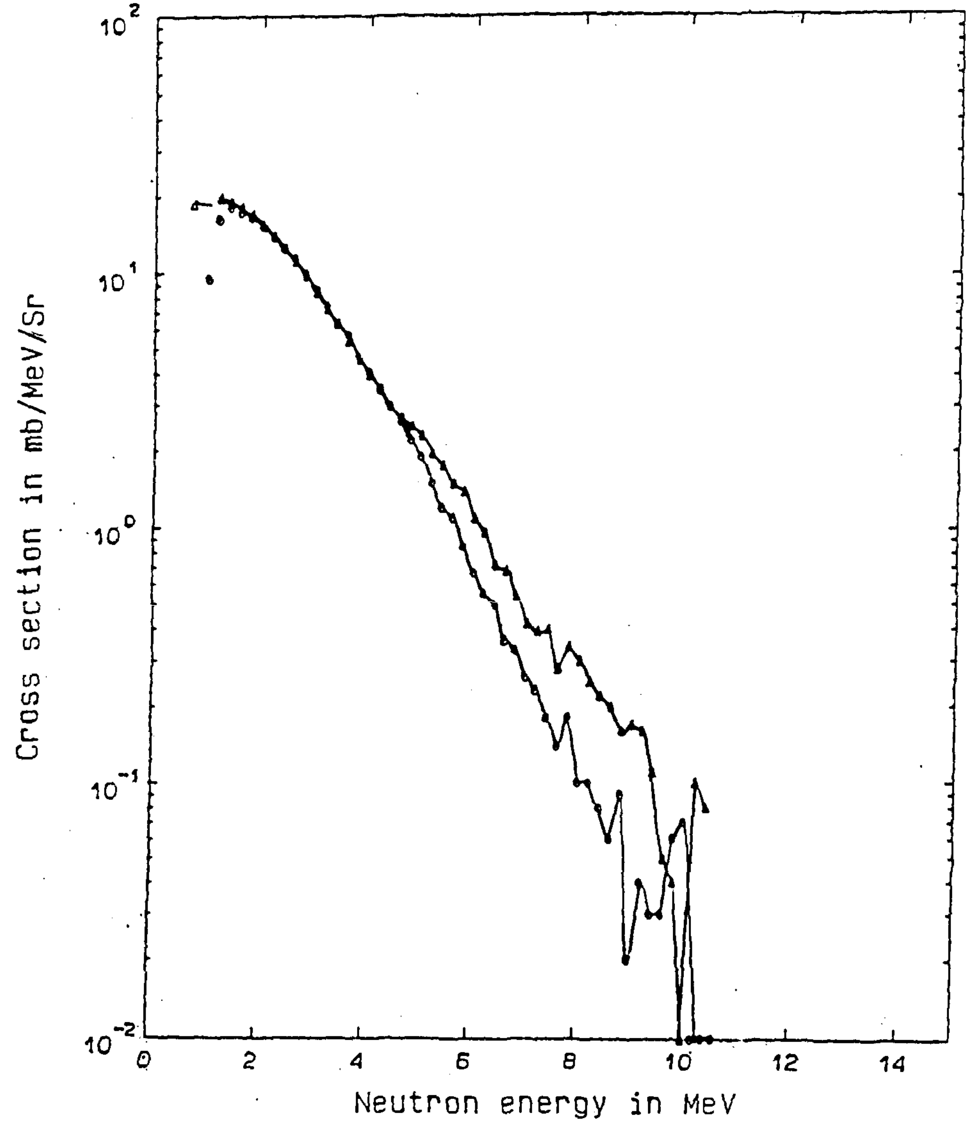

Fig.13 Neutron spectrum of the Mo-95(p,n)Tc-95 reaction

-o- Ep=12.93 MeV, 110°, present work

-▲- Ep=13.1 MeV, 105.5°, Univ. of Hamburg

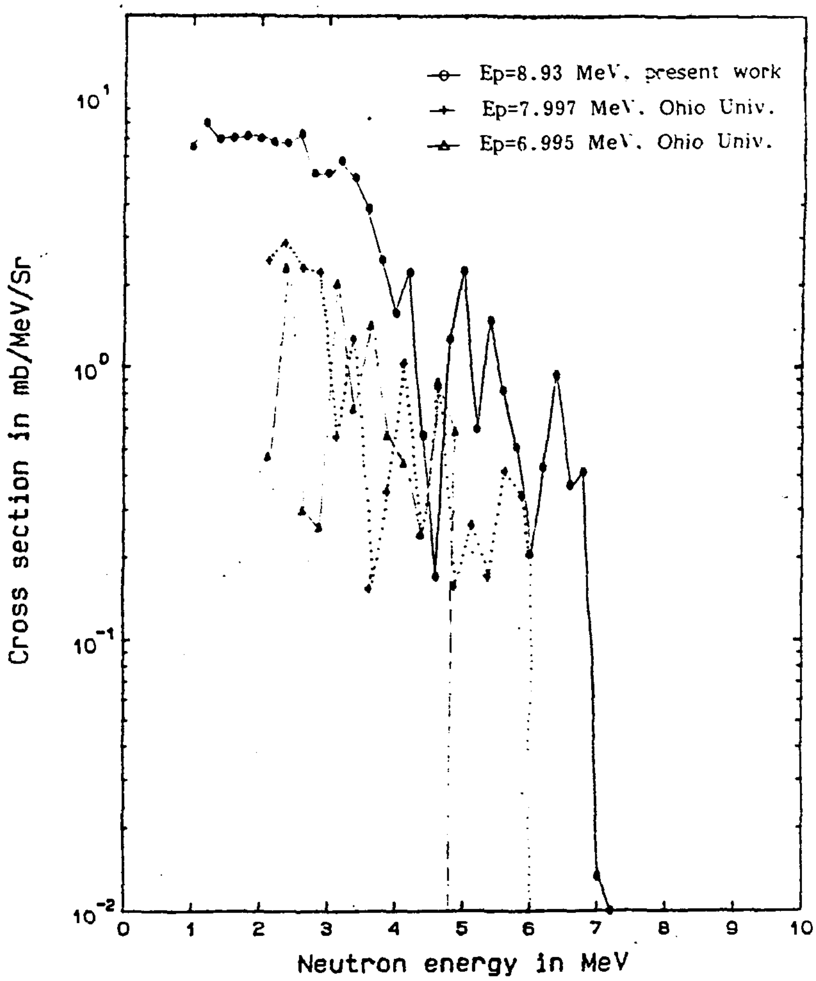

Fig.14 Spectrum of Co59(p, n)Ni59 at 50 deg.

Prior to the measurement, the consistance of different neutron detectors was checked by a radiative neutron source which was placed in the rotation center and in the horizontal plane of the detectors. During the experiment, it was checked by measuring the neutron TOF spectra at the same angle with different detectors. They are in good agreement.

To check the accuracy of determination of target thickness, the double differential neutron emission cross sections of the Mo-95(p,n)Tc-95 reaction using two different Mo-95 targets (one is home made, the other is borrowed from the University of Hamburg) were compared. Good agreement was found between these two Mo-95 targets. These indicates that the uncertainty of the target thickness given in table II is reliable.

A repeat measurement was performed on Mo-96 and Mo-97 at the incident proton energy of 9 MeV after more than half a year since the first measurement. The results of both measurements are consistant within the error.

5. Discussion

The neutron emission energy spectra of the Mo-97(p,n) Tc-97 reaction at 13 MeV proton energy measured by us and by W.Scoble et al.(2) in the University of Hamburg at the angle around 110 degrees are compared in fig.13. In the lower energy part of the spectra (less than 5 MeV), they are in good agreement. However, in the higher energy region they deviate each other. As the energy increases, the present data is lower than that of the University of Hamburg. We checked our measurement carefully, no reason has been found so far. The problem should be further studied.

The neutron emission spectrum of the Co-59(p,n)Ni-59 reaction was compared with the result of Ohio University(3), which is shown in fig.14. The shape of both spectra is similar. However, because the incident energy is different, the absolute value of double differential cross sections is hard to be compared.

6. Acknowledgement

The authers are grateful to professor W.Scoble for his kindness to lend us the Mo isotopic targets.

Reference

1. Sa Jun et al., A multi-detector fast neutron TOF spectrometer at HI-13 tandem accelerator, to be published
2. W.Scoble et al., Private communication
3. S.M.Grimes et al., Private communication

NEUTRON SPECTRA FROM THE (p,n) REACTIONS ON THE ^{165}Ho, ^{204}Pb, ^{206}Pb, ^{207}Pb, ^{208}Pb, ^{209}Bi NUCLEI AND NUCLEAR LEVEL DENSITY

Zhuravlev B.V., Birukov N.S., Rudenko A.P., Titarenko N.N., Trykova V.I.

Institute of Physics and Power Engineering, Obninsk, USSR

ABSTRACT

Neutron spectra from the (p,n) reaction on the ^{165}Ho, ^{207}Pb, ^{208}Pb, ^{209}Bi nuclei have been measured at the proton energy of 6.95$\pm$ 0.15 MeV. The experimental data together with the data obtained earlier at E_p=11 MeV on the ^{165}Ho, ^{204}Pb, ^{206}Pb, ^{207}Pb, ^{208}Pb, ^{209}Bi nuclei have been analyzed within the framework of a statistical nuclear reaction theory using the generalized model of a superfluid nucleus for the nuclear level density. The absolute nuclear level density has been determined in a wide range of excitation energies.

1. Introduction

Since 1986 a coordinated program of investigations "Measurement and analysis of double-differential neutron emission spectra in the (p,n) and (α,n) reactions" has been set up by the IAEA to obtain the information on the nuclear level density. Within the framework of this program the Institute of Physics and Power Engineering has been investigating the (p,n) reactions on the deformed and near-magic nuclei.

In the IPPE reports on the 4322/RO/CF and 4322/R1/CF agreements the measurement and analysis in the framework of the statistical theory of neutron spectra from the (p,n) reaction on the ^{165}Ho, ^{181}Ta, ^{197}Au, ^{204}Pb, ^{206}Pb, ^{207}Pb, ^{208}Pb, ^{209}Bi nuclei at the proton energy of 11 MeV were presented. In the present work the neutron spectra measurements on the ^{165}Ho, ^{207}Pb, ^{208}Pb, ^{209}Bi nuclei have been carried out at E_p=6.95 $\pm$ 0.15 MeV and analysed in the framework of the statistical theory as a continuation of these investigations. The joint analysis of the data obtained at the both proton energies made it possible to determine the absolute nuclear level density in a wide range of excitation energies.

2. Experiment

The measurements were carried out with the time-of-flight neutron spectrometer and the 150-cm cyclotron of the Institute of Physics and Power Engineering /1/. The proton energy mentioned above has been obtained under operating conditions of molecular hydrogen acceleration at the accelerating voltage frequency of 8.9 MHz. The metal foils 13.66, 18.90, 21.87, 13.20 mg/cm^2 thick for ^{165}Ho(99.9%), ^{207}Pb(93.2%), ^{208}Pb(98.3%) and ^{209}Bi (99.8%) respectively were used as targets. The average target current was 1 μA. Neutrons were registered by scintillation detector based on stilbene crystal (d 70 mm, h 50mm) and a photomultiplier FEU-30 with neutron and γ-ray identification on the principle of separate integration of the charge components /2/. Detector efficiency was determined by measuring of the ^{252}Cf prompt fission neutron spectrum by the time-of-flight method with fission fragment registration by a fast ionization chamber /3/. The NBS recommendation was used as a stadard spectrum /4/. The spectrometer time resolution determined from the γ-peak width at a half of the hight is 1.4 ns/m with a flight-path of 2.5 m. The channel width of a time analyzer is 0.89 ns. The minimum neutron energy in spectra is 0.65 MeV.

The neutron spectrum measuring procedure consisted in taking measurements with the target and without it per the equal proton flux registered by the current integrator with the Faraday cup as a current collector. Time of flight spectra measured on the ^{165}Ho nucleus are presented in Fig.1. The background was negligible and in fact non-correlated in time. For the ^{165}Ho and ^{209}Bi nuclei the spectra were measured in the angle range of 75°-150° at 15° interval. Figure 2 shows that the spectra measured at various angles on ^{165}Ho coincide within the limits

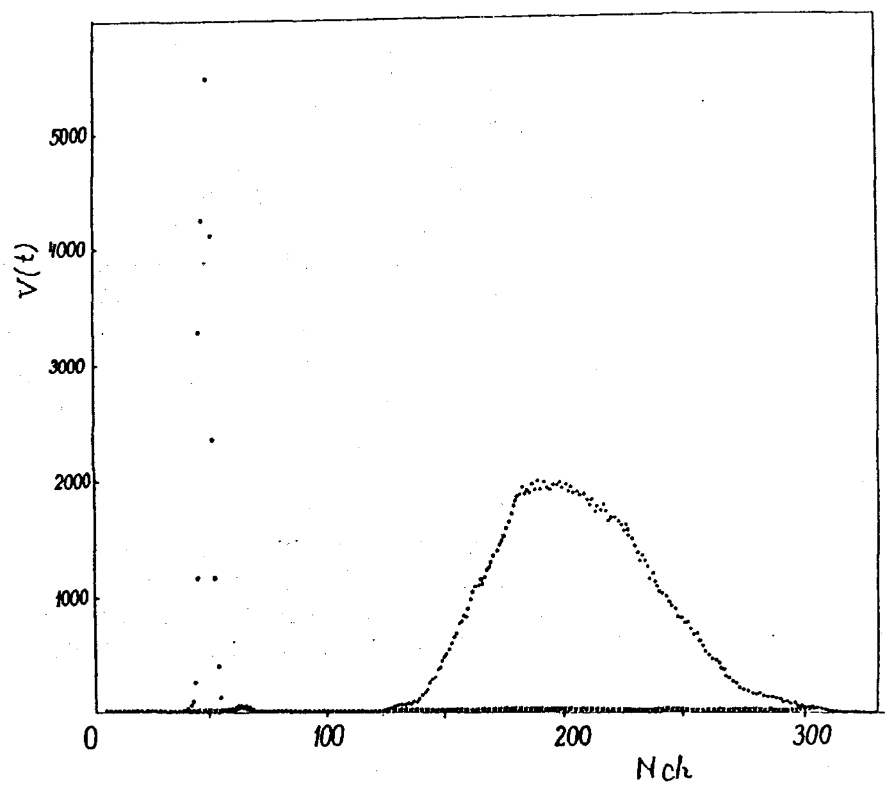

Fig.1. Time of flight spectra from the $^{165}Ho(p,n)$ reaction, θ =105°.
• - effect+background, x - background.

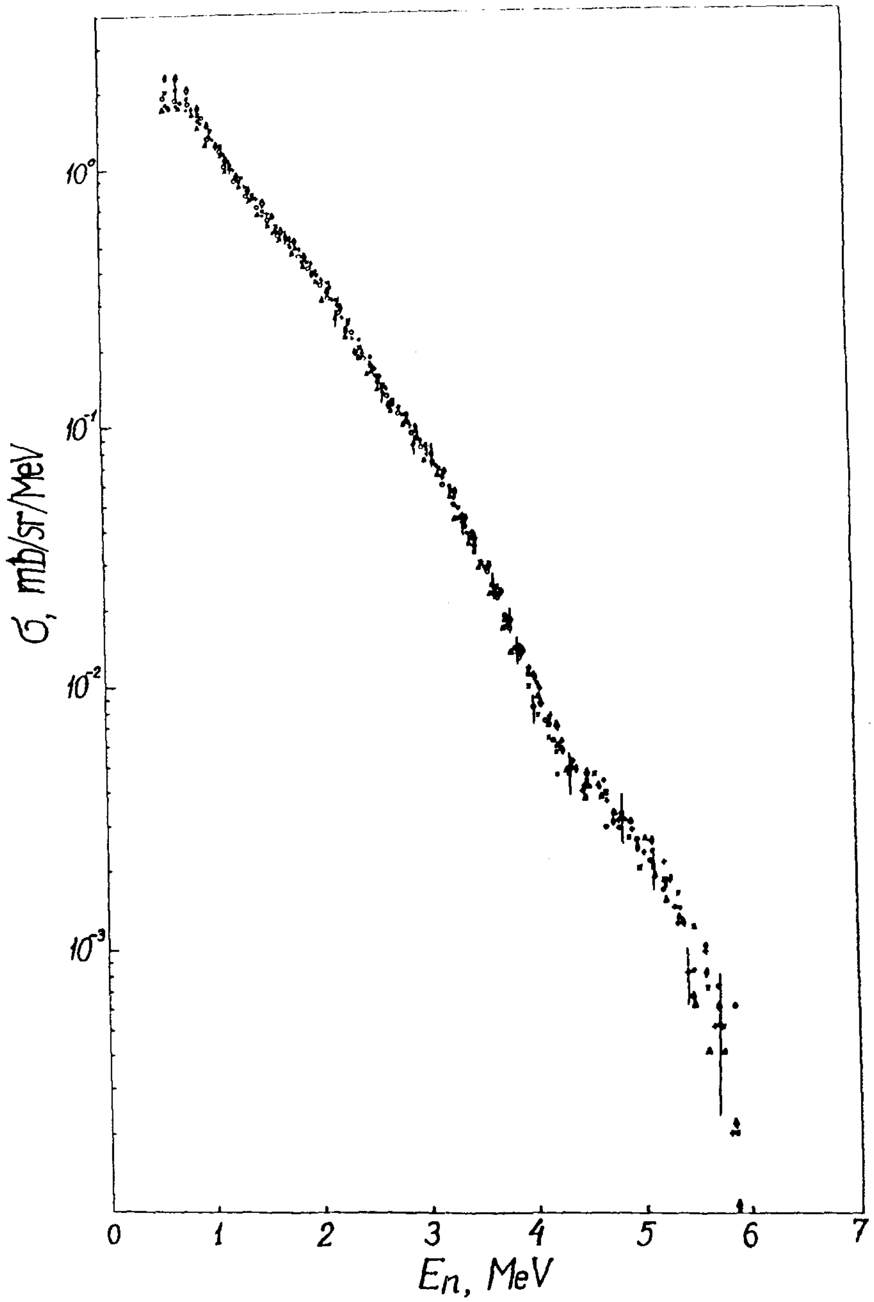

Fig.2. Neutron spectra from the $^{165}Ho(p,n)$ reaction, E_p=6.95 MeV.
• – 75°, x – 90°, o – 105°,
Δ – 120°, + – 135°, ◊ – 150°.

of measuring errors. In the reactions with the greater value of $Q_{p,n}$ the angular disribution should be all the more isotropic. Therefore the ^{207}Pb and ^{208}Pb nuclei measurements have been made only at the angle of 105°. The errors of neutron emission cross-section values measured are determined with allowance for the following factors:

1. The statistical measurement error varied from 1.5 % at E_n =1 MeV to 20 % at the maximum energies;
2. The error of neutron detector absolute efficiency determination – (3 – 5)% ;
3. The error of proton flux measurement – 3% ;
4. The error of target nuclei number determination – 2% ;

5. Errors related to spectrometer calibration $\leq 2\%$. Neutron spectra and measurement errors are presented in tables 1 - 3.

Table I

DOUBLE DIFFERENTIAL NEUTRON CROSS SECTIONS FROM THE REACTION $^{165}Ho(p,n)^{165}Er$ AT PROTON ENERGY 6.95 MEV IN CM-SYSTEM, MB/SR/MEV.

ANG,DEG	75		90		105		120		135		150		ANGLE INTEGRATED	
EN,MEV	σ	Δσ	σ	Δσ	σ	Δσ	σ	Δσ	σ	Δσ	σ	Δσ	σ	Δσ
0.65	1.792	0.108	2.034	0.120	1.895	0.110	1.697	0.101	1.745	0.103	2.419	0.138	23.593	1.238
0.75	1.756	0.097	2.097	0.115	1.833	0.100	1.742	0.095	1.833	0.100	2.405	0.129	23.677	1.224
0.85	1.722	0.092	1.921	0.102	1.736	0.092	1.689	0.090	1.716	0.091	2.128	0.113	22.359	1.149
0.95	1.545	0.082	1.647	0.087	1.522	0.080	1.443	0.076	1.475	0.078	1.734	0.091	19.344	0.993
1.05	1.443	0.076	1.429	0.075	1.312	0.069	1.263	0.067	1.276	0.067	1.471	0.077	17.058	0.875
1.15	1.233	0.065	1.221	0.064	1.143	0.060	1.126	0.059	1.135	0.060	1.265	0.066	14.821	0.760
1.25	1.065	0.056	1.054	0.056	0.983	0.052	0.983	0.052	0.992	0.052	1.099	0.058	12.841	0.658
1.35	0.917	0.049	0.928	0.049	0.867	0.045	0.852	0.045	0.865	0.046	0.955	0.050	11.184	0.574
1.46	0.790	0.042	0.797	0.042	0.767	0.040	0.762	0.040	0.759	0.040	0.846	0.045	9.794	0.503
1.56	0.650	0.035	0.688	0.037	0.671	0.036	0.673	0.036	0.674	0.036	0.751	0.040	8.470	0.435
1.66	0.601	0.032	0.605	0.032	0.588	0.031	0.596	0.032	0.606	0.032	0.653	0.035	7.561	0.389
1.75	0.546	0.030	0.539	0.029	0.522	0.028	0.531	0.028	0.544	0.029	0.584	0.031	6.774	0.349
1.85	0.498	0.027	0.480	0.026	0.475	0.026	0.474	0.026	0.488	0.026	0.526	0.028	6.107	0.315
1.95	0.445	0.024	0.439	0.024	0.425	0.023	0.421	0.023	0.428	0.023	0.448	0.024	5.427	0.280
2.05	0.406	0.022	0.393	0.022	0.376	0.020	0.361	0.020	0.367	0.020	0.378	0.021	4.777	0.247
2.14	0.348	0.020	0.358	0.020	0.323	0.018	0.310	0.017	0.311	0.017	0.328	0.018	4.138	0.215
2.23	0.308	0.017	0.290	0.016	0.278	0.016	0.263	0.015	0.260	0.015	0.281	0.016	3.530	0.184
2.34	0.252	0.014	0.256	0.015	0.235	0.013	0.218	0.012	0.219	0.013	0.233	0.013	2.962	0.155
2.45	0.216	0.014	0.201	0.012	0.191	0.011	0.184	0.011	0.186	0.011	0.196	0.011	2.466	0.130
2.54	0.185	0.011	0.170	0.011	0.163	0.010	0.161	0.010	0.159	0.010	0.169	0.011	2.117	0.112
2.65	0.141	0.009	0.145	0.009	0.138	0.008	0.137	0.008	0.136	0.009	0.145	0.009	1.749	0.093
2.75	0.121	0.008	0.128	0.009	0.117	0.008	0.116	0.008	0.117	0.007	0.122	0.008	1.500	0.081
2.85	0.111	0.008	0.111	0.008	0.102	0.007	0.100	0.006	0.101	0.007	0.105	0.007	1.319	0.072
2.94	0.098	0.007	0.097	0.007	0.089	0.006	0.084	0.006	0.088	0.006	0.091	0.006	1.142	0.063
3.05	0.081	0.006	0.083	0.006	0.075	0.005	0.073	0.005	0.077	0.005	0.077	0.006	0.974	0.054
3.15	0.069	0.005	0.068	0.005	0.061	0.005	0.065	0.005	0.065	0.005	0.066	0.005	0.821	0.046
3.27	0.058	0.004	0.056	0.004	0.051	0.004	0.054	0.004	0.053	0.004	0.055	0.004	0.681	0.038
3.36	0.048	0.004	0.044	0.004	0.043	0.003	0.044	0.004	0.045	0.004	0.044	0.004	0.562	0.032
3.45	0.038	0.003	0.038	0.003	0.035	0.003	0.035	0.003	0.037	0.003	0.037	0.003	0.459	0.027
3.54	0.028	0.003	0.030	0.003	0.029	0.003	0.029	0.003	0.029	0.003	0.030	0.003	0.363	0.022
3.65	0.024	0.002	0.024	0.002	0.023	0.002	0.022	0.002	0.022	0.002	0.024	0.002	0.291	0.018
3.75	0.020	0.002	0.018	0.002	0.018	0.002	0.016	0.002	0.017	0.002	0.018	0.002	0.225	0.014
3.86	0.013	0.002	0.014	0.002	0.014	0.002	0.013	0.002	0.014	0.002	0.014	0.002	0.169	0.011
3.97	0.0088	0.0012	0.0099	0.0013	0.0098	0.0013	0.0111	0.0013	0.011	0.001	0.011	0.001	0.127	0.009
4.06	0.0100	0.0013	0.0076	0.0011	0.0079	0.0011	0.0090	0.0012	0.0098	0.0013	0.0085	0.0011	0.111	0.009
4.14	0.0062	0.0010	0.0063	0.0010	0.0067	0.0010	0.0069	0.0010	0.0075	0.0011	0.0087	0.0013	0.086	0.007
4.22	0.0045	0.0008	0.0055	0.0009	0.0062	0.0009	0.0060	0.0009	0.0058	0.0009	0.0070	0.0011	0.071	0.006
4.35	0.0047	0.0008	0.0046	0.0008	0.0053	0.0008	0.0047	0.0008	0.0045	0.0007	0.0048	0.0008	0.060	0.005
4.49	0.0043	0.0008	0.0043	0.0008	0.0044	0.0007	0.0037	0.0007	0.0039	0.0007	0.0046	0.0008	0.053	0.005
4.58	0.0042	0.0008	0.0046	0.0008	0.0037	0.0007	0.0037	0.0006	0.0036	0.0006	0.0041	0.0007	0.050	0.005
4.68	0.0043	0.0008	0.0039	0.0007	0.0028	0.0006	0.0038	0.0007	0.0038	0.0007	0.0029	0.0003	0.046	0.004
4.79	0.0032	0.0007	0.0032	0.0006	0.0028	0.0006	0.0032	0.0006	0.0030	0.0005	0.0030	0.0003	0.039	0.004
4.89	0.0029	0.0006	0.0026	0.0006	0.0031	0.0006	0.0031	0.0006	0.0028	0.0006	0.0032	0.0004	0.037	0.004
5.00	0.0023	0,0005	0.0020	0.0006	0.0026	0.0006	0.0025	0.0006	0.0023	0.0005	0.0024	0.0003	0.029	0.003
5.11	0.0023	0.0005	0.0020	0.0005	0.0021	0.0006	0.0018	0.0005	0.0024	0.0005	0.0026	0.0003	0.027	0.003
5.23	0.0024	0.0004	0.0018	0.0005	0.0017	0.0006	0.0015	0.0004	0.0021	0.0005	0.0018	0.0002	0.024	0.003
5.35	0.0014	0.0004	0.0016	0.0004	0.0012	0.0004	0.0013	0.0004	0.0014	0.0006	0.0012	0.0002	0.017	0.002
5.47	0.0012	0.0004	0.0012	0.0004	0.0008	0.0003	0.0006	0.0004	0.0008	0.0003	0.0006	0.0001	0.011	0.002
5.60	0.0010	0.0003	0.0007	0.0003	0.0007	0.0003	0.0004	0.0003	0.0010	0.0004	0.0008	0.0001	0.010	0.002
5.73	0.0005	0.0003	0.0005	0.0003	0.0007	0.0003	0.0004	0.0003	0.0005	0.0004	0.0006	0.0001	0.007	0.002
5.87	0.0001	0.0001	0.0002	0.0002	0.0006	0.0002	0.0001	0.0001	0.0002	0.0001	0.0002	0.0001	0.003	0.001

3. Calculation

The analysis of spectra measured was carried out within the framework of Hauser-Feshbach formalism with the nuclear level density according to the superfluid nucleus model with regard to shell effects and collective modes' contribution /5,6/.

Table 2 : Double differential neutron cross sections from the reaction $^{207}Pb(p,n)^{207}Bi$ and $^{208}Pb(p,n)^{208}Bi$ at proton energy 6.95 MeV in cm-system, mb/sr/MeV.

ISOTOPE	207-Pb			208-Pb	
ANG,DEG	105°			105°	
EN,MEV	σ	$\Delta\sigma$	EN,MEV	σ	$\Delta\sigma$
0.65	0.147	0.012	0.65	0.155	0.012
0.75	0.146	0.010	0.75	0.135	0.009
0.85	0.164	0.010	0.85	0.132	0.008
0.95	0.173	0.010	0.95	0.133	0.008
1.05	0.169	0.009	1.05	0.121	0.007
1.15	0.169	0.009	1.15	0.113	0.006
1.25	0.159	0.009	1.25	0.122	0.007
1.35	0.153	0.008	1.35	0.127	0.007
1.45	0.149	0.008	1.45	0.111	0.006
1.55	0.136	0.007	1.55	0.099	0.006
1.65	0.138	0.008	1.65	0.104	0.006
1.75	0.145	0.008	1.75	0.096	0.005
1.85	0.124	0.007	1.85	0.103	0.006
1.95	0.114	0.006	1.95	0.118	0.007
2.05	0.110	0.006	2.05	0.137	0.007
2.14	0.088	0.005	2.14	0.142	0.008
2.24	0.071	0.004	2.24	0.125	0.007
2.34	0.062	0.004	2.34	0.094	0.005
2.45	0.045	0.003	2.45	0.068	0.004
2.55	0.034	0.002	2.55	0.049	0.003
2.64	0.028	0.002	2.64	0.034	0.002
2.75	0.021	0.002	2.75	0.024	0.002
2.86	0.016	0.001	2.86	0.023	0.002
2.96	0.012	0.001	2.96	0.022	0.002
3.07	0.0079	0.0008	3.07	0.020	0.002
3.15	0.0055	0.0006	3.15	0.016	0.001
3.24	0.0042	0.0005	3.24	0.010	0.001
3.36	0.0046	0.0005	3.36	0.005	0.001
3.45	0.0051	0.0006			
3.55	0.0051	0.0006			
3.65	0.0046	0.0005			
3.76	0.0029	0.0004			
3.87	0.0017	0.0003			

$$\rho(U,J) = \rho_{BCS}(U,J) \cdot K_{vib}(U) \cdot K_{rot}(U) \;, \tag{1}$$

$$K_{rot} = \begin{cases} 1 - & \text{for spherical nuclei,} \\ \mathcal{F}_{\perp} \cdot t - & \text{for deformed nuclei} \end{cases} \tag{2}$$

$$K_{vib} = \exp\Big\{ \sum_i (2\lambda_i + 1)\left[(1+\bar{n}_i)\cdot \ln(1+\bar{n}_i) - \bar{n}_i \cdot \ln \bar{n}_i\right] - \\ - \sum_i (2\lambda_i + 1)\cdot \omega_i \cdot \bar{n}_i / t \Big\} \,, \tag{3}$$

$\mathcal{F}_{\perp}$ is the perpendicular moment of inertia;
ω_i is the vibrating state energy;
λ_i is the degree of degeneracy;
$\bar{n}_i$ is the mean occupation numbers at the given temperature t.

Table 3 :

DOUBLE DIFFERENTIAL NEUTRON CROSS SECTIONS FROM THE REACTION $^{209}Bi(p,n)^{209}Po$ AT PROTON ENERGY 6.95 MEV IN CM-SYSTEM,MB/SR/MEV.

ANG,DEG	75		90		I05		I20		I35		I50		ANGLE INTEGRATED	
EN,MEV	σ	$\Delta\sigma$	σ	$\Delta\sigma$	σ	$\Delta\sigma$	σ	$\Delta\sigma$	σ	$\Delta\sigma$	σ	$\Delta\sigma$	σ	$\Delta\sigma$
0.65	0.26I	0.034	0.I7I	0.027	0.I40	0.026	0.2I6	0.03I	0.405	0.046	0.36I	0.04I	3.I02	0.228
0.75	0.327	0.027	0.278	0.025	0.I96	0.020	0.268	0.024	0.277	0.027	0.468	0.035	3.647	0.2I7
0.85	0.282	0.020	0.240	0.0I9	0.227	0.0I8	0.279	0.02I	0.295	0.022	0.4I0	0.028	3.50I	0.I95
0.95	0.252	0.0I7	0.26I	0.0I8	0.24I	0.0I7	0.270	0.0I8	0.26I	0.0I8	0.330	0.022	3.297	0.I79
I.05	0.274	0.0I7	0.255	0.0I6	0.22I	0.0I5	0.228	0.0I5	0.244	0.0I6	0.283	0.0I8	3.I23	0.I68
I.I5	0.279	0.0I7	0.236	0.0I5	0.225	0.0I4	0.239	0.0I5	0.236	0.0I5	0.272	0.0I7	3.II4	0.I66
I.25	0.223	0.0I3	0.233	0.0I4	0.2I7	0.0I3	0.I83	0.0I2	0.I94	0.0I3	0.229	0.0I5	2.660	0.I42
I.35	0.I96	0.0I2	0.I92	0.0I2	0.I72	0.0II	0.I37	0.009	0.I4I	0.0I0	0.I80	0.0I2	2.I4I	0.II5
I.45	0.I47	0.009	0.I22	0.008	0.I24	0.008	0.I24	0.008	0.I30	0.009	0.I42	0.0I0	I.653	0.090
I.55	0.II5	0.008	0.II9	0.008	0.II3	0.008	0.I40	0.009	0.I50	0.0I0	0.I36	0.009	I.586	0.086
I.65	0.I38	0.008	0.I46	0.009	0.I46	0.009	0.I40	0.009	0.I50	0.0I0	0.I53	0.0I0	I.806	0.097
I.74	0.I70	0.0II	0.I58	0.0I0	0.I65	0.0II	0.I3I	0.009	0.I40	0.0I0	0.I59	0.0I0	I.942	0.I05
I.84	0.I57	0.0I0	0.I54	0.0I0	0.I46	0.0I0	0.II6	0.008	0.II9	0.008	0.I47	0.0I0	I.764	0.095
I.94	0.I29	0.009	0.II7	0.008	0.III	0.008	0.I03	0.008	0.099	0.007	0.I2I	0.008	I.430	0.079
2.05	0.099	0.007	0.092	0.007	0.096	0.006	0.083	0.006	0.084	0.007	0.098	0.007	I.I59	0.064
2.I6	0.082	0.006	0.083	0.006	0.080	0.006	0.070	0.006	0.073	0.005	0.087	0.007	0.988	0.056
2.25	0.070	0.006	0.072	0.006	0.07I	0.006	0.066	0.005	0.064	0.005	0.074	0.006	0.869	0.050
2.36	0.063	0.005	0.063	0.005	0.055	0.005	0.058	0.005	0.055	0.005	0.064	0.005	0.745	0.043
2.45	0.057	0.006	0.054	0.004	0.052	0.006	0.049	0.004	0.054	0.006	0.06I	0.006	0.678	0.042
2.55	0.050	0.004	0.045	0.005	0.048	0.004	0.040	0.005	0.047	0.004	0.059	0.005	0.598	0.036
2.65	0.045	0.005	0.043	0.004	0.045	0.005	0.034	0.004	0.037	0.005	0.053	0.006	0.532	0.035
2.74	0.038	0.003	0.034	0.004	0.037	0.004	0.03I	0.003	0.027	0.004	0.045	0.005	0.438	0.028
2.85	0.030	0.004	0.028	0.004	0.03I	0.003	0.026	0.003	0.0I9	0.003	0.032	0.003	0.35I	0.024
2.97	0.024	0.003	0.025	0.003	0.023	0.003	0.0I8	0.003	0.0I6	0.003	0.020	0.003	0.266	0.020
3.05	0.0I7	0.003	0.02I	0.003	0.0I5	0.003	0.0I4	0.002	0.0I4	0.002	0.0I5	0.002	0.I97	0.0I6
3.I3	0.0I5	0.002	0.0I5	0.002	0.0I5	0.002	0.0I2	0.002	0.0II	0.002	0.0I3	0.002	0.I72	0.0I4

3.24	0.014	0.002	0.014	0.002	0.014	0.002	0.011	0.002	0.010	0.002	0.012	0.002	0.157	0.013
3.36	0.0127	0.0020	0.0124	0.0020	0.0119	0.0020	0.0097	0.0018	0.0102	0.0019	0.0129	0.0020	0.146	0.012
3.46	0.0140	0.0021	0.0104	0.0018	0.0105	0.0019	0.0099	0.0017	0.0068	0.0019	0.0138	0.0021	0.138	0.012
3.55	0.0115	0.0019	0.0104	0.0018	0.0107	0.0018	0.0076	0.0017	0.0048	0.0012	0.0109	0.0021	0.119	0.011
3.65	0.0123	0.0019	0.0070	0.0015	0.0066	0.0016	0.0061	0.0013	0.0036	0.0013	0.0063	0.0016	0.094	0.010
3.76	0.0052	0.0013	0.0055	0.0013	0.0049	0.0012	0.0057	0.0013	0.0029	0.0009	0.0044	0.0011	0.061	0.007
3.87	0.0051	0.0012	0.0046	0.0011	0.0045	0.0011	0.0041	0.0012	0.0031	0.0009	0.0052	0.0011	0.056	0.007
3.94	0.0057	0.0012	0.0026	0.0010	0.0032	0.0011	0.0039	0.0010	0.0027	0.0010	0.0045	0.0020	0.049	0.007
4.02	0.0044	0.0011	0.0019	0.0007	0.0013	0.0010	0.0036	0.0011	0.0022	0.0008	0.0022	0.0006	0.034	0.005
4.15	0.0051	0.0011	0.0019	0.0007	0.0022	0.0007	0.0012	0.0011	0.0018	0.0008	0.0035	0.0009	0.035	0.005
4.27	0.0031	0.0009	0.0022	0.0007	0.0033	0.0009	0.0010	0.0004	0.0033	0.0008	0.0035	0.0010	0.034	0.005
4.36	0.0028	0.0008	0.0020	0.0007	0.0016	0.0010	0.0022	0.0006	0.0035	0.0011	0.0036	0.0009	0.032	0.005
4.45	0.0022	0.0007	0.0010	0.0007	0.0012	0.0006	0.0022	0.0009	0.0027	0.0007	0.0042	0.0010	0.028	0.004

$$\bar{n}_i = \frac{\exp\left(- \frac{C_v \cdot (\omega_i^2 + 4\pi^2 t^2)}{\omega_i} \right)}{\exp(-\omega_i/t) - 1} \qquad (4)$$

C_v is the constant of level density vibrating enhancement. The nuclear level density in the superfluid nucleus model can be presented in the follwing form:

$$\rho_{BCS} = \frac{(2J+1)}{2\sqrt{2\pi} \cdot \sigma^3_{eff} \cdot Det^{1/2}} \cdot \exp\left\{ S - \frac{(J+1/2)^2}{2\sigma^2_{eff}} \right\} . \qquad (5)$$

The relationship between the entropy S, preexponential factor Det and other thermodynamic functions and the excitation energy is determined by the equations of superfluid nucleus model state /5/. The main parameters of the model are the correlation function "Δ_0" and the parameter of level density "a". Above the critical point the superfluid nucleus model equations differ from the Fermi-gas model equations only by a shift of excitation energy equal to the energy of condensation $(E_{cond} = \frac{3}{2\pi^2} \cdot a_{cr} \cdot \Delta_o^2)$.

To take into account the shell effects the authors of the Ref. /5/ suggested to use the empirical "a"-parameter dependence on the excitation energy and shell correction in nuclear binding energy "$\delta W(Z,A)$".

$$a(U,Z,A) = \begin{cases} \tilde{a} \cdot \left[1 + (1-\exp(-\gamma \cdot U_{eff})) \cdot \frac{\delta W(Z,A)}{U_{eff}}\right] & \text{for } U > U_{cr} \\ a_{cr}(U_{cr}, Z, A) & \text{for } U \leq U_{cr} \end{cases} \qquad (6)$$

Even-odd differences in thermodynamic functions are determined by the shift of the ground state energy.

$$U = U_{eff} + \begin{cases} 0 - & \text{for even-even nuclei} \\ \Delta_o - & \text{for odd nuclei} \\ 2\Delta_o - & \text{for odd-odd nuclei} \end{cases} \qquad (7)$$

The correlation function for a one-component description was determined by Δ_{OZ} and Δ_{ON} /7/ in the following way:

$$\Delta_0 = \frac{\sqrt{\Delta^2_{ON} + \Delta^2_{OZ} \cdot (Z/N)^{1/3}}}{\sqrt{1 + (Z/N)^{1/3}}} . \qquad (8)$$

All calculations within the framework of the opticostatistical approach have been made according to the SMT-80 code /8/. When the excitation energy was below the U_c value, transitions

Table 4 : The parameters of the nuclear level density.

Parameter / Residual nucleus	O.P.	U_c, MeV	N_{lev},	$\tilde{a}$, MeV^{-1}	Δ_o, MeV	δW, MeV	γ, MeV	K_{rot}	C_v, MeV^{-1}	ω_{2^+}, MeV	ω_{3^-}, MeV	$\bar{D}_o$, eV	$Q_{p,n}$, MeV
^{165}Er	p /9/ n /10/	0.92	20	15.40	1.04	-0.17	0.073	$\mathcal{F}_{\perp} \cdot t$ (β =0.3)	0.0300	0.50	1.00	23 20±3 /13/ 22 /14/	-1.155
^{204}Bi	p /9/ n /9/	1.00	3	19.00	0.70	-8.65	0.070	1	0.0294	0.90	1.44	383	-5.177
^{206}Bi	p /9/ n /9/	1.00	3	19.18	0.58	-9.42	0.070	1	0.0295	0.45	1.43	753	-4.433
^{207}Bi	p /9/ n /9/	1.00	6	19.27	0.54	-9.96	0.050	1	0.0296	0.30	1.43	109	-3.188
^{208}Bi	p /9/ n /9/	1.00	12	19.36	0.47	-11.09	0.047	1	0.0296	0.35	1.42	313	-3.651
^{209}Po	p /9/ n /10/	1.00	3	19.46	0.62	-9.71	0.048	1	0.0250	0.50	1.42	1925	-2.675

to the discrete nuclear levels were calculated. Cross-section values obtained to be compared with the experimental data were averaged over excitation energy in terms of the normal law. The distribution dispersion corresponded to the spectrometer energy resolution. To calculate particle emission spectra above U_c all the excitation energy area was devided with the equable interval (~ 0.2 MeV) into a number of quasilevels. Each interval was assumed to have up to 30 different spin states of one parity and the same number of another parity with the $\rho(U,J)$ probability. Then such quasi-levels were processed as usual discrete nuclear states with efficient transmission coefficients. Calculations were made using the global optical potential systematics obtained in the investigations /9,10/.

The equations (1 - 8) show that in the generalized superfluid nucleus model there are rather many parameters - $\tilde{a}$, Δ_o, δW, γ , C_v, ω_i . However some of them can be determined from the independent experimental data. In the investigations /5,6/ the $\tilde{a}$ values were obtained from the analysis of experimental data on $\rho(B_n,J)$.

$$\tilde{a} = 0.0931 \cdot A \qquad (9)$$

The experimentally-based determination of correlation functions for the proton Δ_{OZ} and neutron Δ_{ON} systems has been made from the nuclei mass difference in the Ref./7/ and according to (8) Δ_o is calculated.

The values of shell correction δW were determined in the Ref. /11/ on the basis of experimental data on the mass-defect value and its liquid-drop component. In the Ref. /5/ the value of 0.064 MeV^{-1} is recommended for the γ parameter reflecting the energy dependence of the nuclear level density parameter and in the Ref. /12/ this value is equal to $0.4/A^{1/3}$ MeV^{-1}. These both recommendations are based on the analysis of the data on neutron resonance density $\rho(B_n,J)$, embracing a rather narrow range of excitation energies, and refer to the A - averaged description. The values of energies of the first vibrating

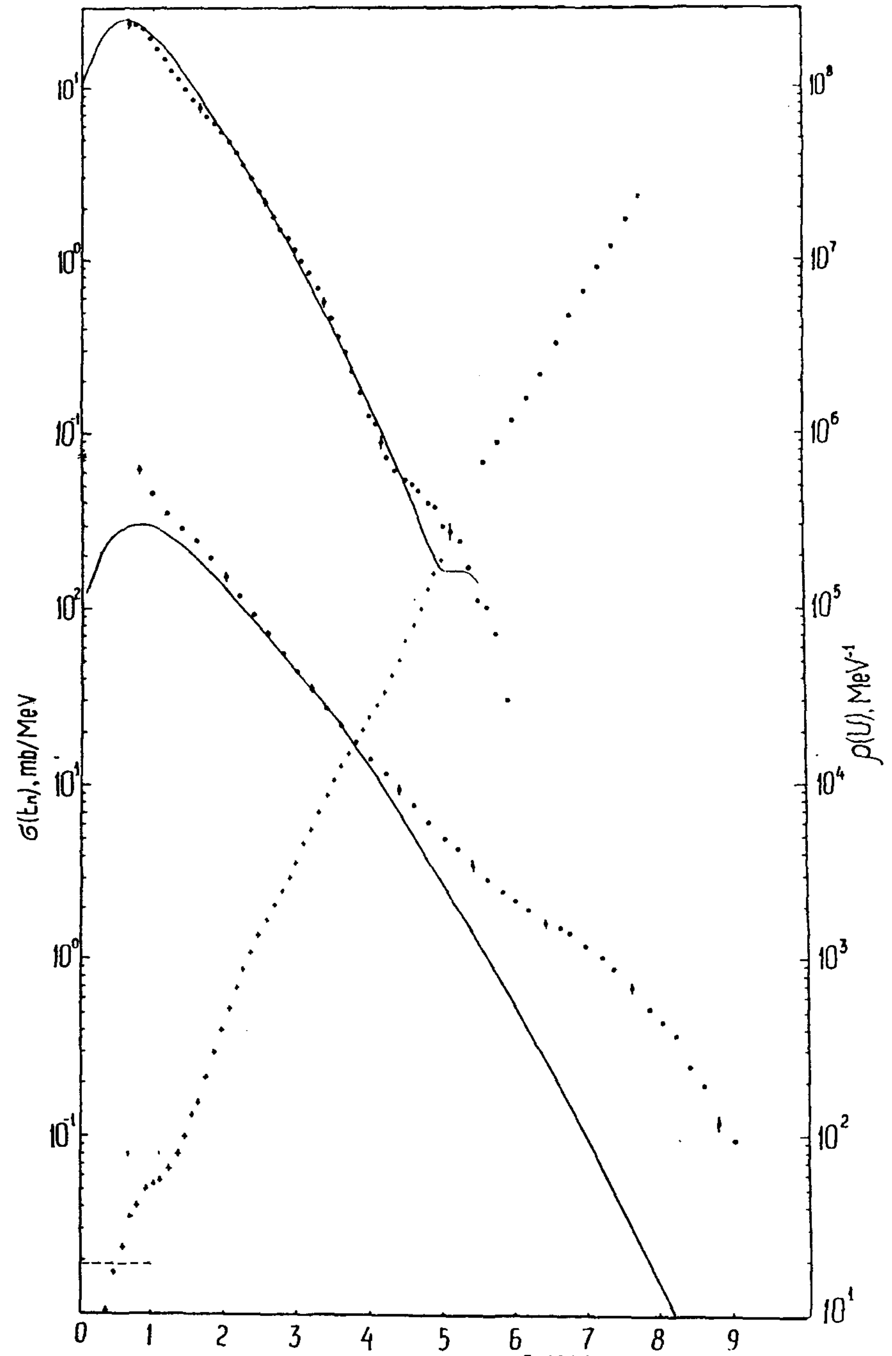

Fig.3. Integral neutron spectra from the $^{165}Ho(p,n)^{165}Er$ reaction at E_p=6.95 MeV (top) and 11.2 MeV (bottom). Curves - calculations. + and o are the absolute level density (right scale), determined from the data at E_p=6.95 MeV and 11.2 MeV, respectively. The horizontal dotted line shows level density at low excitation energy according to the level scheme /16/.

states ω_i and that of the enhancement factor C_v for odd and odd-odd nuclei, investigated in the present paper, can significantly differ from the even-even nuclei recommendations. Therefore in calculations these parameters (γ, ω_i, C_v) varied in searching for the agreement with the neutron spectra measured.

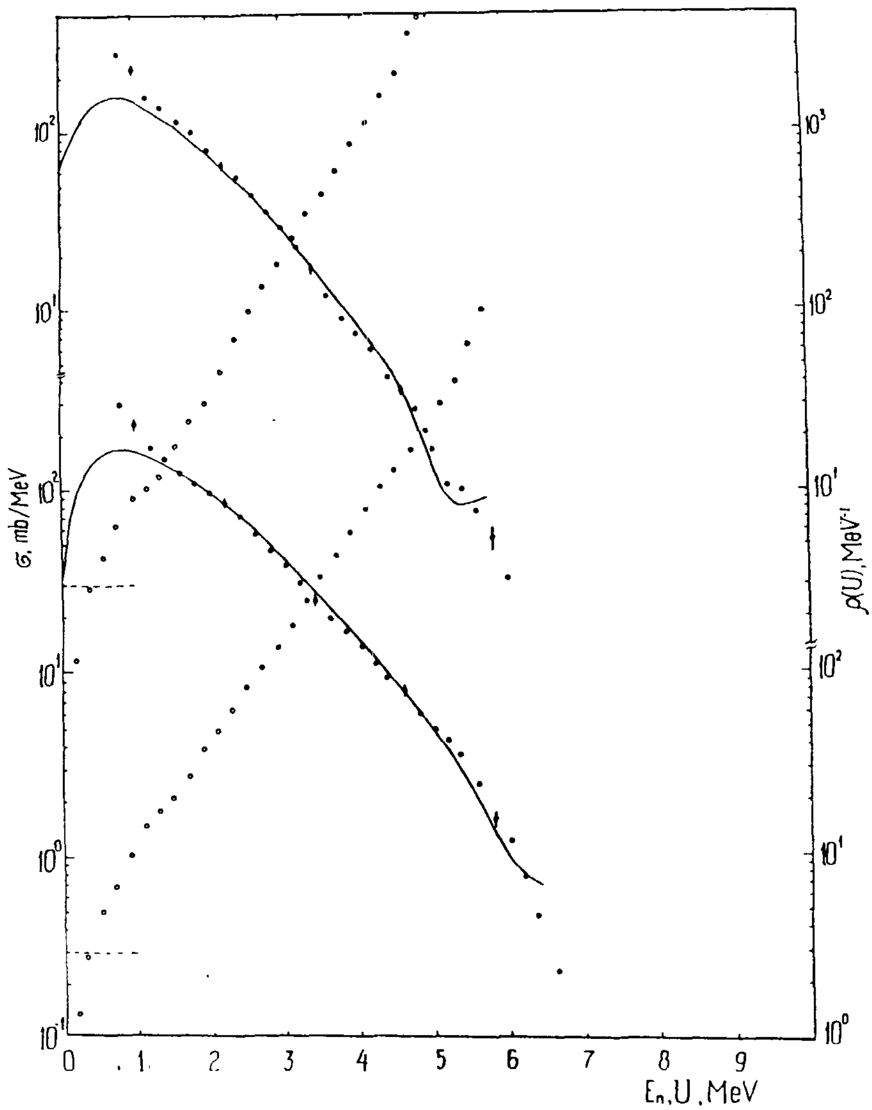

Fig.4. Integral neutron spectra from the $^{204}Pb(p,n)^{204}Bi$ reaction (top) and the $^{206}Pb(p,n)^{206}Bi$ reaction (bottom) at E_p=11.2 MeV.
Designation is the same as in Fig.3.

4. Results

Figures 3 - 7 show the neutron spectra from the (p,n) reaction on the ^{165}Ho, ^{204}Pb, ^{206}Pb, ^{207}Pb, ^{208}Pb, ^{209}Bi nuclei, measured at the proton energies of 6.95 and 11.2 MeV and the calculational results with the parameters presented in tables. At first calculations were made for $E_p=6.95\pm0.15$ MeV, because for such energy the contribution of non-equilibrium processes can be neglected. The agreement of absolute cross-section values was achieved by the proton energy variation within the limits of its uncertainty. A satisfactory description of the spectra from the (p,n) reaction on the ^{165}Ho, ^{208}Pb, ^{209}Bi nuclei can be observed. For ^{207}Pb a somewhat better agreement with the experiment is achieved for the calculation with the level density according to the Fermi-gas model with the parameters

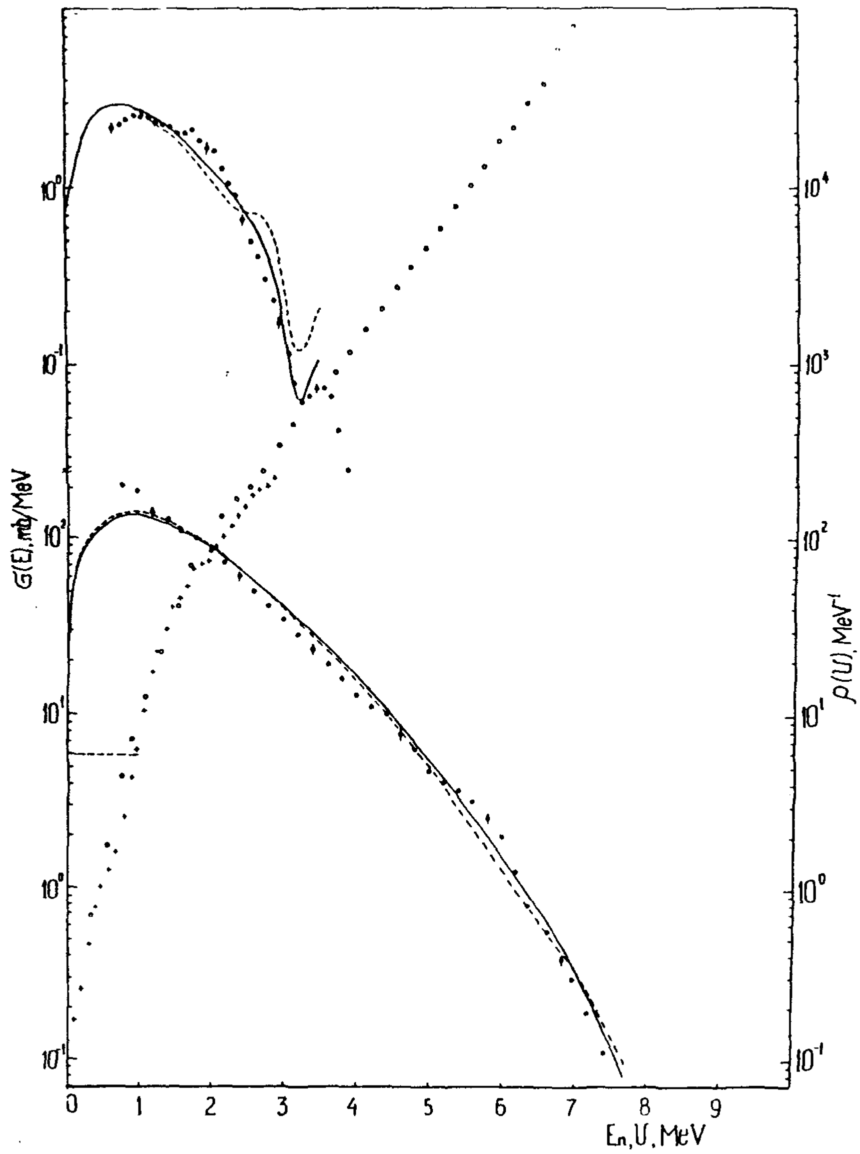

Fig.5. Integral neutron spectra from the $^{207}Pb(p,n)^{207}Bi$ reaction at E_p=6.95 MeV (top) and 11.2 MeV (bottom). Curves - calculations: - - - is a superfluid nucleus model, ——— is a back-shifted Fermi-gas model (a =12.5 MeV^{-1}, Δ =-0.9 MeV).

a =12.5 Mev^{-1}, Δ =-0.9 MeV. Then neutron spectra were calculated at E_p=11.2 MeV with the parameters determined at E_p=6.95 MeV. The comparison of the spectra calculated and measured for ^{207}Pb and ^{208}Pb shows the mechanism of the (p,n) reaction on these nuclei at E_p=11.2 MeV to be compound. It allows to suppose the identical mechanism for the reactions on ^{204}Pb and ^{206}Pb nuclei having a higher values of threshold energy $Q_{p,n}$ and to determine the parameters of nuclear level density from the spectra measured. With the $Q_{p,n}$ decrease, that corresponds to the increase of the energy of the neutrons emitted and of the nucleus excitation energy, a non-equilibrium neutron emission appears

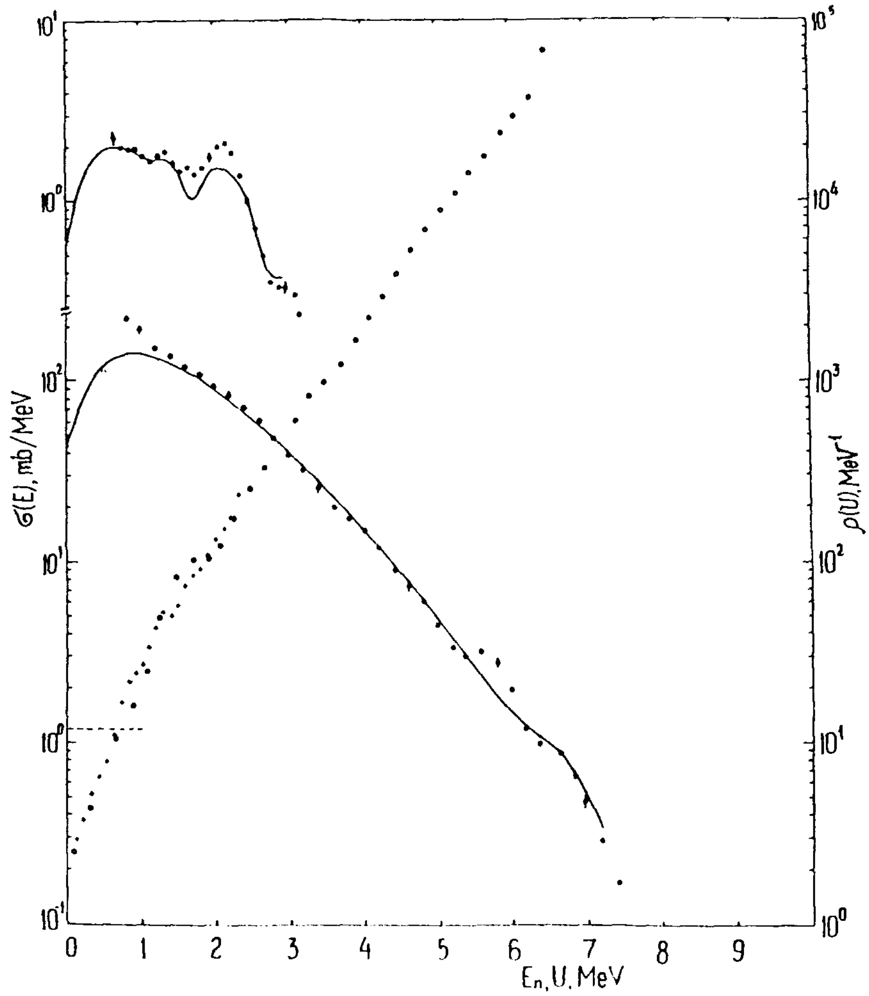

Fig.6. Integral neutron spectra from the $^{208}Pb(p,n)^{208}Bi$ reaction at E_p=6.95 MeV (top) and 11.2 MeV (bottom). Designations are the same as in Fig.3.

in the high-energy part of spectra in the $^{209}Bi(p,n)$ reaction and to a greater extent in the $^{165}Ho(p,n)$ reaction.

Let us discuss the values of nuclear level density parameters varied in searching for the optimal description of the neutron spectra measured. The "γ" parameter for the ^{165}Er, ^{204}Bi and ^{206}Bi nuclei is in good agreement with the recommendation /12/ but is $\sim$ 1.5 times lower for ^{207}Bi, ^{208}Bi, ^{209}Po. This fact corresponds to a weaker energy dependence of the nuclear level density parameter "a" for the nuclei close to the double-magic one (82, 126). The vibrating enhancement of the level density, calculated in terms of the expressions (3, 4), is very sensitive to the energies of the first 2^+, for which there is the vast experimental material for even-even spherical nuclei. The ω_{2^+} values obtained for ^{204}Bi and ^{209}Po are close to the known values for ^{202}Pb(0.96 MeV) and ^{208}Po(0.66 MeV), but for the ^{206}Bi, ^{207}Bi, ^{208}Bi nuclei the values are half as much as the corresponding values for ^{204}Pb and ^{206}Pb. The values of a vibrating enhancement factor C_v are close to the recommendation of the work /6/ (C_v=0.05$\cdot$ $A^{1/3}$MeV^{-1}) obtained from

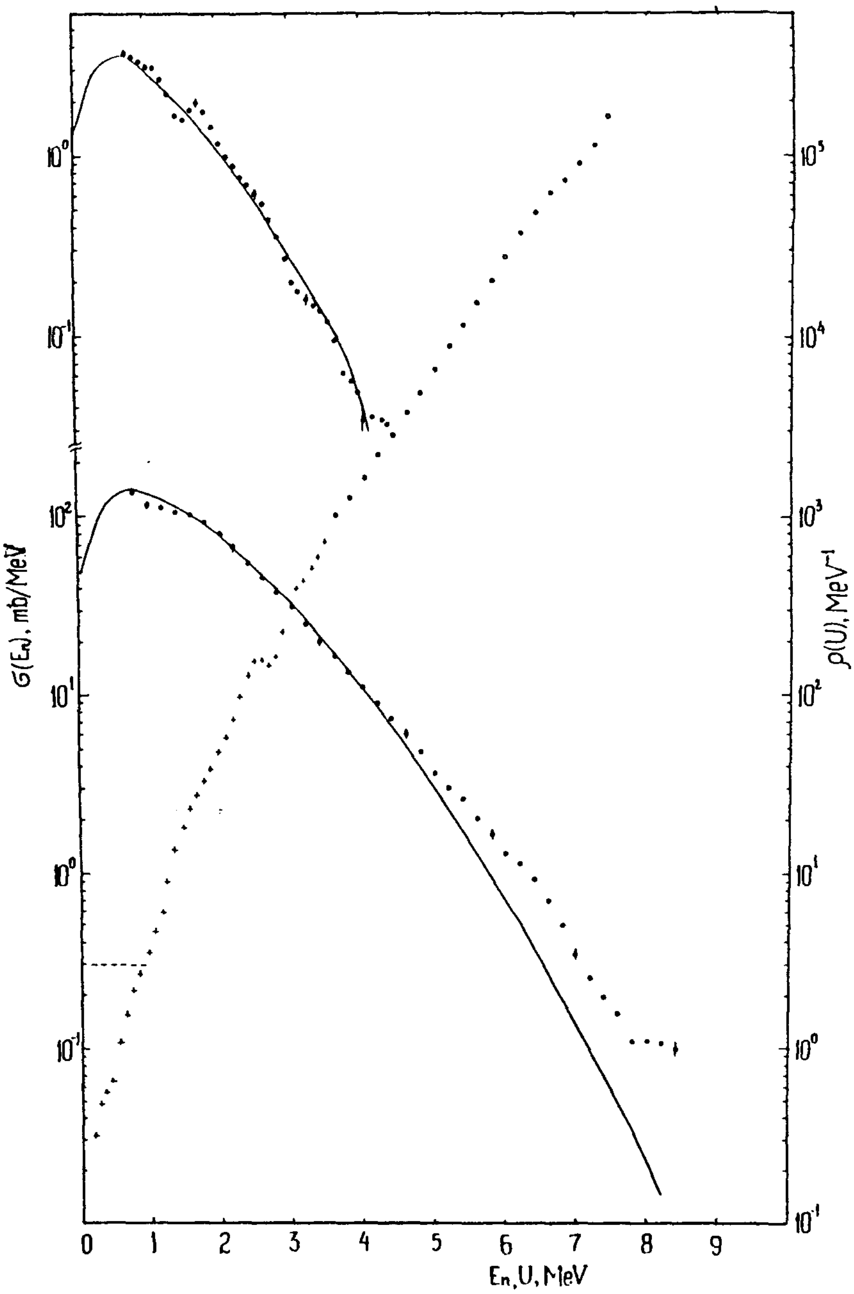

Fig.7. Integral neutron spectra from the $^{209}Bi(p,n)^{209}Po$ reaction at E_p=6.95 MeV (top) and 11.2 MeV (bottom). Designations are the same as in Fig.3.

the width analysis of the giant quadrupole isoscalar resonance observed.

If the measured values of neutron emission cross-section with the excitation of the known low-lying levels are reproduced in calculations the absolute density of nuclear levels in a wide range of excitation energies can be determined by comparing the spectra calculated and measured /15/.

$$\rho(U) = \rho(U)_{mod} \frac{(d\sigma/dE_n)_{meas}}{(d\sigma/dE_n)_{cal}} \qquad (10)$$

Determined according to the equation (10) the absolute nuclear level density of ^{165}Er, ^{204}Bi, ^{206}Bi, ^{207}Bi, ^{208}Bi, ^{209}Po is presented in Fig.-s 3÷7 as a function of excitation energy. For all nuclei at low excitation energies a good agreement is observed with the level counting data, and for ^{165}Er there is an agreement with the data on the average S-wave neutron resonance spacing $\bar{D}_o$ (see table 4). An error in determination of the absolute nuclear level density according to (10) can be estimated from the accuracy achieved in measuring the $\frac{d\sigma}{dE_n}/\sigma_{lev}$ value (~ 10 ÷ 15%) and in calculating it, caused mainly by the uncertainties of neutron optical potential (~ 10%) and spin dependence (~ 7%). Proceeding from this, we estimate the accuracy of determination of the absolute level density in (~ 15 ÷ 20%).

5. Conclusion

Neutron spectra from the (p,n) reaction on the ^{165}Ho, ^{207}Pb, ^{208}Pb, ^{209}Bi nuclei have been measured at the proton energy of 6.95±0.15 MeV. The experimental data obtained, together with the data measured earlier at E_p=11 MeV, have been analyzed within the framework of the Hauser-Feshbach formalism using the generalized superfluid nucleus model for level density. The level density parameters are determined, corresponding to the optimal description of the spectra measured both in the range of discrete states and continuum. The attenuation of the "a" parameter energy dependence for the nuclei close to the double-magic one (82, 126), and the decrease of energy of the first vibrating state ω_{2^+} for the ^{206}Bi, ^{207}Bi, ^{208}Bi nuclei are observed. The absolute nuclear level density was determined within a wide range of excitation energies by comparing the model calculations with the neutron spectra measured. The results obtained showed a good agreement with the level-counting data at low excitation energy and for ^{165}Er with the data on the average S-wave neutron resonance spacing.

The authors would like to acknowledge Dr. Ignatuk A.V. for his useful advice and discussions.

6. References

1. Baryba V.Ya., Birukov N.S., Zhuravlev B.V. et al. IPPE preprint-910. Obninsk. 1979.
2. Birukov N.S., Zhuravlev B.V. //Experimental devices and technique. 1983. V.6. P.22.
3. Baryba V.Ya., Kornilov N.V. et al. //Questions of atomic science and engineering. Reactor construction series. 1977. Issue 5(19). P. 45.
4. Grundl J., Eisenhauer C. //NBS-493. 1977.
5. Ignatuk A.V., Istekov K.K., Smirenkin G.N. //Yadernaya Fisika. 1979. V.29. Is.4. P.875.

6. Grudzevich O.T., Ignatuk A.V., Plaskin V.I. //Neutron Physics. Materials of the I-st International Conference on Neutron Physics. Kiev. 1987. V.2. M.: Nauka. 1988. P.96.
7. Solovyov V.G. Complex nuclei theory. M.: Nauka. 1971. P.164.
8. Titarenko N.N. IPPE preprint-1260. Obninsk. 1982.
9. Becchetti F.D., Greenless G.W. //Phys.Rev. 1969. V.182. P1190.
10. Holmqvist B., Wiedling T. //J.Nucl.Energy. 1973. V.27. P.543.
11. Myers W.D., Swiatecki W.S. //Ark.Fysik. 1967. V.36. P.593.
12. Ramamurthy V.S. et al. //INDC-092/L. 1983. P.187.
13. Mughabghab S.F. //Neutron cross sections. 1984. V.1. Part B.
14. Dilg W., Schantl W., Vonach H. //Nucl.Phys. 1973. V.A217. P.269.
15. Vonach H. //INDC(USA)-092/L. 1983. P.247.
16. Lederer C.M., Shirley V.S. Tables of Isotopes. 7-th Ed. Wiley. N.Y. 1978.

FINAL CONCLUSIONS AND RECOMMENDATIONS

The following conclusions emerged as a result of extensive discussions reviewing the progress made towards achieving the objectives of the CRP in view of the results reported by each participant:

1) Extensive new measurements have been carried out under the CRP spanning 18 nuclides in the mass regions 45-65, 90-100, 180-210. The bombarding energies used ranged from 5 to 25 MeV for protons and 9 to 12 MeV for alpha particles and 5 to 11 MeV for neutrons. This information is summarized in the Appendix. It is possible to extract level density information in the maximum range of 0-10.5 MeV excitation energy for the corresponding residual nuclei from these data.

   It is pointed out that the errors reported for all the measurements were within the accuracy limits required for the proposed level density analysis. However, it was necessary to recognize that the errors in the neutron energy at the higher end of the spectrum were critical factors for matching the extracted level density information with the experimental values based on the discrete level information, especially for those odd-odd nuclides where discrete level densities were already as high as 50/MeV. It was realized that inherent errors in the timing for the time-of-flight technique were the major contribution to this error which was about 200 keV for most of the reported data. In this connection the participants recommended that work to extend the determination of level densities based on discrete level counting to higher energies should be encouraged.

   Analyses of some of the data were reported which brought out the importance of contributions from non-equilibrium processes.

2) The participants agreed that sufficient data were reported to carry out the second stage of the CRP work namely extraction of level density information using consistent analytical procedures. It was suggested, however, that measurements on Pb isotopes at around 14 MeV and on Au-197 at 9 MeV would add useful information towards extending the range of nuclear level densities for those nuclides.

3) It was agreed that, while the experimental part of the CRP was completed, follow-up systematic analyses for extracting the level density information using all the data generated under the CRP were still to be done. It was also suggested that "nuclide specific" or "regional" parameters would be preferrable to "global" parameter sets. The analysis should also explicitly report on the non-compound contributions, if any, and the way in which they have been accounted for.

4) The participants concluded that the CRP may be formally terminated at this stage, however, the analysis work mentioned above should be carried out by all the participants who should send the results to the Nuclear Data Section by the end of 1990. It is recommended that IAEA hold a Consultants' Meeting in the first half of 1991 to intercompare the results of these analyses and to prepare a report containing recommendations of nuclear level density formalisms and data for general use in calculations related to nuclear data needed for nuclear technology applications.

APPENDIX

Table 1. Reactions investigated under this CRP

Reaction	E_{in} (MeV)	Q(MeV)	U_{max} (MeV)	Lab
$^{56}Fe(\alpha,n)^{59}Ni$	12.40	-5.10	6.45	Ohio
	8.95	"	3.25	"
	10.92	"	5.	"
$^{48}Ti(\alpha,n)^{51}Cr$	8.96	-2.70	5.55	Ohio
	10.93	"	7.35	"
	12.40	"	8.70	"
$^{51}V(p,n)^{51}Cr$	5.	-1.5	3.4	Ohio
	6.	"	4.4	"
	7.	"	5.4	"
	8.	"	6.35	"
	8.49	"	6.85	"
$^{59}Co(p,n)^{59}Ni$	5.	-1.9	3.00	Ohio
	6.	"	4.00	"
	7.	"	5.00	"
	8.	"	5.95	"
	8.93	"	6.9	Beijing
	10.93	"	8.85	"
	12.93	"	10.80	"
	14.93	"	12.75	"

Table 1 continued

$^{95}Mo(p,n)^{95}Tc$	8.95 15.00 25.60	-2.25 " "	6.35 10.5 22.9	Beijing Hamburg "
$^{94}Mo(p,n)^{94}Tc$	13.10 25.60	-5.0 "	8.0 20.4	Hamburg "
$^{96}Mo(p,n)^{96}Tc$	8.95 13.10 25.60	-3.79 " "	5.1 9.2 21.6	Beijing Hamburg "
$^{97}Mo(p,n)^{97}Tc$	8.95 13.10 25.60	-1.20 " "	7.65 11.8 24.1	Beijing Hamburg "
$^{98}Mo(p,n)^{98}Tc$	8.95 13.10 25.60	-2.48 " "	6.4 10.5 22.9	Beijing Hamburg "
$^{100}Mo(p,n)^{100}Tc$	8.95 13.10 25.60	-1.12 " "	7.75 11.85 24.3	Beijing Hamburg "
$^{181}Ta(p,n)^{181}W$	11.2 7. 8. 9. 10.	-1.0 " " " "	10.1 " " " "	Obninsk " " " "
$^{165}Ho(p,n)^{165}Er$	11.2 6.95	-1.2 "	9.9 "	Obninsk "
$^{197}Au(p,n)^{197}Hg$	11.2	-1.2	9.9	"
$^{204}Pb(p,n)^{204}Bi$	11.2	-5.8	5.3	"
$^{206}Pb(p,n)^{206}Bi$	11.2	-4.4	6.7	"
$^{207}Pb(p,n)^{207}Bi$	11.2 6.95	-3.2 "	7.9 3.7	" "
$^{208}Pb(p,n)^{208}Bi$	11.2 6.95	-3.6 "	7.5 3.3	" "
$^{209}Bi(p,n)^{209}Po$	11.2 6.95	-2.7 "	8.4 4.2	" "

Table 2. Possible energy range for absolute level density determinations from the results of CRP measurements

Nucleus	Excitation energy range (MeV)	Measurements		Resolved level range (MeV) (no. of levels)
^{51}Cr	0 - 7.7	$^{51}V(p,n)$ and $^{48}Ti(\alpha,n)$		0 - 3.5 (43)
^{59}Ni	0 - 10.5	$^{59}Co(p,n)$ and $^{56}Fe(\alpha,n)$		0 - 2.0 (13)
^{94}Tc	0 - 7	$^{94}Mo(p,n)$	at E_n = 8.9 and 13.1 MeV	0 - 1.5 (26)
^{95}Tc	0 - 9	$^{95}Mo(p,n)$	"	0 - 1.5 (22)
^{96}Tc	0 - 8	$^{96}Mo(p,n)$	"	0 - 0.5 (21)
^{97}Tc	0 - 10.5	$^{97}Mo(p,n)$	"	0 - 1.0 (16)
^{98}Tc	0 - 9	$^{98}Mo(p,n)$	"	0 - 0.5 (24)
^{100}Tc	0 - 10.5	$^{100}Mo(p,n)$	"	
^{165}Er	0 - 9	$^{165}Ho(p,n)$	at E_n = 11.2 and 6.95 MeV	0 - 1.0 (55)
^{181}W	0 - 9	$^{181}Ta(p,n)$	at E_n = 6 - 11.2 MeV	0 - 1.0 (30)
^{204}Bi	0 - 4.3	$^{204}Pb(p,n)$	at E_n = 11.2 MeV	0 - 1.5 (23)
^{206}Bi	0 - 5.7	$^{206}Pb(p,n)$	"	
^{207}Bi	0 - 6.9	$^{207}Pb(p,n)$	at E_n = 11.2 and 6.95 MeV	0 - 2.0 (31)
^{208}Bi	0 - 6.5	$^{208}Pb(p,n)$	"	0 - 1.7 (28)
^{209}Po	0 - 7.4	$^{209}Pb(p,n)$	"	

Third Research Coordination Meeting of the
Coordinated Research Programme on

MEASUREMENT AND ANALYSIS OF DOUBLE DIFFERENTIAL
NEUTRON EMISSION SPECTRA IN (P,N) AND (α,N) REACTIONS

ENEA, Bologna, Italy
13-15 November 1989

AGENDA

A. Opening
   Election of Chairman
   Adoption of Agenda

B. Chairman's Remarks

C. Reports by participants on the progress of their programmes

   1. S.A. Egorov, Radium Institute, Leningrad
   2. S.M. Grimes, Ohio University
   3. P.T. Guenther, Argoone National Laboratory
   4. A.V. Ignatyuk, FEI Obninsk
   5 S.K. Kataria, BARC Bombay
   6. H. Märten, TU Dresden
   7. W. Scobel, Inst. für Exp. Physik, Hamburg
   8. Tang Hongqing, IAE Beijing
   9. H.K. Vonach, IRK Vienna
   10. B.V. Zhuravlev, FEI Obninsk

D. Discussions on special problems encountered

E. Further discussions (in detail) on future activities and actions

F. Conclusions and Recommendations

G. Joint session with the NEANDC Level Density Meeting

Proposed Time Schedule

9:30 - 10:30
11:00 - 12:30
14:00 - 16:00
16:30 - 18:30

IAEA Research Coordination Meeting (Third) on
MEASUREMENT AND ANALYSIS OF DOUBLE DIFFERENTIAL NEUTRON
EMISSION SPECTRA IN (P,N) and (α,N) Reactions"

Bologna, Italy
13 - 15 November 1989

LIST OF PARTICIPANTS

AUSTRIA	Dr. H.K. Vonach Institut für Radiumforschung und Kernphysik Boltzmanngasse 3 A-1090 Vienna
CHINA	Dr. Tang Hongqing Institute of Atomic Energy P.O. Box 275 (3) Beijing
GERMAN Dem. Republic	Dr. H. Märten Sektion Physik Technische Universität Dresden Mommsenstrasse 13 DDR-8027 Dresden
GERMANY, Fed. Republic of	Dr. W. Scobel I. Institut für Experimentalphysik Universität Hamburg Luruper Chaussee 149 D-2000 Hamburg 50
INDIA	Dr. S.K. Kataria Nuclear Physics Division Bhabha Atomic Research Centre Trombay, Bombay 400 085
	Dr. M.K. Mehta Vikram Sarabhai Community Science Centre Navrangpura, Ahmedabad 380009
ITALY	Dr. E. Menapace E.N.E.A.-C.R.E. "E. Clementel" Viale Ercolan 8 I-40138 Bologna
	Dr. G. Reffo E.N.E.A. - C.R.E. "E. Clementel" Div. Fis. e Calcolo Scientifico Via Mazzini 2 I-40138 Bologna
	Dr. M. Herman E.N.E.A. - C.R.E. "E. Clementel" Div. Fis. e Calcolo Scientifico Via Mazzini 2 I-40138 Bologna